Macromolecules
REVIEW

Macromolecules **2009**, *42*, 7221–7250 **7221**
DOI: 10.1021/ma9009593

Ordered Network Mesostructures in Block Polymer Materials

Adam J. Meuler,[†] Marc A. Hillmyer,*[,‡] and Frank S. Bates*[,†]

[†]*Department of Chemical Engineering and Materials Science and* [‡]*Department of Chemistry, University of Minnesota, Minneapolis, Minnesota 55455*

Received May 1, 2009; Revised Manuscript Received August 2, 2009

ABSTRACT: Block polymers are formed by the covalent union of two or more chemically distinct homopolymers. These composite macromolecules self-assemble into a variety of ordered morphologies with features on the nanometer length scale, a phenomenon that has interested researchers for roughly four decades. The known ordered morphologies include numerous multiply continuous network mesostructures, the focus of this review. Multiply continuous network morphologies contain two or more chemically distinct domains that continuously percolate through the specimen in all three dimensions. They have captivated researchers because of their superior mechanical properties and could potentially find utility in technologies such as catalysis, photonic materials, solar cells, and separations. This review summarizes experimental and theoretical investigations of the structures and properties of network morphologies in AB block copolymer and ABC block terpolymer systems and includes a discussion of some proposed technological applications of these intriguing mesostructures.

Introduction

Block polymers are hybrid macromolecules formed by coupling together two or more chemically distinct homopolymers. They have been the focus of extensive research efforts since Szwarc's development of living anionic polymerization as a relatively facile means of block polymer synthesis in 1956.[1] There are a number of block polymer architectures, the simplest of which is the linear AB diblock copolymer. Early experimental research revealed that these materials self-assemble primarily into three periodically ordered mesostructures: lamellae (LAM), hexagonally packed cylinders (HEX), and body-centered-cubic spheres (BCC);[2−4] real space representations of these morphologies are provided in Figure 1. Theoretical studies followed these experimental reports and elucidated the statistical mechanical phenomena governing mesostructure formation in block copolymers.[5−7] (Here we note that the packing of the spherical morphology as BCC was not definitively established until 1980.[7])

AB diblock copolymers are generally characterized by the overall degree of polymerization N, the volume fraction f_A of block A, and the segment−segment (Flory−Huggins) interaction parameter χ_{AB}, where the product $\chi_{AB}N$ scales with the segregation strength of the system (note that both χ_{AB} and N must be defined with respect to the same segment reference volume).[9,10] Above a minimum value of $\chi_{AB}N$, the constituent blocks are thermodynamically incompatible and, like oil and water, segregate to minimize the system free energy. Unlike oil and water, the covalent linkages between blocks prevent macrophase separation and constrain block separation to a length scale commensurate with the size of the polymer chains (typically 5−100 nm). Free energy minimization drives block copolymers to adopt periodically ordered morphologies, and a balance of interfacial tension and entropic stretching energy considerations governs selection of the equilibrium state.[9,10] In AB diblock copolymers, the identity of the equilibrium morphology depends largely on f_A and $\chi_{AB}N$.[7,11−13]

BCC, HEX, and LAM have been identified as the equilibrium morphologies for the majority (>80% at $\chi_{AB}N = 100$) of AB diblock copolymer compositions.[13] None of these mesostructures have multiple domains that continuously percolate across the specimen in three dimensions. A multiply continuous, percolating domain structure would provide physical attributes that could be useful in many technological applications. From a mechanical property standpoint, a multiply continuous morphology permits each domain to contribute directly to the modulus of the material[14] and may allow for synergistic improvements in toughness, stress at failure, and creep resistance.[15−17] Multiply continuous block polymer mesostructures are characterized by a high interfacial area per specimen volume, an attribute that could facilitate gas separation[18] or the separation and extraction of free charges (and thus improved efficiency) in solar cells.[19−23] Percolating domain structures could be useful in membranes for water purification; HEX-forming diblock copolymers have been employed, following the degradation and removal of the minority components, as water filtration membranes.[24,25] Anisotropic structures such as HEX often require costly and/or time-consuming alignment procedures to minimize pore dead ends and maximize flux through the membrane. The percolating domains of multiply continuous mesostructures are not likely to terminate at grain boundaries, rendering these alignment procedures unnecessary.[26] Three-dimensional (3-D) domain connectivity may also enhance ionic transport in, for example, battery or fuel cell membranes, when the mesostructure contains a conducting domain.[27] Triply periodic order is also important in 3-D photonic crystals,[28−36]and multiply continuous block polymer morphologies may find application in this emerging technology.[37]

Scriven first suggested, in 1976, that morphologies with multiple continuous, percolating domains could arise in complex fluids.[38] Numerous types of multiply continuous structures have since been identified in polymeric materials, including cocontinuous blends,[14,17] bicontinuous microemulsions,[39−41] disordered bicontinuous structures,[26,42,43] and multiply continuous morphologies with long-range translational order (i.e., multiply continuous network morphologies).[44−46] Ordered network morphologies are arguably the most versatile multiply continuous mesostructures in polymeric materials, as they are characterized by translational order that may be important in photonic crystal[28−36] or solar cell[47] applications. This review chronicles

*To whom correspondence should be addressed. E-mail: hillmyer@umn.edu (M.A.H.); bates@cems.umn.edu (F.S.B.).

Published on Web 09/10/2009

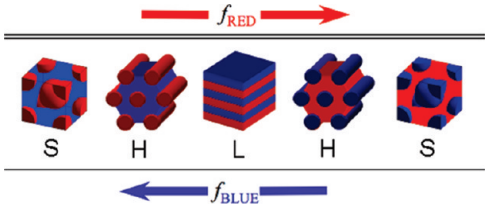

Figure 1. Real space representations of the (S) BCC, (H) HEX, and (L) LAM morphologies that are accepted as equilibrium mesostructures for AB diblock copolymers. Morphologies are presented, from left to right, in the order of increasing volume fraction of the red block. Reproduced with permission from ref 8. Copyright 2008 Elsevier.

theoretical and experimental investigations of multiply continuous ordered network morphologies in block polymer materials. It details the symmetries and microdomain structures of all known multiply continuous block polymer based network morphologies, discusses network stability with respect to various system perturbations (e.g., solvent or homopolymer addition, block polydispersity), and describes the mechanical properties and some potential applications of network mesostructures.

Definition of "Network Morphology"

Network lattices (nets) are comprised of polyhedra that tile (i.e., completely cover the surface area of) triply periodic hyperbolic surfaces that are free of self-intersections.[48] (Hyperbolic surfaces have negative and positive curvature (e.g., saddle surfaces) and are described in more detail in geometry textbooks such as ref 49.) These nets are characterized by translational symmetry in three dimensions and divide space into independent, intertwining domains. The topologies of structures in a variety of materials, including zeolites[50] and low molecular weight surfactants,[51−54] can be represented by triply periodic network lattices. Two important characteristics of a network lattice are the connectivity of each node (p) and the smallest number of such nodes that form a closed loop in the lattice (n). Wells proposed a (n,p) labeling scheme to characterize nets,[55] and we utilize this scheme in this review. Schematics of nodes with 3-fold, 4-fold, and 6-fold connectivity (i.e., different values of p) are provided in Figure 2; these connectors clearly have a different local structure. Differences in n values are subtly related to translational symmetry and are not as readily visualized as the differences in the connectivities of the nodes. In this review, the term "network morphology" refers to a mesostructure whose domain topology can be represented by a network lattice. Multiply continuous network morphologies are characterized by 3-D translational order and contain two or more domains continuously percolating in three dimensions.

Network Morphologies Formed by Block Copolymers

Ordered Bicontinuous Double Diamond. Scriven first hypothesized that bicontinuous structures could arise in complex fluids in 1976.[38] In that prescient publication, he described a bicontinuous structure as "a bicontinuous partitioning in which each subvolume is filled with a distinct, not necessarily uniform composition or state of matter." Here we generalize Scriven's notation by describing structures containing two or more continuous, percolating domains as "multiply continuous" structures. Scriven noted that, for certain subvolume ratios, bicontinuous geometries have less interfacial area than structures comprised of discrete spheres of one component packed in a continuum of the other component.[38] Thermodynamic considerations that favor a minimization of interfacial area could thus drive formation of a bicontinuous structure. Scriven pointed out that at some

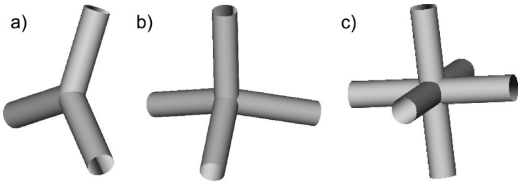

Figure 2. Schematic representations of (a) 3-fold, (b) 4-fold, and (c) 6-fold connecting elements.

compositions the dividing surfaces that minimize interfacial area are periodic minimal surfaces;[38] Schoen had mathematically described 17 such surfaces in 1970.[56] Constant mean curvature surfaces minimize interfacial area at other compositions, and Anderson et al. subsequently made a comprehensive assessment of the relationships between periodic surfaces of prescribed mean curvature as a function of the symmetry and composition.[57]

The phrase "ordered bicontinuous structure" was first used to describe a block copolymer morphology by Alward et al. in 1986.[58] These researchers characterized starblock copolymers comprised of PS−PI arms. (Note that a list of abbreviations for all of the polymers dicussed in this review is provided in Table 4 at the end of the review.) They obtained, from materials with 8, 12, and 18 branches and 30 wt % PS, transmission electron microscopy (TEM) images with both "wagon-wheel" and square arrangements; representative micrographs are provided in Figure 3.[58] Aggarwal had published a similar wagon-wheel micrograph 10 years prior (acquired from a 15-arm PS−PI starblock copolymer with 30 wt % PS) but, unlike Alward et al., did not comment on the nature of the underlying mesostructure.[59] Alward and coworkers suggested that both of the projections provided in Figure 3 were the product of a single ordered bicontinuous morphology, as tilting a specimen in the TEM led to a transformation of one projection into the other. They probed the bicontinuity of the materials using gas sorption and dynamic mechanical spectroscopy measurements; the high rates of gas diffusion and the large elastic moduli (G') suggested continuity of the PI and PS domains, respectively.[58] Ordered bicontinuous mesostructures were subsequently reported in various other PS−PI starblock copolymers.[60,61]

Thomas and colleagues attempted to elucidate the detailed microdomain structure of the ordered bicontinuous morphology depicted in the images in Figure 3.[44] They noted that the micrographs provided in Figure 3 contain both 4-fold (a) and 3-fold (b) axes of symmetry and concluded that the space group must be cubic, as only cubic space groups contain both of these symmetry elements. Small-angle X-ray scattering (SAXS) measurements were used to probe the space group symmetry, but the Bragg patterns contained features that were artifacts of the data desmearing process and were thus not reflective of the underlying mesostructure.[62] TEM images obtained from particularly thin (∼30 nm thick) polymer slices revealed 3-fold connected PS rods separated by 120°. Thomas et al. suggested these rods were part of a 4-fold connector, with the fourth rod being perpendicular to the plane of the image, and proposed a 3-D model for the ordered bicontinuous structure based upon $Pn3m$ symmetry and (6,4) nets.[44] Simulated TEM images were generated using this model, and they generally resembled the experimental micrographs. Thomas et al. cited this agreement as evidence in support of their model and called the bicontinuous mesostructure the ordered bicontinuous double diamond (OBDD).[44] Solvent casting and thermal annealing experiments provided some evidence that the bicontinuous struc-

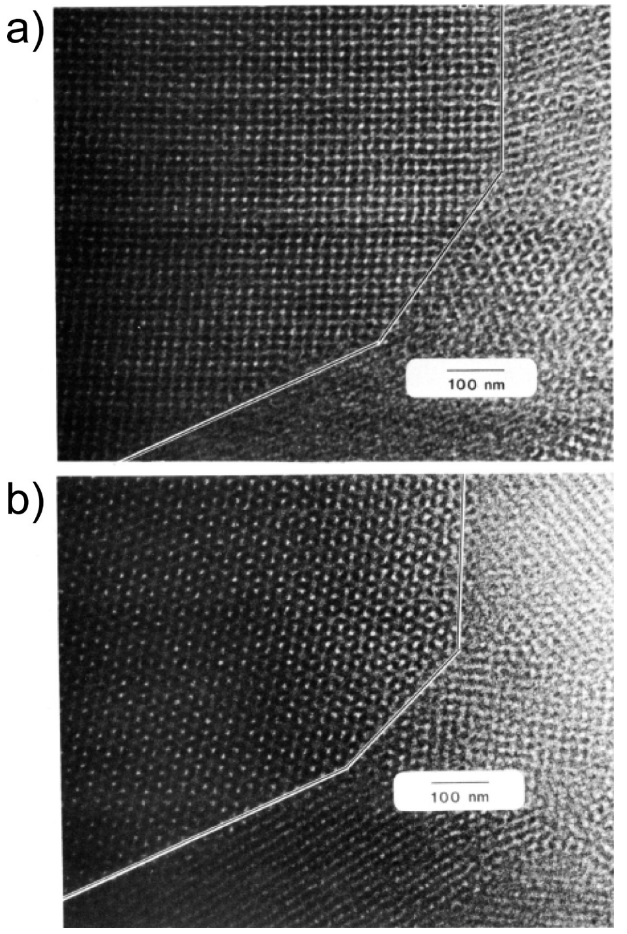

Figure 3. TEM micrographs obtained from a starblock copolymer material comprised of PS−PI arms with 30 wt % PS. The majority PI appears black because it was stained with OsO_4. Tilting the specimen in the TEM converted the square projection in (a) into the wagon-wheel arrangement in (b); Alward et al. suggested these projections are the product of an ordered bicontinuous mesostructure, and the micrographs are reproduced from the original publication.[58] Aggarwal had published a similar wagon-wheel micrograph without comment 10 years earlier.[59]

ture was the equilibrium phase. Films cast from toluene adopted OBDD that persisted upon thermal annealing, while those cast from cyclohexane initially formed HEX and subsequently transitioned to the bicontinuous network morphology following thermal treatment.[44]

At roughly the same time as the Thomas et al. publication,[44] Hasegawa and co-workers independently reported an ordered bicontinuous mesostructure in solvent cast films of linear PS−PI diblock copolymers.[63] TEM micrographs comparable to those provided in Figure 3 (but with opposite contrast) were acquired from specimens with PS volume fractions ranging from 0.62 to 0.66.[63] Like Thomas et al.,[44] Hasegawa and co-workers suggested the TEM images were consistent with interpenetrating networks connected by 4-fold elements. They considered models of all three of the possible 4-fold-connected cubic network structures and reported that simulated TEM images generated from the OBDD lattice model with *Pn3m* symmetry and (6,4) nets were the most consistent with the experimental micrographs.[63] The bicontinuous mesostructure in the PS−PI specimens was further interrogated using SAXS. The acquired Bragg patterns did not contain all of the allowed reflections[64] for the *Pn3m* space group of OBDD but appeared to be consistent with a Bravais lattice with hexagonal symmetry. Hasegawa et al. suggested that some peaks

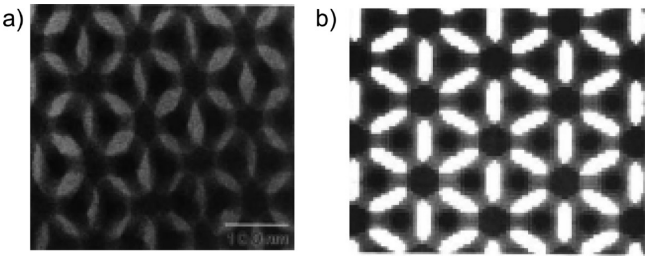

Figure 4. (a) TEM micrograph obtained from a PS−PI diblock copolymer with a PS volume fraction of 0.62 (PS appears light in the image because the PI is stained). (b) Simulated [111] projection from a model OBDD structure with CMC interfaces and the same composition as the experimental material probed in (a). Reproduced with permission from ref 65. Copyright 1988 Macmillan Publishers Ltd.

were not visible in SAXS patterns due to either detector resolution issues or form factor extinctions, and largely on the basis of TEM analysis, they identified the bicontinuous mesostructure as OBDD.[63]

Thomas et al. attempted to elucidate the molecular factors driving the selection of the OBDD mesostructure.[65] They noted that the interfacial width in strongly segregated diblock copolymers is small relative to the domain periodicity and suggested that, in this limit, the minimization of interfacial tension becomes more significant than the minimization of the entropic free energies associated with chain stretching. It was reasoned that block copolymers adopt morphologies with minimal-surface area interfaces separating the chemically distinct domains to minimize segment−segment contacts and interfacial tension.[65] The surfaces that mathematically minimize area are known as constant mean curvature (CMC) surfaces, and Anderson et al. calculated that it is possible to have CMC surfaces with OBDD symmetry provided the volume fraction of the minority component is at least 0.262.[57] Thomas et al. pointed out that this CMC volume fraction limit agreed remarkably well with block copolymer experiments,[65] as OBDD had been identified only in block copolymer materials with minority volume fractions above 0.26 (ranging from 0.27 to 0.38).[44,61,63] Thomas et al. generated simulated TEM projections using the CMC OBDD model and compared them to experimental TEM micrographs; both the simulated and experimental images are provided in Figure 4.[65] The agreement between the experimental and simulated images was cited as evidence that block copolymers form mesostructures with CMC, although Thomas et al. pointed out the visual similarities did not provide definitive proof.[65]

A number of additional experimental reports[66−69] of the OBDD mesostructure appeared in the literature following the seminal publications by Thomas et al.[44,58,60,61,65] and Hasegawa et al.[63] These investigations focused on binary blends of block copolymers and homopolymers. Winey et al. noted[66] that the OBDD morphology was only reported over narrow ranges of composition (a volume fraction range of ~0.05) in both diblock[63] and starblock[44,58,60,61] copolymers. Targeting this narrow composition window can be synthetically challenging, and numerous reports demonstrated that blending could be used to overcome the stringent synthetic requirements.[66−69] Winey et al. studied blends of PS−PI or PS−PB diblock copolymers and a constituent homopolymer (either PS, PI, or PB).[66] Most of the blends formed a single morphology with long-range order that was qualitatively comparable to the long-range order in mesostructures formed by neat diblock copolymers (e.g., a similar number of Bragg peaks in the SAXS data). The blends reportedly formed the OBDD network in the appropriate composition

range and generally behaved like neat diblocks with the same overall composition, provided (i) the homopolymer weight fraction in the blend was below 0.40 and (ii) the homopolymer molecular weight was roughly equal to or less than the appropriate block molecular weight. Higher homopolymer fractions and/or higher molecular weight homopolymers usually triggered macrophase separation.[66] Spontak et al. extended Winey et al.'s investigations[66] of blends of PS−PI diblocks and PS or PI homopolymers to additional absolute and relative molecular weights.[67,68] Generally, the reported results were consistent with Winey et al.'s study,[66] although some higher molecular weight blends formed poorly ordered mesostructures with both cylindrical and network features, and not well-ordered bicontinuous morphologies, possibly due to kinetic limitations.[67] Xie and co-workers examined blends of symmetric PS−PB−PS triblock copolymers (28 wt % PS, overall PDI = 1.35) and PVME homopolymers (PDI = 1.70).[69] The HEX mesostructure was identified using TEM in the neat PS−PB−PS triblock, and the OBDD mesostructure was reported in binary blends containing 10, 12, and 15 wt % PVME (a total volume fraction of 0.33−0.37 for the mixed PS/PVME domains). The authors reported that there was no evidence of macrophase separation, and this work demonstrated that monodisperse materials are not required to form an ordered bicontinuous network mesostructure.[69]

A number of theoretical investigations also followed the Thomas et al.[44,58,60,61,65] and Hasegawa et al.[63] publications. These studies largely focused on the stability of the OBDD network mesostructure relative to LAM, HEX, and BCC.[70−74] Wang and Safran studied model ternary blends comprised of an AB diblock copolymer and the constituent A and B homopolymers.[70] They calculated the curvature free energy of the block copolymer interface and suggested that the OBDD morphology was stable for systems with certain compositions and molecular weights, although the analysis was not rigorously valid for neat block copolymer materials.[70] Anderson and Thomas used a mean-field theory to calculate the free energies of the LAM, HEX, BCC, and OBDD morphologies for AB diblock and starblock copolymers in the strong-segregation limit (SSL).[71] The lowest free energy OBDD configuration (microdomains separated by CMC interfaces) never was predicted to be the equilibrium morphology; at least one of the BCC, HEX, and LAM morphologies always had a computed free energy that was at least 1% lower than that of OBDD. Anderson and Thomas suggested that non-Gaussian behavior of core chains unaccounted for by the theory prevented OBDD from being identified as the equilibrium mesostructure.[71] Two other groups employed alternative strong-segregation theory (SST) calculations to re-examine Anderson and Thomas' conclusion regarding the stability of the OBDD morphology in AB diblock copolymers in the SSL.[72,73] Likhtman and Semenov used a more accurate mean-field approach to compute the free energies of competing morphologies in linear AB diblock copolymers with a minority block volume fraction ranging from 0.27 to 0.37.[72] They calculated that the OBDD morphology has a free energy at least 4% higher than either the LAM or HEX mesostructure over this composition range and suggested that free energy differences of this magnitude could not be accounted for by errors associated with either model assumptions or numerical approximations. Likhtman and Semenov hypothesized that the reported[63] OBDD morphologies in AB diblock copolymers were metastable structures.[72] Olmsted and Milner modified the SST approach by relaxing the assumption of CMC interfaces.[73,74] This methodology allegedly improved the realism of the unit cells used in the calculations and, unlike studies based on Semenov's original SST approach,[75] enabled differentiation of the free energies associated with different packing arrangements (e.g., it could distinguish between BCC and FCC packing of spheres). Olmsted and Milner calculated that the free energy of the OBDD mesostructure was always at least ~3% higher than the competing LAM and HEX morphologies,[73,74] a result in good agreement with Likhtman and Semenov's report.[72] (Note that Olmsted and Milner corrected[74] a numerical mistake in their initial publication[73] that had led to an initial erroneous identification of ODBB as an equilibrium morphology.) None of these studies provided a theoretical basis for considering OBDD an equilibrium mesostructure in strongly segregated AB diblock copolymers.

Gyroid (Q^{230}). While the OBDD morphology was the only bicontinuous mesostructure described in the block copolymer literature prior to 1994, additional interpenetrating phases were well-known in lipid−water systems. An ordered structure with $Ia\bar{3}d$ symmetry that could be represented using (10,3) nets was first identified in strontium saturated soaps by Luzzati and Spegt in 1967.[51] Schoen mathematically described a minimal surface that could be used to model this structure in 1970 and called it the gyroid[56] (others have referred to it as Schoen's G surface).[45] The name "gyroid" has subsequently been widely used in the literature to describe structures with $Ia\bar{3}d$ symmetry. (Here we note that Schoen's G surface is characterized by $I4_132$ symmetry.[56] A structure will have $Ia\bar{3}d$ symmetry when it contains two parallel Schoen's G surfaces that are related by inversion. Some researchers have therefore used the term "double gyroid" to describe morphologies with $Ia\bar{3}d$ symmetry;[45] we will use "gyroid" to describe these mesostructures in this review but note that the two terms are often used interchangeably in the literature.) The gyroid structure was reported in a number of water−lipid systems by 1991[51−54] but was not known in block copolymer materials until 1994 when two experimental groups[45,46] and one theoretical team[76] independently identified the gyroid morphology in weakly segregated diblock copolymer materials. (Gobran had, in 1990, reported SAXS and TEM data obtained from a PS−PI diblock copolymer (f_s = 0.34) that he speculated could be consistent with the gyroid morphology, although no definitive morphological assignment could be made on the basis of just two Bragg peaks in the SAXS data.[77])

Fetters synthesized a 27.4 kg/mol PS−PI diblock copolymer containing 37 wt % PS.[45] This diblock specimen was annealed at least 1 h in the melt to allow the material to approach equilibrium and improve the long-range order of the resulting morphology. SAXS data acquired following a 150 °C heat treatment contained two peaks at relative reciprocal space positions of $\sqrt{3}$:$\sqrt{4}$, with the second peak having ~10% of the intensity of the primary peak. Hajduk et al. noted that although these relative peak positions did not definitively eliminate HEX, BCC spheres, or OBDD as morphological candidates, the absence of peaks at relative q positions of 1 (for HEX and BCC) and $\sqrt{2}$ (for OBDD) were strongly suggestive of a new mesostructure.[45] Several complementary characterization techniques were employed in an attempt to determine the identity of this morphology. A representative TEM micrograph from this specimen is provided in Figure 5a. Both the PS and PI domains appear to be continuous in the image, eliminating HEX and BCC as mesostructural candidates.[45] This PS−PI sample had a measured birefringence of zero and, consequently, an optically isotropic structure, consistent with cubic symmetry.[45] Since neither the TEM nor the birefringence experiments eliminated OBDD as a mesostructural candidate, Hajduk et al.

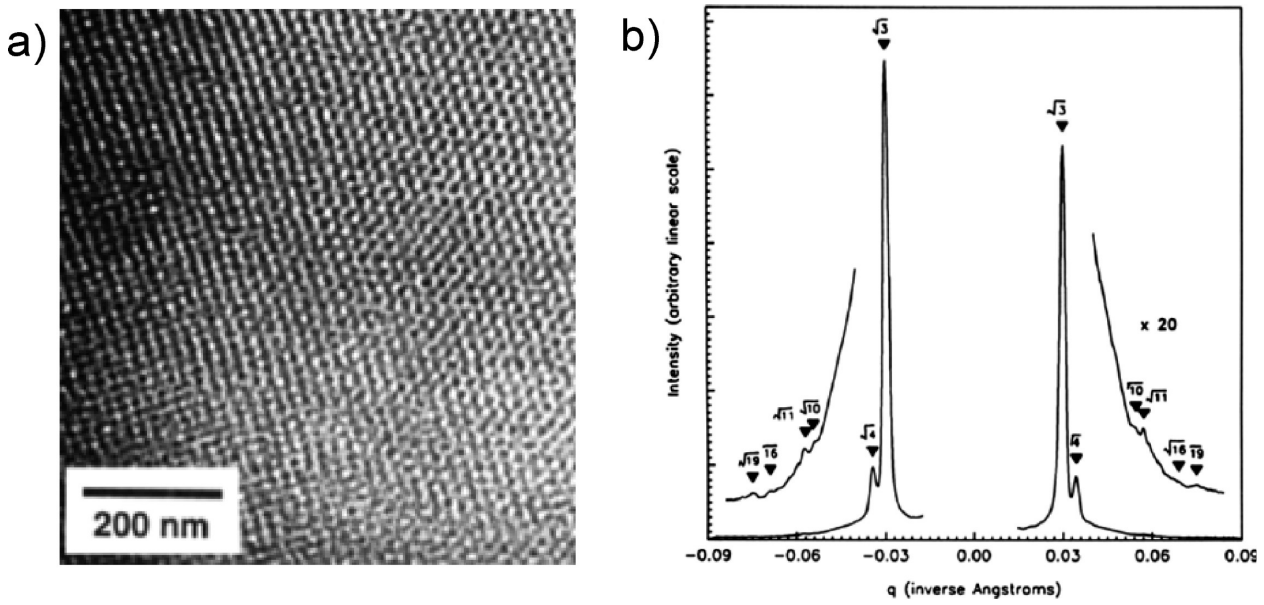

Figure 5. (a) TEM micrograph acquired from a PS−PI diblock copolymer with 37 wt % PS. Prior to TEM analysis, the sample was annealed for 22 h at 160 °C and then quenched in liquid nitrogen to preserve the high-temperature morphology. (b) One-dimensional SAXS profile acquired from the PS-PI diblock that formed the morphology imaged in (a). Reproduced from ref 45.

returned to SAXS analysis and modified their procedure to maximize the number of higher order Bragg peaks obtained from the experiment. The sample was annealed for 8 h and then exposed to X-rays for 8 h, yielding the one-dimensional profile provided in Figure 5b. Bragg reflections are present at relative q positions of $\sqrt{3}$, $\sqrt{4}$, $\sqrt{10}$, $\sqrt{11}$, $\sqrt{16}$, and $\sqrt{19}$. Hajduk et al. noted that the $\sqrt{10}$, $\sqrt{11}$, and $\sqrt{19}$ reflections are inconsistent with noncubic space groups, a result in accord with the birefringence experiment.[45] Only 3 of the 17 possible cubic extinction symbols (P..., $P4_2$.., and Pn...) have allowed reflections at the relative $\sqrt{3}$, $\sqrt{4}$, $\sqrt{10}$, $\sqrt{11}$, $\sqrt{16}$, and $\sqrt{19}$ Bragg locations. However, each of these symbols also have at least eight allowed reflections that are not present in the SAXS data provided in Figure 5b. Hajduk et al. noted that while a couple of these absences can be rationalized as minima in the structure factor, such reasoning is unlikely to account for the large number of peaks absent from the SAXS data. They argued that these data suggest the new morphology does not belong to either the P..., $P4_2$..., or Pn... space groups and could not be OBDD.[45]

Hajduk et al. pointed out that the Bragg peak locations can be rescaled, as the $\sqrt{3}$, $\sqrt{4}$, $\sqrt{10}$, $\sqrt{11}$, $\sqrt{16}$, and $\sqrt{19}$ values simply represent the lowest magnitudes consistent with the relative positions.[45] Additional possibilities for the space group arise when all of these values are multiplied by $\sqrt{2}$, an operation that leaves the peak ratios unchanged. The reinterpretation of the peak positions as $\sqrt{6}$, $\sqrt{8}$, $\sqrt{20}$, $\sqrt{22}$, $\sqrt{32}$, and $\sqrt{38}$ reflections is supported by the fact that this renormalization yields better agreement between the unit cell dimensions measured by SAXS and those measured using TEM than the previous $\sqrt{3}$, $\sqrt{4}$, $\sqrt{10}$, $\sqrt{11}$, $\sqrt{16}$, and $\sqrt{19}$ assignments. Twelve cubic space groups (all of those with P or I symmetry) allow Bragg reflections at the rescaled peak positions. However, all of these space groups have at least seven allowed reflections that are not present in the experimental Bragg pattern, except for $Ia\bar{3}d$, which is only missing five allowed reflections. Hajduk et al. suggested the gyroid was the mesostructure that was the most consistent with the SAXS data. (Hajduk et al. use the term "double gyroid" to describe the morphology with $Ia\bar{3}d$ symmetry.[45])

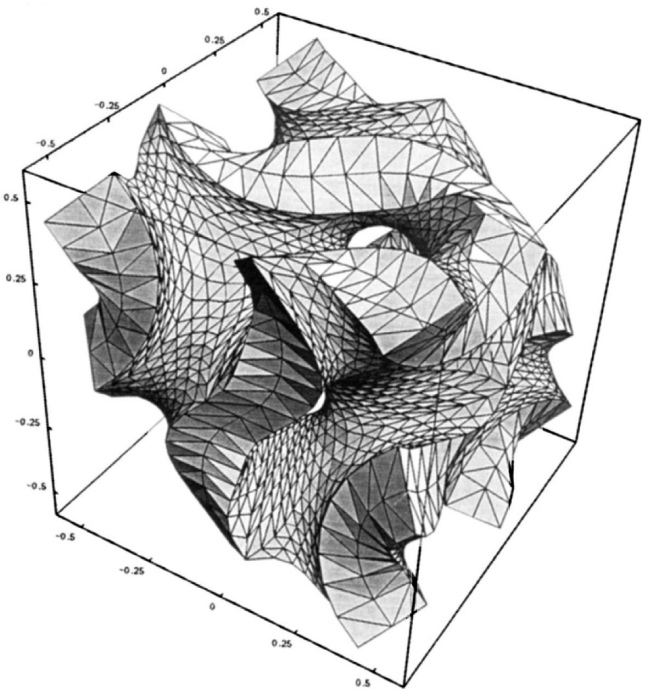

Figure 6. Space-filling model of the gyroid morphology proposed by Hajduk et al.[45] The model contains two parallel Schoen's minimal G surfaces that are related by inversion and contains a minority volume fraction of 0.33. The regime illustrated in this figure is the matrix; the two independent networks are depicted as the white/void regions. Reproduced from ref 45.

This analysis of the relative peak positions helped establish the space group symmetry of the gyroid morphology but did not lead to an understanding of the detailed microdomain structure. Hajduk et al. therefore generated a microdomain space-filling model containing two Schoen's G surfaces[56] that is reproduced in Figure 6. They used this model to predict both the relative intensities of the SAXS peaks and the projections that should be obtained using TEM.[45] Analysis of the model depicted in Figure 6 suggests that the

$\sqrt{6}$ and $\sqrt{8}$ reflections in the SAXS data should be strong and all other peaks should have low intensities; this prediction agrees with the experimental SAXS data reproduced in Figure 5b. The simulated TEM images obtained using the model contained both 3-fold and 4-fold symmetry elements, as is characteristic of cubic morphologies. Hajduk et al. obtained TEM micrographs from the sample that agreed with both the [111] and [100] simulated projections. The good general agreement between the predicted and experimental SAXS and TEM data suggests the model displayed in Figure 6 which contains two parallel Schoen's G surfaces related by inversion is a valid representation of the microdomain structure of the gyroid.[45]

Here we note that schematics of network morphologies are often depicted using "ball and stick" models containing connecting elements similar to those provided in Figure 2. While these models provide appealing visualizations of the network lattice (a (10,3) net in the case of the gyroid), the space-filling model presented in Figure 6 is a better representation of the actual microdomain structure of a block copolymer material.

Hajduk et al. noted that the gyroid mesostructure resembles the previously proposed OBDD morphology[44,65,71] in a number of ways.[45] Namely, both are bicontinuous mesostructures with infinite triply periodic cubic symmetry minimal surfaces underlying their topology. As a result, the TEM images obtained from the gyroid closely mirror those expected from the OBDD mesostructure. Hajduk et al. warned that differentiating the two morphologies on the basis of only TEM was very difficult and noted that SAXS was integral in their identification of the gyroid.[45] One key difference between OBDD and the gyroid is the local structure of the connecting nodes in the interpenetrating networks; the OBDD mesostructure can be represented using a (6,4) net with 4-fold connectors while the gyroid is described by a (10,3) net containing 3-fold connectors.

Schulz et al. independently identified the bicontinuous gyroid mesostructure in a weakly segregated blend of PS−P2VP diblock copolymers that had an overall PS volume fraction of 0.37.[46] The PS blocks were deuterated to provide contrast for small-angle neutron scattering (SANS), an integral characterization technique employed in the study. The sample was aligned using a dynamic shearing device[78] and then quenched to room temperature to preserve the high-temperature structure prior to exposure to neutrons. Rheological measurements revealed that the blend underwent an order−order transition (OOT) upon heating, with G' increasing by about an order of magnitude as the temperature was increased from 150 to 170 °C.[46] SANS experiments were employed to probe the morphology of the blend above and below the OOT. Data consistent with a HEX morphology were obtained from the sample sheared at 140 °C, and a Bragg pattern consistent with the gyroid was acquired from the material aligned at 175 °C. Schulz et al. were able to identify epitaxial relationships between the HEX and gyroid morphologies because they investigated aligned mesostructures. (Note, the (10) ↔ (211) correspondence between the HEX and gyroid phases was mistakenly rotated by 90° in this initial paper.[46])

These experimental investigations[45,46] were augmented by the self-consistent mean-field theory (SCFT) calculations reported by Matsen and Schick.[76] With this method, the free energies of various mesostructural candidates are computed for a model block copolymer with a given composition and segregation strength, ignoring fluctuation effects. The morphology with the lowest free energy is accepted as the equilibrium phase. Matsen and Schick considered a number

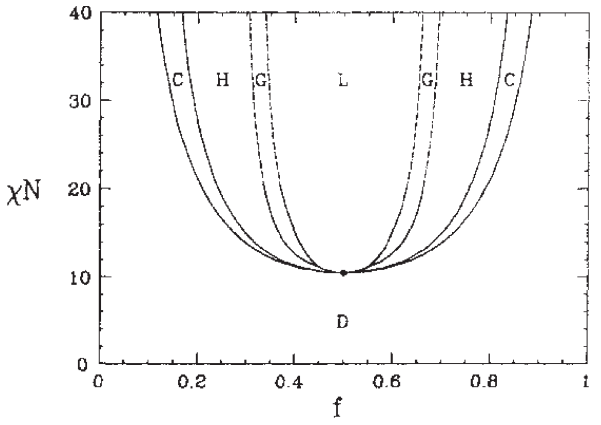

Figure 7. SCFT phase portrait depicting the predicted stable regions for various morphologies in conformationally symmetric linear AB diblock copolymers: (D) disordered, (L) LAM, (G) gyroid, (H) HEX, and (C) BCC. Dashed lines represent extrapolated mesostructural boundaries, and the critical point is marked by a dot. The gyroid stability region does not reach the critical point but terminates at a HEX/gyroid/LAM triple point. OBDD is not predicted to be an equilibrium phase. Reproduced with permission from ref 76. Copyright 1994 American Physical Society.

of mesostructural candidates, including LAM, HEX, BCC, OBDD, gyroid, and various stackings of perforated lamellae. They noted that the consideration of these morphologies was largely guided by experimental reports, and their work illustrates the synergies that arise when theoreticians and experimentalists work in concert on a problem. The initial study focused on conformationally symmetric diblock copolymers with $\chi_{AB}N$ values below 20, and the predicted SCFT phase portrait generated by Matsen and Schick is reproduced in Figure 7.[76] The BCC, HEX, gyroid, and LAM morphologies were predicted to be equilibrium mesostructures in this weak segregation regime, and the predicted stability range for the gyroid generally agreed with the experimental reports of Hajduk et al.[45] and Schulz et al.[46] The OBDD and perforated lamellar morphologies never produced the lowest computed free energy, although they closely competed with the equilibrium HEX, gyroid, and LAM mesostructures at some compositions and segregation strengths.[76]

Matsen and Schick subsequently utilized the same general SCFT methodology to investigate linear multiblock,[79] starblock,[80] and conformationally asymmetric linear diblock[79] copolymers. Asymmetry in the statistical segment lengths (i.e., conformational asymmetry) drives a shift in the boundaries of the phase portrait depicted in Figure 7 and changes the sizes of the various stability windows but does not destabilize the gyroid or stabilize either the OBDD or perforated lamellar morphologies when the ratio of statistical segment lengths is equal to 1.5 or 2.[79] Altering the molecular architecture to a linear multiblock (e.g., ABA, ABABA, etc.) or starblock $((AB)_n$ with the number of arms $n = 3$, 5, or 9) configuration also does not significantly alter the topology of the phase portrait; only the positions of the boundaries change, and the gyroid remains the only bicontinuous morphology predicted to be stable.[79,80] Interestingly, Matsen and Schick predicted that the gyroid windows (i.e., the range of compositions at which gyroid is stable) widen as the number of arms increases, intimating that the starblock architecture could provide a means of stabilizing the bicontinuous network mesostructure.[80] These SCFT results[80] are in good agreement with the previously demonstrated stability of ordered bicontinuous network morphologies at higher arm numbers in PS-PI starblock materials.[58]

Re-examining the OBDD Morphology. The gyroid appears to be a stable morphology, consistent with predictions for conformationally symmetric[76] and asymmetric[79] linear diblock, linear multiblock,[79] and starblock[80] copolymers. The calculated free energies of the OBDD and perforated lamellar morphologies are close to, but never lower than, the computed free energy of the gyroid for these weakly segregated materials.[76,79,80] Similarly, the OBDD morphology was never predicted to be the equilibrium mesostructure for strongly segregated block copolymer materials.[71−74] Rigorous experimental analyses[45,46] also identified the gyroid, and not OBDD, as a bicontinuous network structure in linear diblock copolymers. These theoretical[71−74,76,79,80] and experimental[45,46] results stimulated a re-examination of the morphological assignments of the OBDD network in the previously discussed 6-arm and 18-arm PS−PI starblock copolymers.[62] During this re-examination, the 6-arm and 18-arm materials were annealed at 120 °C for 3 and 11 days, respectively, to improve long-range order, cooled to ambient temperatures, and probed using SAXS. The resulting Bragg patterns contained peaks at relative q positions of $\sqrt{3}$, $\sqrt{4}$, $\sqrt{10}$, and $\sqrt{11}$; Hajduk et al. suggested that, while not definitive, these relative positions were most consistent with $Ia\bar{3}d$ space group symmetry (i.e., the gyroid), and good general agreement between the experimental peak intensities and computed intensities based upon a mesostructural model supported this claim. A reversible, thermally induced OOT from gyroid to HEX in the 6-arm material provided compelling evidence that gyroid was in fact the equilibrium morphology.[62]

Hajduk et al.'s reclassification of the OBDD mesostructure as gyroid in the starblock samples[62] led some to wonder if OBDD was ever the stable morphology for block copolymer materials. As discussed earlier, several groups had reported the OBDD network in binary blends comprised of AB diblock copolymer and a constituent homopolymer.[66−68] Matsen theoretically interrogated this system in the weak segregation regime using SCFT and presented phase portraits for several ratios of homopolymer chain length to diblock chain length ($\alpha = N_{homo}/N_{AB}$).[81,82] The broad features of the phase diagrams could be understood by viewing the addition of homopolymer as equivalent to an increase in the volume fraction of the constituent block,[81,82] and the gyroid windows were comparable in size to those depicted in Figure 7 for the neat AB diblock copolymers.[76] Matsen did, however, predict that OBDD would be stable over very narrow ranges of composition for systems with certain values of α.[81,82] However, since these predicted OBDD windows were so narrow, Matsen believed that previous experimental studies[66−68] had actually produced gyroid and not OBDD. He implied that at least some[66] of these experimental materials had been re-examined and reclassified as gyroid.[81] Martínez-Veracoechea and Escobedo investigated blends of AB diblock and A homopolymer ($\alpha = 0.8$) using lattice Monte Carlo (MC) simulations and predicted that the OBDD network would be stable for some blend compositions,[83] a result in qualitative agreement with Matsen's SCFT calculations.[81,82] This MC analysis also suggested that blends can form the 6-fold-connected primitive phase with $Im3m$ symmetry known as plumber's nightmare[84] at certain compositions.[83] The stability of both the OBDD and plumber's nightmare network morphologies was attributed to a reduction in packing frustration (see next paragraph for a discussion of this term) that resulted when the relatively long homopolymer chains filled the center of the domains.[83] Martínez-Veracoechea and Escobedo subsequently employed MC, molecular dynamics (MD), and SCFT to extend the theoretical investigation of blends of AB diblock copolymers and the minority-block homopolymer ($\alpha = 0.8$) to the intermediate segregation regime ($25 \leq \chi N \leq 35$).[85] They found that OBDD represents the equilibrium state over a significant range of compositions ($\sim$0.05 in f_A) in these blends and predicted that plumber's nightmare, while metastable at all investigated compositions, may exist as a long-lived state in some experimental materials.[85] We are not aware of any reports that have confirmed these theoretical predictions by definitively identifying either the OBDD or plumber's nightmare network mesostructure in purely polymeric materials.

Matsen and Bates attempted to elucidate why gyroid is more stable than OBDD in nearly all block copolymer materials.[86,87] Thomas et al. had previously proposed that interfacial tension dominated block copolymer self-assembly, with the materials adopting constant mean curvature (CMC) mesostructures to minimize interfacial area.[65] Matsen and Bates used SCFT to demonstrate that a second factor, termed "packing frustration",[88] played an equally important role in block copolymer phase behavior.[86,87] Packing frustration is minimized when block copolymers adopt morphologies with uniform domain thicknesses because polymer chains do not have to excessively stretch (compress) to fill space. SCFT provided Matsen and Bates with a theoretical tool to investigate the relative importance of packing frustration. Unlike some other theoretical calculations,[71−74] SCFT does not require a priori assumptions about the shapes of domain interfaces. Rather, the chains in the unit cell of each mesostructural candidate adjust conformations (and thus the shape of the interface) to minimize free energy.[86,87] Matsen and Bates noted that while the classical LAM, HEX, and BCC mesostructures simultaneously minimize both interfacial area (with nearly CMC interfaces) and packing frustration (with nearly uniform domain thicknesses), the complex gyroid, OBDD, and perforated lamellar phases do not. If these latter structures were to have domain interfaces described by CMC surfaces, significant variations in domain thicknesses (i.e., high levels of packing frustration) would result. The actual free energy minimizing domain interfaces computed using SCFT deviated from these complex CMC surfaces to alleviate the packing frustration associated with nonuniform domain thicknesses. Matsen and Bates found that, of the complex mesostructural candidates, the gyroid had a calculated interfacial shape that varied the least from a CMC surface (i.e., it had the lowest standard deviation of the mean curvature distribution, as illustrated in Figure 8), and they therefore reasoned that packing frustration considerations stabilized gyroid relative to OBDD and perforated lamellae.[86,87] Additional support for this deduction came from SCFT calculations of AB diblock/A homopolymer blends.[81,82] These SCFT analyses predicted that the homopolymer that was added to the minority domains in the blend preferentially filled space in the center of the domains, relieving packing frustration and stabilizing OBDD because the minority blocks no longer had to excessively stretch to fill the centers of the domains.[86] Martínez-Veracoechea and Escobedo presented a similar rationale for OBDD stabilization in their recent investigations of AB diblock/A homopolymer blends.[83,85] Jinnai et al. directly measured the interfacial curvature distributions in gyroid-forming PS−PI−PS triblock copolymer materials using 3-D image reconstruction of TEM micrographs and verified the SCFT predictions[86,87] that gyroid mesostructures would not contain CMC interfaces.[89]

Gyroid: An Accepted Equilibrium Bicontinuous Morphology in Block Copolymer Systems. The gyroid morphology became widely accepted as an equilibrium block copolymer

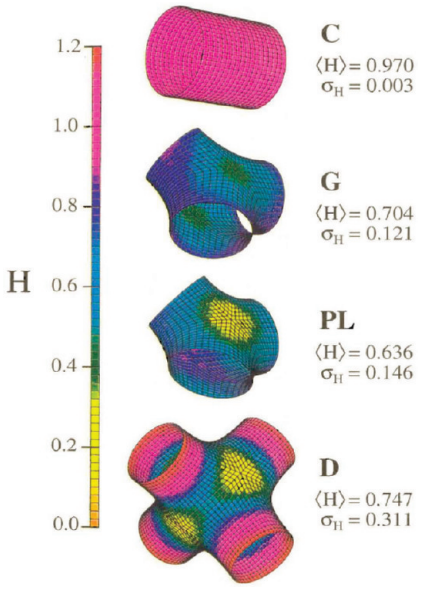

Figure 8. SCFT-calculated interfacial surfaces associated with the elementary units of the (C) HEX, (G) gyroid, (PL) perforated lamellar, and (D) OBDD morphologies for model AB diblock copolymers with $\chi N = 20$ and $f_A = 0.3378$ (i.e., at the HEX/gyroid phase boundary). The distribution of mean curvature H over the surface is indicated using the color scale, and the area-average $\langle H \rangle$ and standard deviation of H (σ_H) are provided. Note that the 3-fold connector of the gyroid is planar, while that of perforated lamellae is slightly nonplanar. Figure reproduced from ref 86.

mesostructure following the extensive experimental[45,46,62] and theoretical[76,79,80,86,87] publications described in the previous sections. The gyroid network has been reported in many AB diblock, AB starblock, and ABA triblock copolymer systems, including those listed in Table 1. A bevy of theoretical investigations have augmented these experimental reports and concluded that the bicontinuous gyroid is a stable block copolymer mesostructure.[12,76,79−83,85−87,90−99]

One aspect of the equilibrium nature of the gyroid morphology has only recently been resolved. Typically the gyroid has been identified in block copolymers with weak to intermediate segregation strengths ($\chi_{AB}N < \sim 40$),[11,45,46,101,128,131] although some groups[37,44,63,67,68] reported a bicontinuous mesostructure in strongly segregated block copolymer films prepared by solvent casting. It was uncertain whether the gyroid represented the equilibrium state in these strongly segregated materials[37,44,63,67,68] given the slow chain dynamics that are common in high molecular weight polymers. SST analyses predicted that gyroid is not an equilibrium structure,[149,150] and SCFT calculations were not performed for the gyroid phase when $\chi_{AB}N > \sim 40$ due to the prohibitively large number of basis functions (i.e., computational time) required to accurately evaluate the free energy of triply periodic network structures.[12,76,79] Matsen and Bates posited that increased packing frustration at higher segregation strengths would destabilize the gyroid in favor of LAM or HEX when $\chi_{AB}N > \sim 60$.[86,87] They suggested that the bicontinuous mesostructures reported in the slowly solvent cast strongly segregated block copolymers[37,44,63,67,68] were metastable.[12] Davidock and colleagues tested Matsen and Bates' hypothesis[12] by examining the phase behavior of difluorocarbene-modified PI−PEE diblock copolymers.[136,137] These samples, unlike the previously investigated[37,44,63,67,68] strongly segregated block copolymers, were designed to have relatively low molecular weights and thus relatively fast chain dynamics.[136,137] Davidock et al. reported that materials with $\chi_{AB}N$ as high as ~120 formed the gyroid, and two types of experiments provided evidence that this network was the equilibrium phase. First, the gyroid persisted following 4 weeks of melt-phase thermal annealing.[136] Second, metastable samples containing LAM or HEX were prepared by solvent casting from preferential solvents, and these specimens always transitioned to gyroid following thermal annealing.[137] While these reports provided convincing experimental evidence that the gyroid is an equilibrium morphology in the limit of strong segregation,[136,137] drawing such conclusions must be done with caution due to the difficulties associated with achieving thermodynamic equilibrium even in intermediately segregated experimental systems.[151] Cochran et al. used an improved SCFT methodology that overcame the numerical hurdles encountered by Matsen et al.[12,76] to theoretically re-examine the stability of the gyroid in the strong segregation regime.[13] They found that the gyroid had the lowest free energy over a narrow range of compositions ($\Delta f_A \approx 0.015$) for $\chi_{AB}N$ values up to 100. Theory[13] and experiment[37,44,63,67,68,136,137] are now in agreement that gyroid persists as an equilibrium morphology into the strong segregation regime and possibly[13] all the way to the $\chi_{AB}N = \infty$ limit. (Here we note that SST calculations, all of which involve some approximations, predict that gyroid is not an equilibrium mesostructure in this $\chi_{AB}N = \infty$ limit.[149,150])

Table 1. Block Copolymer Systems in Which the Gyroid (Q^{230}) Has Been Identified

block copolymer	reference(s)
starblock PS−PI	62, 100
PS−PI	11, 37, 45, 101−115
PS−P2VP	46, 116
PS−P4VP	117
PI−P2VP	108, 118
PEO−PBO	119, 120
PS−PDMS	121
PS−PLA	122
PS−PEO	122
PI−PEO	123−126
PI−PDMS	127
PEP−PEE	128, 129
PEP−PLA	130
PEP−PDMS	127, 131
PEE−PEO	129, 132−134
PEE−PE	128, 135
PE−PCHE	129
P4FS−PLA	22, 23
difluorocarbene-modified PI−PEE	136, 137
PSS−PMB	138
PFCDMS−PMMA	139
PS−PI−PS	15, 16, 89, 140−142
PI−PS−PI	141, 143
PS−PB−PS	144, 145, 253
PI−PPMDS−PI	146, 147
PS−PNIPAM−PS	148
PEO−PEE−PEO	129
PCHE−PE−PCHE	129

Gyroid Epitaxial Relationships. Epitaxial relationships between the gyroid and other phases were proposed in lyotropic liquid crystals[53] prior to the identification of the gyroid in block copolymer materials.[45,46] Schulz and colleagues were the first to discuss epitaxial relationships between the gyroid and other mesostructures in block copolymer materials.[46] They investigated shear-aligned HEX mesostructures that directly transformed to gyroid upon heating and identified epitaxial relationships between the HEX and gyroid morphologies using SANS data.[46] The correspondence between the (10) lattice plane in the HEX morphology and the $(1\bar{2}1)$ cubic plane controlled the orientation of the gyroid that was grown from the aligned HEX mesostructure.[101]

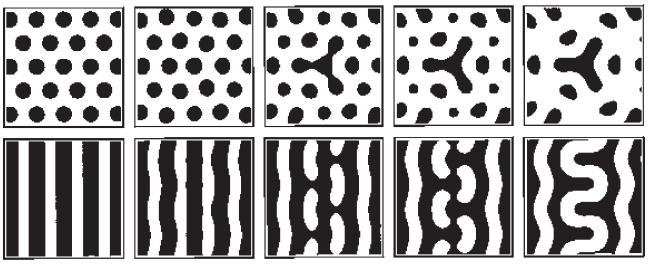

Figure 9. Calculated pathway for the evolution of HEX into the gyroid. Here black represents the minority A domain ($f_A = 0.35$). The horizontal axes are oriented in the [1$\bar{1}$0] direction, and the vertical axes are oriented in the [111] (bottom panel) and [11$\bar{2}$] (top panel) directions. Figure reproduced with permission from ref 152. Copyright 1998 American Physical Society.

A number of subsequent investigations have focused on the transition mechanisms and epitaxial relationships between gyroid and the LAM and HEX morphologies.[101,106,110,116,123,124,131,134,152−157] Förster et al. identified epitaxial relationships between the equilibrium gyroid and the metastable hexagonally perforated lamellar (HPL) mesostructure.[101] HPL may appear as an intermediate state during the ordering of gyroid from a disordered melt[111,155] or in morphological transitions between the gyroid and LAM morphologies[134] Matsen used SCFT to examine the Landau free energy surface of a diblock copolymer melt.[152] A low-energy pathway connecting the gyroid and HEX mesostructures was reported, and the calculated evolution between the two morphologies is provided in Figure 9. The computed energy barriers and stability limits implied that the HEX-to-gyroid morphological transition proceeds by a nucleation and growth mechanism,[152] a prediction validated by subsequent experiments.[124,131,153] Gyroid does not always grow directly from the HEX morphology, however; the HPL mesostructure may appear as an intermediate state during this morphological transition.[153,154]

Network Morphologies Formed by Multiblock Terpolymers

The phase behavior of AB diblock copolymers was generally understood by about 1995. Both experimentalists[11] and theoreticians[76] presented the equilibrium morphologies formed by block copolymers on a "universal" phase portrait with the composition (f_A) as the abscissa and the segregation strength ($\chi_{AB}N$) as the ordinate, and generally good agreement exists between theoretical predictions and experimental results. In contrast, no such "universal" understanding exists for linear ABC triblock terpolymers. (Note that "triblock" describes the number of blocks in the polymer chain while "terpolymer" indicates the material contains three chemically distinct repeat units.) There are more molecular variables in ABC triblock systems than in AB diblock materials, including two independent composition variables, three χ_{ij}'s (χ_{AB}, χ_{BC}, χ_{AC}), and three statistical segment lengths (b_A, b_B, b_C). This increased number of molecular variables results in more complex phase behavior, and more than 30 distinct mesostructures have been identified in the ABC triblock terpolymer literature.[158] Included among these triblock morphologies are a number of multiply continuous network mesostructures that are the focus of this section.

Ordered Tricontinuous Double Diamond (OTDD). Mogi and co-workers reported the first multiply continuous network structure in ABC triblock terpolymers in 1992.[159−161] They prepared a series of PI−PS−P2VP triblock terpolymers with narrow molecular weight distributions (PDI ≤ 1.05) and roughly equivalent PI and P2VP volume fractions, but different lengths of middle PS chains.[159] PI−PS−P2VP triblock terpolymers have roughly symmetric interfacial tensions and a large enthalpic incompatibility between the terminal blocks (i.e., $\chi_{IV} > \chi_{IS} \approx \chi_{SV}$);[162] Bailey et al. described block terpolymers with this block sequence as "nonfrustrated" because the most enthalpically incompatible blocks (i.e., those with the largest χ) are not required by chain connectivity to form domain interfaces.[163] We will use this "nonfrustrated" terminology in this review. Mogi et al. used TEM to interrogate the mesostructures of films of PI−PS−P2VP triblock terpolymers that were prepared by solvent casting and subsequent thermal annealing. The polymers containing PS volume fractions of 0.48 to 0.66 formed the same morphology, and representative TEM micrographs of this mesostructure are provided in Figure 10.[160] Mogi et al. suggested, on the basis of the agreement between the experimental and simulated micrographs provided in Figure 10, that this morphology was an ordered tricontinuous double diamond (OTDD) mesostructure.[160] The model of this postulated OTDD network is a three domain analogue of the OBDD morphology;[44,58,60,63] it consisted of cylindrical struts connected by 4-fold connectors and contained two chemically distinct interpenetrating networks ((6,4) nets), one comprised of PI and the other of P2VP, in a PS matrix.[160] Mogi et al. pointed out a flaw in their proposed OTDD model. Namely, a 55° rotation of the sample in the TEM experiments never resulted in the transition between the [111] and [001] projections that was predicted (for a 54.7° rotation) by the model.[160] Mogi et al.'s study is particularly notable because it established that multiply continuous network morphologies could persist over much broader ranges of compositions in ABC triblock terpolymers than they do in AB diblock copolymers. The network mesostructure formed in the PI−PS−P2VP materials over a range of ~0.18 in the PS volume fraction,[160] while

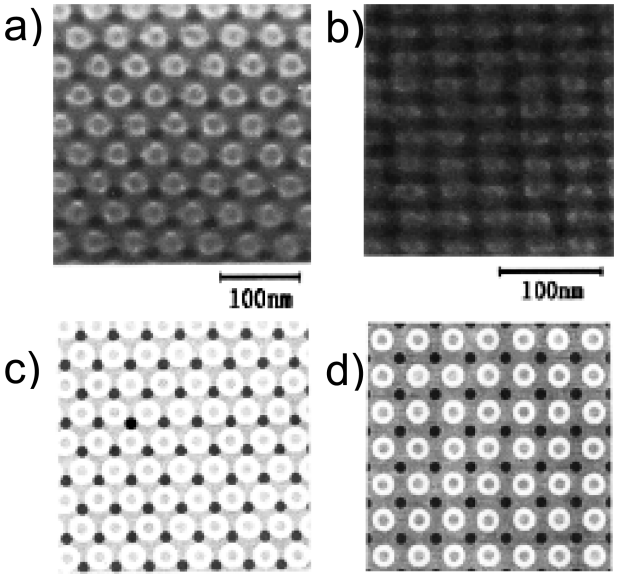

Figure 10. (a, b) Representative TEM micrographs obtained from PI−PS−P2VP triblocks with PS volume fractions ranging from 0.48 to 0.66. The polymer samples were stained with OsO_4, and the black, white, and gray images correspond to domains rich in PI, PS, and P2VP, respectively. Mogi et al. suggested that these images were consistent with the (a) [111] and (b) [001] projections of an ordered tricontinuous double diamond (OTDD) network containing independent interpenetrating domains of PI and P2VP in a PS matrix. (c, d) Simulated TEM images corresponding to the (c) [111] and (d) [001] projections. These simulated micrographs were obtained using a model comprised of cylindrical struts and 4-fold connectors. Images reproduced from ref 160.

the gyroid only occurs over a volume fraction range of ~0.04 in AB diblock copolymers.[11]

Revisiting OTDD and the Alternating Gyroid (Q^{214}). Mogi et al.'s series of publications[159−161] catalyzed many investigations of multiply continuous network morphologies in block terpolymers. Several theoretical studies directly built upon Mogi et al.'s work and focused on "symmetric" (i.e., equal volumes of A and C domains) ABC triblock terpolymers.[162,164−166] Both Matsen[162] and Phan and Fredrickson[164] suggested that, given the initial misidentification of the gyroid as OBDD in block copolymer systems,[62] the OTDD should be accepted as an equilibrium morphology with caution.[162,164] Phan and Fredrickson extended the theoretical approaches of Likhtman and Semenov[72] and Milner et al.[73,74,167] from AB diblocks to ABC triblocks and investigated "symmetric" ABC triblock terpolymers in the SSL.[164] Two network morphologies were considered in this study: OTDD and an alternating gyroid with $I4_132$ symmetry that can be represented by (10,3) nets (herein called Q^{214}, with "214" being the number of the space group[64]). While both mesostructures contain two chemically distinct, interpenetrating lattices, the local structures of the connecting elements are different, with OTDD characterized by 4-fold-connected nets while Q^{214} is represented by 3-fold-connected nets. Phan and Fredrickson constructed approximate representations of the OTDD and Q^{214} domain interfaces and computed the free energies of these networks and a number of other mesostructural candidates.[164] The equilibrium morphology was predicted to change from BCC to tetragonally packed cylinders to LAM as the combined volume fraction of the terminal A and C blocks was increased from 0 to 0.4. While Q^{214} always had a lower computed free energy than OTDD, neither of these networks was predicted to be the equilibrium mesostructure for any of the investigated compositions. Phan and Fredrickson suggested Q^{214} could become stable for intermediate segregation strengths, and since it was always stable relative to OTDD in their calculations, they suggested Mogi et al.'s assignment[159−161] of OTDD should be revisited, with Q^{214} being considered as an alternative.[164]

Dotera and Hatano developed a diagonal bond method based on the Verdier−Stockmayer model[168] to perform MC simulations on block copolymer melts.[165,166] This method has the benefit of not requiring the selection of mesostructural candidates (i.e., simulations progressed from a random initial configuration), although it does rely on the selection of unit cell dimensions, and metastable structures may be wrongly identified as equilibrium morphologies when the simulation box sizes are not commensurate with equilibrium mesostructural lattice parameters. A series of "symmetric" ABC triblock terpolymers encompassing the OTDD window reported by Mogi et al.[159] were "annealed" in the MC simulations from random initial configurations.[165,166] A twice-periodic strategy was utilized to minimize metastability effects related to the simulation box size, and Q^{214}, and not OTDD, was predicted to be the equilibrium morphology over the composition range $0.14 < f_A < 0.23$.[166] Dotera also examined blends containing ABC triblocks and constituent A and C homopolymers and predicted that these materials form, in addition to Q^{214}, the 4-fold-connected OTDD and a 6-fold-connected plumber's nightmare at certain compositions.[166] We are not aware of any experimental reports that have validated this prediction.

Matsen used a spectral implementation of SCFT to interrogate the phase behavior of "symmetric" ($b_A = b_B = b_C$, $\chi_{AB} = \chi_{BC} = \chi$, and $f_A = f_C$) ABC triblock terpolymers in the intermediate segregation regime ($\chi N < 65$).[162] These ABC triblocks can be characterized by three parameters: the volume fraction of one of the terminal blocks (f), χN, and χ_{AC}/χ.[162] Matsen determined that, for compositions with $f \leq 0.3$, the morphology selection is not sensitive to either the χ_{AC}/χ ratio or χN, and the equilibrium mesostructure was largely selected based on the composition of the triblock terpolymer. Pseudo-BCC spheres with alternating A and C spheres (i.e., the A and C domains are packed in a CsCl structure with $Pm\bar{3}m$ symmetry), hexagonally and tetragonally packed cylinders, Q^{214}, OTDD, and LAM were considered as mesostructural candidates in the SCFT calculations. The sequence of equilibrium morphologies was predicted to be pseudo-BCC spheres → tetragonally packed cylinders → Q^{214} (for $0.145 \leq f \leq 0.198$ when $\chi N = 50$) → LAM with increasing f. Matsen noted that this sequence was analogous to that predicted in AB diblock copolymers (see Figure 7), with tetragonally packed cylinders replacing HEX due to packing frustration. This packing frustration also reduces the width of the cylinder window and, consequently, widens the network window in ABC triblocks relative to AB diblocks.[162]

OTDD, like OBDD in diblock copolymers, never had the lowest SCFT-computed free energy in these single-component model ABC triblock systems.[162] Matsen posited that a minimization of packing frustration drives ABC triblock terpolymers to form Q^{214}, and not OTDD, much like it drives ABA triblock copolymers to adopt the gyroid with $Ia\bar{3}d$ symmetry,[140,141] and not OBDD.[162] The SCFT predictions were in excellent agreement with Dotera's MC simulations[166] and contained many of the same features as Phan and Fredrickson's SST results.[164] Approximations in the SST involving chain trajectories and the shape of internal interfaces[164] may account for the fact that SCFT[162] and MC simulations[166] identified Q^{214} as an equilibrium structure, but SST[164] did not.[162] Matsen also re-examined some of Mogi et al.'s experimental data[160] obtained from the network-forming PI−PS−P2VP materials. He argued in detail that the simulated Q^{214} projections more closely matched the experimental micrographs than the simulated OTDD images did. Notably, a simulated tilt of the Q^{214} unit cell yielded projections that qualitatively resembled the micrographs obtained by tilting the PI−PS−P2VP specimen while a simulated tilt of the OTDD unit cell did not.[162]

Matsushita et al., independent of Matsen,[162] reconsidered the OTDD assignment in the PI−PS−P2VP triblock terpolymer system.[169−172] They generated model unit cells in which the domain interfaces were parallel surfaces to either the gyroid or diamond minimal surface. These constructions illustrated how blocks could fill space with a given space group symmetry but, unlike SCFT results, did not have any connection to the statistical mechanics of the individual chains. Matsushita et al. used these space-filling models to simulate the TEM projections that would be obtained from samples with varying thicknesses. When film thickness was considered, the simulated images from the Q^{214} model matched the experimental TEM micrographs acquired from three PI−PS−P2VP specimens ($f_I = f_V = 0.26$,[169−171] $f_I = 0.20$, $f_V = 0.14$,[171] and $f_I = 0.22$, $f_V = 0.19$[172]) much better than did the predicted OTDD projections, as is illustrated in Figure 11. Matsushita and colleagues also utilized the space-filling models to predict the intensities of SAXS peaks from the Q^{214} morphology.[170−172] The predicted intensities of the allowed reflections qualitatively agreed with experimental data obtained at the three different compositions ($f_I = f_V = 0.26$,[170,171] $f_I = 0.20$, $f_V = 0.14$,[171] and $f_I = 0.22$, $f_V = 0.19$[172]), corroborating the TEM analysis and further supporting the change in the assignment of the tricontinuous mesostructure from OTDD to Q^{214}.[170−172]

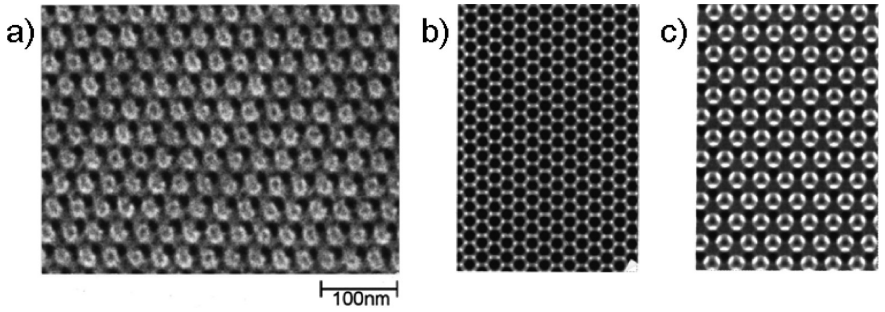

Figure 11. (a) TEM micrograph obtained from an 80 nm thick section of a PI−PS−P2VP triblock terpolymer with M_n = 64 kg/mol, f_I = 0.22, and f_V = 0.19. (b, c) Simulated TEM projections of an 80 nm thick slice of a model PI−PS−P2VP material forming (b) OTDD and (c) Q^{214}. The Q^{214} simulation (c) more closely resembles the experimental micrograph (a) than does the OTDD image (b). Images reproduced with permission from ref 172. Copyright 2000 American Institute of Physics.

The OTDD network was also reported in a PS−PI−P2VP triblock terpolymer sample.[173] The mesostuctural assignment of OTDD in the PS−PI−P2VP system was made based upon general agreement between simulated TEM images and experimental micrographs.[173] This PS−PI−P2VP specimen is similar to the network-forming PI−PS−P2VP samples[159,160] in terms of the compositions of the middle and terminal blocks, but as pointed out by Matsen,[162] the PS−PI−P2VP block sequencing does not yield symmetry in the A/B and B/C interfacial tensions. Matsen questioned the OTDD assignment and suggested that no indication of minority domain continuity was present in the reported[173] experimental TEM micrographs. He speculated, based on Zheng and Wang's theoretical investigation[174] of triblock terpolymers with asymmetric interfacial tensions, that the reported OTDD morphology in the PS−PI−P2VP specimen[173] was in fact a pseudo-BCC sphere (CsCl packing) mesostructure.[162] Matsen argued that simulated TEM images obtained from a pseudo-BCC sphere unit cell[162] were consistent with the experimental micrographs attributed[173] to the OTDD mesostructure. To our knowledge, this OTDD assignment has not been revisited experimentally. Given the reclassification of the OTDD network in PI−PS−P2VP triblocks,[169−172] the reported identification[173] of OTDD in the PS−PI−P2VP sample should be accepted with caution.

The reassignment of the tricontinuous morphology formed by PI−PS−P2VP triblock terpolymers from OTDD to Q^{214} in many ways paralleled the change in the accepted identity of the bicontinuous network structure commonly formed by block copolymers from OBDD to gyroid. The initial OBDD[44,63] and OTDD[160] assignments were both made primarily using TEM micrographs and did not include definitive scattering data or theoretical support for the identification of the diamond mesostructures. While TEM is a very powerful and useful characterization technique, interpreting the two-dimensional projections of an inherently 3-D structure can be difficult.[45] In both the OBDD and OTDD cases, scattering (either X-ray or neutron) data[45,46,170,171] and SCFT calculations[76,162] were crucial corroborative elements used to correctly interpret the experimental data and identify the gyroid (Q^{230}, $Ia\bar{3}d$ symmetry) and Q^{214} ($I4_132$ symmetry) morphologies.

Several investigations of Q^{214} followed Matsushita et al.'s definitive identification[169−172] of Q^{214} in the PI−PS−P2VP materials. Suzuki and co-workers focused on the mechanism driving the Q^{214} morphology to preferentially orient with [110] normal to the film surface in solvent cast films of PI−PS−P2VP.[175] A PI−PS−P2VP triblock sample (f_I = f_V = 0.26) was solvent cast from THF and the morphology of the polymer film was probed using a combination of TEM and synchrotron SAXS following various lengths of thermal annealing times at 150 °C. The as-cast PI−PS−P2VP specimen contained a lamellar mesostructure oriented with [001] normal to the film surface. Subsequent annealing at 150 °C drove a morphological transition, over a period of 2 days, to a Q^{214} network that was, according to the analysis of two-dimensional SAXS data, oriented with the [110] normal to the film surface. Suzuki et al. suggested that the metastable lamellar morphology formed with [001] normal to the film surface as a result of the affinity between the P2VP block and the Teflon substrate on which the film was cast. The subsequent thermal annealing yielded a stable Q^{214} morphology with [110] oriented normal to the surface due to the epitaxial relationship between the [001] of lamellae and the [110] of Q^{214}. Generally a strategy of preparing films of aligned metastable morphologies followed by thermal annealing could prove useful in the preparation of polymer films containing stable oriented network mesostructures.[175]

Epps and Cochran et al. investigated PI−PS−PEO triblock terpolymers over a wide range of compositions.[176,177] PI−PS−PEO triblock terpolymers, like PI−PS−P2VP samples,[162] have symmetric interfacial tensions and are "non-frustrated" (i.e., $\chi_{IO} > \chi_{IS} \approx \chi_{SO}$).[178] The melt-phase morphologies of PI−PS−PEO materials were probed using a combination of synchrotron SAXS, TEM, dynamic mechanical spectroscopy (DMS), and static birefringence. This thorough characterization process identified Q^{214} in seven samples along two different isopleths: (i) f_I/f_S = 0.64, 0.14 < f_O < 0.18 and (ii) f_I/f_S = 0.45, 0.17 < f_O < 0.29.[176,177] This Q^{214} composition window is broadly consistent with Matsen's calculations[162] and Matsushita et al.'s PI−PS−P2VP investigations,[159−161,169−172] although Q^{214} is stable in more asymmetric materials in the PI−PS−PEO system than in the PI−PS−P2VP materials, possibly due to differences in the statistical segment lengths of the PEO and P2VP chains.[176,177] The PI−PS−PEO system will be discussed in more detail later in this review.

Core−Shell Gyroid (Q^{230}). Q^{214} topologically resembles the gyroid morphology identified in AB block copolymers in that it contains two independent, interpenetrating domains embedded in a matrix. However, these two morphologies are characterized by different space groups for two possible reasons: the two independent domains are chemically distinct and/or may have different volume fractions in Q^{214} ($I4_132$) while they are chemically identical and have identical volume fractions in the gyroid ($Ia\bar{3}d$). One could envision that a block terpolymer could also form a core−shell version of the gyroid structure with $Ia\bar{3}d$ symmetry, with two chemically identical interpenetrating networks that are comprised of cores of C encased in shells of B and embedded in a

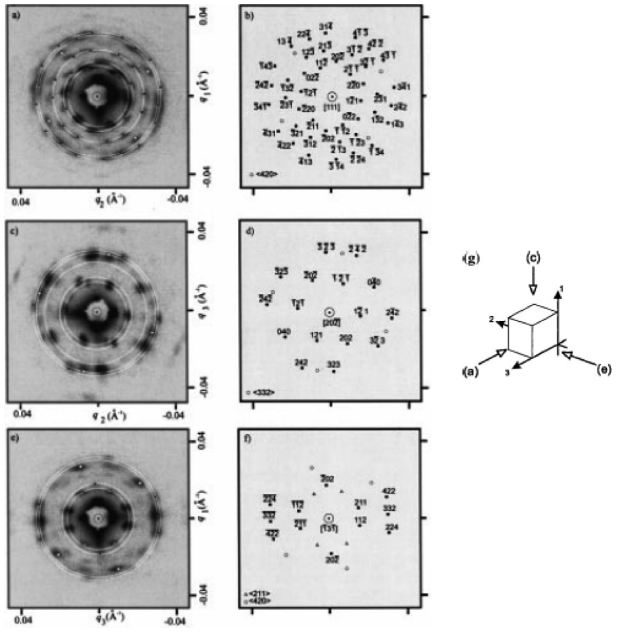

Figure 12. SAXS diffraction patterns obtained from a sheared sample of PI−PS−PDMS. SAXS data (a, c, e) are presented next to the indexing scheme (b, d, f) for each orientation. All peaks are indexed to Q^{230}. The black squares mark the expected peak positions in a "single-crystal" pattern while the open circles and triangles connote out-of-plane reflections that are consistent with twinning (i.e., the sample contains multiple grains of Q^{230} oriented in different directions). (g) Schematic illustrating the orientations at which the SAXS data were obtained. Reproduced from ref 18.

matrix of A blocks. Core−shell versions of the HEX and BCC morphologies had been reported in other terpolymer systems,[158] and there was no reason an analogous core−shell gyroid mesostructure would not form. Two independent groups simultaneously identified the core−shell gyroid (Q^{230}) morphology with $Ia\bar{3}d$ symmetry in block terpolymer systems in 1999.[18,179]

Shefelbine et al. synthesized a PI−PS−PDMS triblock terpolymer ($f_I = 0.40$, $f_S = 0.41$) and interrogated its melt-phase morphology using a combination of SAXS, SANS, TEM, and static birefringence.[18] PI−PS−PDMS triblocks are "frustrated",[163] as the PS and PDMS blocks have the largest χ parameter ($\chi_{SD} = 0.12$, $\chi_{ID} = 0.09$, and $\chi_{IS} = 0.033$ at 150 °C)[18] and are required by chain connectivity to form an interface. The PI−PS−PDMS polymer powder was heated to 200 °C and subjected to large-amplitude oscillatory shear to reduce mesostructural defects and facilitate the formation of large grains. Both the sheared sample and unsheared powder were nonbirefringent, an indication that the morphology formed by the PI−PS−PDMS triblock had cubic symmetry. X-rays were passed, at ambient temperature, through the sheared material in all three directions orthogonal to the sample surfaces (see schematic in Figure 12). Discrete spots, and not continuous rings, were present in these Bragg patterns, indicating relatively large mesostructural grains were present in the sheared PI−PS−PDMS specimen. These 2-D SAXS data are provided in Figure 12. Shefelbine et al. considered all of the cubic space groups as candidates when fitting these data. Space groups with *F* symmetry were eliminated from consideration because those groups do not allow the 211 reflections present in the data in Figure 12, while all space groups with *P* symmetry and most with *I* symmetry were ruled out because a large number of reflections consistent with the space groups were not present in the SAXS data. Shefelbine et al. reported that, while both the radial positions and relative angular positions of all of these reflections are consistent with a Q^{230} mesostructure, a morphology with $I\bar{4}3d$ symmetry could not be ruled out solely on the basis of scattering data.[18]

TEM was used to examine how the PI−PS−PDMS microdomains filled space and to try to distinguish between the two possible space group symmetries.[18] Micrographs consistent with a Q^{230} mesostructure were acquired from PI−PS−PDMS samples in both the native state and following staining with OsO_4. Shefelbine et al. did not yet rule out a mesostructure with $I\bar{4}3d$ symmetry, however,[18] given the difficulties associated with interpretation of TEM images from multiply continuous morphologies.[45] Rather, they supplemented their experimental analysis with SCFT calculations. The segment distributions for a Q^{230} network were computed and used to predict the intensities of SAXS and SANS peaks. The predicted scattering intensities generally matched the experimental SAXS and SANS data, and the predictions even captured the extinctions of the first two peaks in the SANS data.[18] The computed segment distributions were also used to simulate the projections expected in TEM experiments. Excellent agreement was found between predicted projections and experimental micrographs for both the unstained and stained materials. Shefelbine et al. concluded, on the basis of all of these results, that the PI−PS−PDMS triblock terpolymer had formed a pentacontinuous Q^{230} morphology with two discrete domains of PDMS cores, two separate domains of PS shells, and a PI matrix. They noted that this mesostructure made intuitive physical sense, as the area of the enthalpically costly PS/PDMS interface was smaller than that of the less costly PI/PS interface because the PDMS occupied the cores of the interpenetrating networks. It was intimated that the Q^{230} network persisted over a relatively narrow range of compositions in the PI−PS−PDMS system.[18]

At approximately the same time that Shefelbine et al.'s paper[18] appeared, Goldacker and Abetz detailed a morphological investigation of binary blends of PS−PB−PtBMA triblock terpolymers ($f_S = 0.33$, $f_B = 0.37$) and PB−PtBMA diblock copolymers ($f_B = 0.58$).[179] While these ABC/BC blends were initially targeted to produce noncentrosymmetric lamellae,[180] Goldacker and Abetz reported that PS−PB−PtBMA/PB−PtBMA blends with a PB−PtBMA volume fraction of 0.22 predominantly formed a Q^{230} morphology.[179] This network assignment was made by comparing TEM micrographs to simulated [110] and [112] projections of a Q^{230} mesostructure comprised of two interpenetrating networks of PS that are encased in shells of PB and embedded in a matrix of PtBMA. Notably the microtomed slices used in the TEM analysis had a thickness less than that of a single Q^{230} unit cell. As a result, the experimental micrographs contained, due to variations in the film thicknesses, a near-continuum of images that represented the same projection viewed through different fractions of the Q^{230} unit cell.[179] This experimental feature allowed for a more definitive morphology assignment than is typical of TEM analyses.[169] Goldacker and Abetz hypothesized that the increase in PB/PtBMA junction points resulting from the addition of the PB−PtBMA diblock to the PS−PB−PtBMA triblock increased the chain crowding at the PB/PtBMA interface and drove a morphological transition from lamellae to Q^{230}.[179]

Many reports[163,176,177,181−186] of the pentacontinuous Q^{230} morphology followed the two initial publications[18,179] identifying the network mesostructure. Hückstädt and co-workers investigated the melt-phase morphologies of linear PS−PB−P2VP triblock and heteroarm PS−PB−P2VP starblock

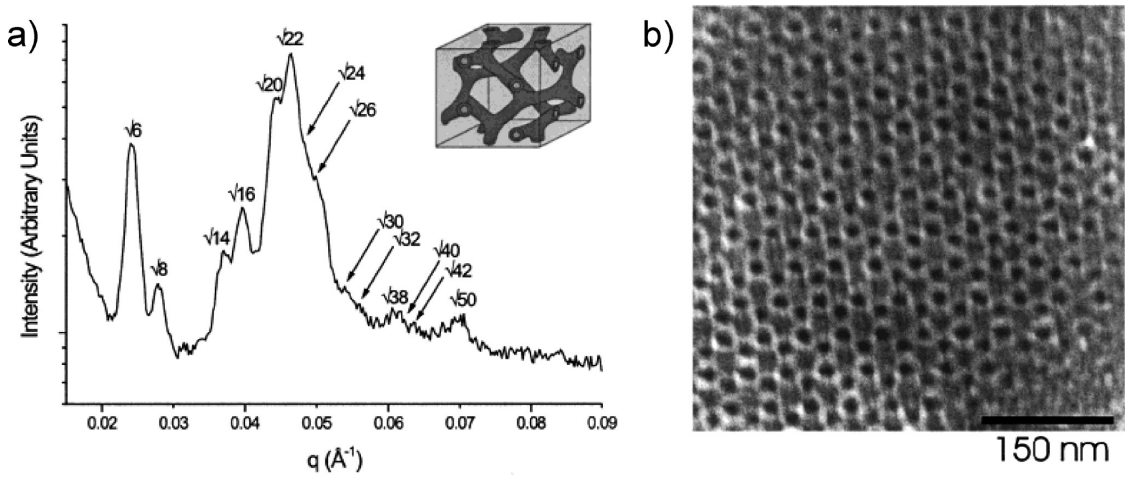

Figure 13. Data acquired from a PS−PI−PEO sample with $f_O = 0.21$. (a) SAXS data obtained at 180 °C. The first 14 reflections allowed for Q^{230} are marked. (b) TEM micrograph corresponding to the [111] projection of Q^{230}. Figure reproduced from ref 163.

terpolymers using TEM.[181] The linear PS−PB−P2VP sample (PS wt % = 0.48, PB wt % = 0.31), like Shefelbine et al.'s PI−PS−PDMS material,[18] is frustrated ($\chi_{BV} > \chi_{BS} \approx \chi_{SV}$) and has a terminal block that comprises ~20% of the volume of the polymer.[181] Analysis of the experimental and simulated TEM micrographs led to the identification of a Q^{230} network containing P2VP cores, PB shells, and a PS matrix in the linear PS−PB−P2VP specimen. Hückstädt et al. suggested that Q^{230} was restricted to a narrow range of compositions in these linear triblock terpolymer materials. The PS−PB−P2VP starblock sample (PS wt % = 0.14, PB wt % = 0.37), unlike the linear PS−PB−P2VP triblock, contained multiple morphologies. Hückstädt et al. compared experimental TEM micrographs obtained from samples that contained various fractions of a unit cell (i.e., slices of continuously varying thicknesses) with simulated projections through various fractions of a unit cell and concluded that a minority of the PS−PB−P2VP starblock sample contained a Q^{230} network. The "shell" in this starblock Q^{230} morphology must, as a result of chain connectivity, be a mixed domain. Notably, the interpenetrating networks in this Q^{230} morphology were largely comprised of P2VP and had a volume fraction (>0.45) larger than is typically obtained in gyroid mesostructures formed by materials with linear architectures. Hückstädt et al. offered several hypotheses to account for this feature of Q^{230} in the starblock sample.[181]

Bailey et al. investigated the melt-phase morphological behavior of frustrated PS−PI−PEO triblock terpolymers ($\chi_{IO} > \chi_{IS} \approx \chi_{SO}$).[163] Ten neat PS−PI−PEO triblock samples with $0.03 < f_O < 0.33$ were synthesized from a parent PS−PI−OH diblock with $f_I \approx f_S$. In addition, 13 PS−PI−PEO specimens with intermediate compositions were prepared by blending consecutive pairs (to minimize polydispersity effects) of neat PS−PI−PEO triblocks. The mesostructures of these 23 intermediate and weakly segregated materials were probed using a combination of rheological measurements, SAXS, and TEM. This complement of experimental data allowed Bailey et al. to identify pentacontinuous Q^{230} in four PS−PI−PEO samples (a neat triblock and three blends) with $0.19 < f_O < 0.23$; representative SAXS and TEM data are provided in Figure 13.[163] The range of compositions over which Q^{230} forms in the PS−PI−PEO samples includes the composition of the Q^{230}-forming PI−PS−PDMS material reported by Shefelbine et al.;[18] these two frustrated ABC systems have a comparable sequence of χ parameters ($\chi_{BC} > \chi_{AB} \approx \chi_{AC}$).[163] All of the Q^{230}-forming PS−PI−PEO materials underwent an OOT from Q^{230} to core−shell cylinders upon heating. While this transition was reversible, the formation of Q^{230} upon cooling exhibited significant hysteresis. Bailey et al. investigated the hysteresis at a variety of cooling/quenching rates and reported a complex kinetic rate dependence, with some PS−PI−PEO materials requiring more than 12 h of thermal annealing to reach the (presumably) equilibrium Q^{230} morphology. The core−shell cylinder-to-Q^{230} transition likely occurred through a rearrangement process that resulted in the formation of a metastable semiperforated lamellar intermediate.[163]

Sugiyama and colleagues studied a variation of the triblock terpolymer system investigated by Shefelbine et al.;[18] the materials contained the same PI, PS, and PDMS components, but the block architecture was changed from the frustrated PI−PS−PDMS sequence to the nonfrustrated PS−PI−PDMS arrangement.[182] Sugiyama et al. synthesized a PS−PI−PDMS triblock terpolymer (M_n = 42 kg/mol, $f_S = 0.20$, $f_I = 0.59$) and subsequently solution blended it in toluene with various equal volume fractions of PS ($M_n = 2.4$ kg/mol) and PDMS (M_n = 2.2 kg/mol) homopolymers. SAXS, SANS, and TEM measurements were used to interrogate the morphologies of the samples. Sugiyama et al. reported that the neat PS−PI−PDMS triblock specimen formed a complex mesostructure, but they were unable to ascertain its exact state of order;[182] Epps and Cochran et al. later suggested this morphology was actually O^{70} (see next section for a description of this multiply continuous network mesostructure).[177] Q^{230} was identified in PS−PI−PDMS blends containing an overall homopolymer volume fraction ranging from 0.15 to 0.45 ($0.25 < f_S (f_D) < 0.34$). Sugiyama et al. suggested that the slight asymmetry in χ parameters ($\chi_{SI} < \chi_{ID}$) led to the formation of core−shell morphologies (Q^{230} and core−shell cylinders) in the PS−PI−PDMS system.[182] Hardy et al. expanded upon this work by investigating a variety of weakly segregated triblock terpolymer materials with segment volume fractions near 0.33, including frustrated PI−PS−PDMS triblocks, nonfrustrated PS−PI−PDMS triblocks, and blends of PI−PS−PDMS and PS−PI−PDMS triblock terpolymers with varying intermediate amounts of frustration.[183] The morphologies of these materials were characterized using a combination of DMS, SAXS, and SANS measurements. While the neat triblock samples adopted cylindrical or LAM morphologies, several blends with intermediate levels of frustration adopted

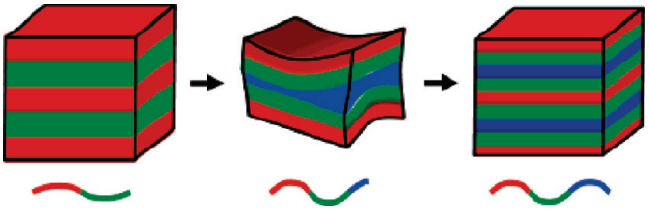

Figure 14. A cartoon illustration of Bailey et al.'s strategy for inducing network formation in nonfrustrated ABC triblock terpolymers with symmetric interfacial tensions. The left and right structures depict the flat interfaces preferred by samples with symmetric compositions. The middle polymer contains an intermediate length of the terminal C chains. It was hypothesized that this intermediate chain length would destabilize the flat interfaces, leading to saddle surfaces and network morphologies. Reproduced from ref 177.

a Q^{230} mesostructure, as evidenced by SAXS reflections with a relative spacing of $\sqrt{6}q^*$ to $\sqrt{8}q^*$ and an intensity ratio of 10:1.[183] (The Q^{230} structure has been determined to yield Bragg diffraction with scattering amplitudes that have a ratio of intensities from 211 to 220 powder pattern reflections of approximately 10 to 1, in all types of block polymers and aqueous mixtures of lipids, soaps and surfactants.[18,45,51,177]) Hardy et al. noted that the composition near the PDMS interface (i.e., a thin "shell") must, due to chain connectivity, depend on the relative amounts of the PI−PS−PDMS and PS−PI−PDMS chains in the blend. It was hypothesized that changing this interfacial composition altered the interfacial tension and drove the morphological transitions from cylinders or LAM to the Q^{230} mesostructure. These results demonstrated that frustration effects can be used to manipulate the state of order of triblock terpolymer materials with the same overall chemical composition and molecular weight.[183]

Epps and Cochran et al. identified Q^{230} during their investigation of the nonfrustrated PI−PS−PEO system.[176,177] Definitive SAXS data, complemented by TEM, DMS, and static birefringence measurements, led to the identification of Q^{230} in six samples along two different isopleths: (i) $f_I/f_S = 1.38$, $0.14 < f_O < 0.20$ and (ii) $f_I/f_S = 1.27$, $0.11 < f_O < 0.20$.[176,177] Chatterjee et al. expanded the investigation of the PI−PS−PEO system to PEO-rich specimens and identified Q^{230} in six PEO-rich samples.[184] The PI−PS−PEO system will be discussed in more detail in the following sections.

The pentacontinuous Q^{230} with the familiar $Ia\bar{3}d$ space group symmetry has been reported in both frustrated[18,163,181] and nonfrustrated[176,177,179,182,184−186] triblock terpolymer systems. In addition, the Q^{230} mesostructure was reported in blends containing both frustrated PI−PS−PDMS and nonfrustrated PS−PI−PDMS components.[183] Clearly, many block copolymer and block terpolymer materials can minimize the overall system free energy by forming a structure with $Ia\bar{3}d$ symmetry. This fact renders the gyroid something of a universal network mesostructure, albeit one whose precise phase boundaries are sensitive to the block sequence, χ values, and block statistical segment lengths.

O^{70}, the Orthorhombic *Fddd* Network. The previous two sections demonstrated that a number of groups[18,159−161,163,169−172,179,181−183] had, by 2002, identified multiply continuous network morphologies in a host of block terpolymer systems. The associated publications did not, however, establish a systematic framework for preparing network-forming materials.[187] Bailey sought such an approach and began by noting that symmetric diblock copolymers form LAM with flat interfaces. He surmised that an ABC triblock with equivalent block volume fractions (prepared by adding a similarly sized third block to a symmetric AB diblock) and roughly symmetric interfacial tensions ($\chi_{AB} \approx \chi_{BC}$) would form a LAM morphology with two flat interfaces (A/B and B/C), provided there was no thermodynamic driving force for the formation of an A/C interface (i.e., provided $\chi_{AC} \gg \chi_{AB}, \chi_{BC}$). He suggested that ABC triblocks with intermediate, asymmetric compositions would have packing frustrations that would best be accommodated by the hyperbolic interfacial surfaces (i.e., saddle surfaces) of network morphologies.[187] A cartoon illustrating this concept is provided in Figure 14.

Bailey and colleagues selected PI−PS−PEO triblock terpolymers as the model system to test this hypothesis.[188] This system was chosen for several reasons. First, PI−PS−PEO triblock terpolymers are nonfrustrated ($\chi_{IO} > \chi_{IS} \approx \chi_{SO}$), and formation of PI/PEO interfaces is enthalpically unfavorable. Thus, only the PI/PS and PS/PEO interfaces required by chain connectivity should form, and Bailey et al. hoped to use these competing interfaces to drive network formation. Second, the magnitudes of the χ parameters placed the order−disorder transition temperatures (T_{ODT}'s) at experimentally feasible temperatures when the molecular weight ranged from approximately 15 to 25 kg/mol. These chain lengths were convenient for experimental characterization while also being long enough to permit comparison with SCFT. Finally, the PI−PS−PEO system was synthetically tractable, as many PI−PS−PEO triblock samples could be prepared from a single parent PI−PS−OH diblock. This synthetic methodology minimized variation across triblock specimens, with only the length of the PEO blocks being altered. Thirteen PI−PS−PEO samples with $0 < f_O < 0.34$ were synthesized from a parent PI−PS−OH diblock (M_n = 13.6 kg/mol, $f_I \approx f_S$).[188] The melt-phase morphologies of these materials were probed using DMS, SAXS, TEM, static birefringence, and differential scanning calorimetry (DSC). As expected, lamellar mesostructures were reported for samples in two different regimes: (i) short terminal PEO chains ($f_O < 0.10$) or (ii) approximately equal volume fractions in each of the three domains ($0.27 < f_O < 0.34$). Bailey et al. classified the mesostructures formed by the low PEO-content materials as two-domain lamellae (LAM_2), as the short PEO chains mixed with the segments in the PS domain. The morphologies adopted by the PEO-rich materials were called three-domain lamellae (LAM_3), as striped domains rich in each of the three components were identified.[188]

Characterization data inconsistent with LAM mesostructures were acquired from six samples with intermediate compositions ($0.13 < f_O < 0.24$). The nonlamellar symmetry of this mesostructure is readily apparent upon inspection of the TEM micrographs provided in Figure 15. Bailey et al. reported that both of these images were frequently observed during their TEM analysis and concluded that these micrographs represent different directional orientations of the same structural element.[188] These micrographs resemble those acquired from gyroid-forming materials but do not contain any regions with true 3-fold or 4-fold symmetries.[177] Additionally, lab-source SAXS data were not consistent with either Q^{230} or Q^{214}.[188]

Bailey et al. utilized a systematic approach to elucidate the symmetry of this unknown mesostructure. DSC measurements were employed to probe the percent crystallinity of the PEO block. The crystallinity was negligible for short PEO chains, which Bailey et al. attributed to mixing of the PEO and PS chains. The fractional crystallinity sharply increased to ~0.5 as f_O changed from 0.10 to 0.13 and remained roughly constant as f_O was further increased to 0.34. Bailey et al. suggested the increase in crystallinity corresponded to the formation of relatively pure PEO domains.[188] Rheological measurements were used to probe the viscoelastic

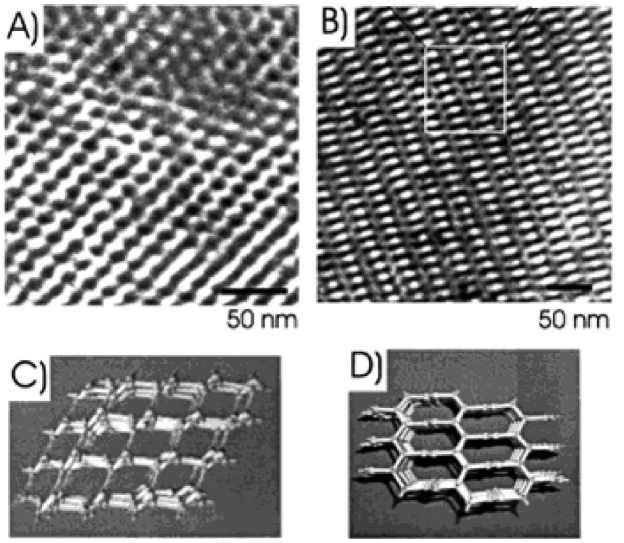

Figure 15. (A, B) Representative TEM images of the two predominate projections obtained by Bailey et al. from a PI−PS−PEO specimen with $f_O = 0.18$. The black regions correspond to OsO_4-stained PI while the white areas represent unstained PS and/or PEO domains (C, D) Two orientations of a lattice model of the O^{70} network morphology. The open channels in this model correspond to the black (PI) regions of the TEM micrographs, while the model struts represent the white (PS and PEO) portions of the images. Figure reproduced from ref 188.

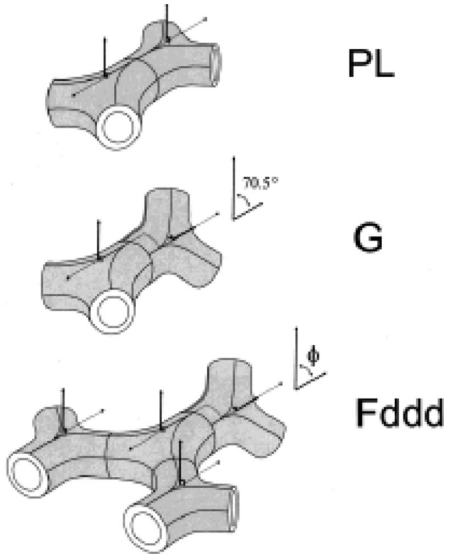

Figure 16. Local configurations of 3-fold connectors in the perforated lamellar (PL), gyroid (G), and O^{70} (*Fddd*) morphologies. The O^{70} lattice was constructed using two parts PL and one part G (with some distortion in Φ). Reproduced from ref 188.

response of the materials. The unknown mesostructure was highly elastic, with a nearly frequency-independent elastic modulus (G') that was orders of magnitude larger than the loss modulus (G'').[188] This viscoelastic pattern was known to be associated with triply periodic cubic mesostructures such as gyroid or BCC.[129] Bailey et al. employed melt-phase static birefringence measurements to definitively establish if the unknown mesostructure had a cubic symmetry. Optically isotropic phases, such as those with cubic symmetry, are nonbirefringent. This unknown mesostructure was strongly birefringent, leading Bailey et al. to deduce that it was noncubic.[188] Bailey et al. reasoned that, since it was noncubic, the unknown mesostructure had to be a triply periodic morphology; other phases were not consistent with both the birefringence and rheological measurements.[188]

Bailey and colleagues next turned to TEM analysis to try and develop a microdomain model of the unknown mesostructure. They pointed out that the TEM micrograph provided in Figure 15B contains an array of bright white, stain deficient spots that are indicative of continuous channels comprised of PS and/or PEO chains and they posited that these continuous PS/PEO channels percolated through a continuous PI matrix.[188] Using these TEM images as a guide, Bailey et al. built a simple network model consisting of tubes connected by 3-fold connectors ((10,3) nets). This model contained elements of both the gyroid and perforated lamellar morphologies, as shown in Figure 16, and had *Fddd* symmetry.[188] (This morphology was subsequently called O^{70},[176] with "O" indicating an orthorhombic unit cell and "70" referring to the number of the space group in the crystallographic tables.[64] The O^{70} notation is used in this review.) The two projections of this lattice model that most closely match the experimental micrographs are provided in Figure 15; the model captures the qualitative features present in the TEM images and is also consistent with the rheological and birefringence measurements.[188] (Tyler et al.[189] later noted that Bailey et al.'s simplistic geometrical model could not account for the lattice parameter ratios obtained from SAXS experiments and should not be considered quantitatively accurate.) Bailey et al. then reconsidered the SAXS data in the context of the O^{70} morphology. (Note that the allowed reflections for the orthorhombic lattice of O^{70} are not simple multiples of the primary peak q^*, as they are for a cubic lattice such as Q^{230}. Rather, orthorhombic peak positions change with the lattice dimensions a, b, and c according to $q_{hkl} = 2\pi[h^2/a^2 + k^2/b^2 + l^2/c^2]^{1/2}$, where h, k, and l are the associated Miller indices. Specific orthorhombic space groups are associated with different sets of allowed reflections, as identified in the crystallographic tables.[64] The a, b, and c parameters must be varied to obtain optimal least-squares fits of the allowed reflections for O^{70} to the recorded SAXS peaks.) The peaks in the experimental 1-D data were accommodated by the allowed reflections for the O^{70} structure, although there were many more allowed reflections than there were experimental Bragg peaks. (Here we note that the absence of allowed reflections does not disqualify a particular space group, as peak intensities are sensitive to the specific electron density distribution within a unit cell. Familiar cases include form factor extinctions in ordered spherical,[184] cylindrical,[184] and lamellar[177,184] block polymers.) In addition, four spots on a 2-D SAXS pattern were found to be consistent with O^{70} Bragg scattering. Bailey et al. tentatively concluded that the PI−PS−PEO specimens had formed the O^{70} network morphology but noted that higher resolution scattering data with an improved signal-to-noise ratio would be required to make the claim definitive. Regardless of the network structure's symmetry, this report validated the strategy for producing multiply continuous network morphologies that was highlighted in Figure 14.[188]

Epps and Cochran et al. extended Bailey et al.'s[188] investigation of PI−PS−PEO materials along the $f_I \approx f_S$ isopleth by probing the specimens with synchrotron X-ray radiation; the resulting data had a higher resolution and higher signal-to-noise ratio[176,177] than the lab-source data previously reported by Bailey et al.[188] SAXS data acquired from eight PI−PS−PEO samples (not all along the $f_I \approx f_S$ isopleth) are provided in Figure 17; Epps and Cochran et al. indexed all of these Bragg patterns to the O^{70} mesostructure.[176,177] Interestingly, in all cases, the 111, 022, and 004 peaks are nearly coincident. The reflections absent from these data match the extinction rules for O^{70}, and

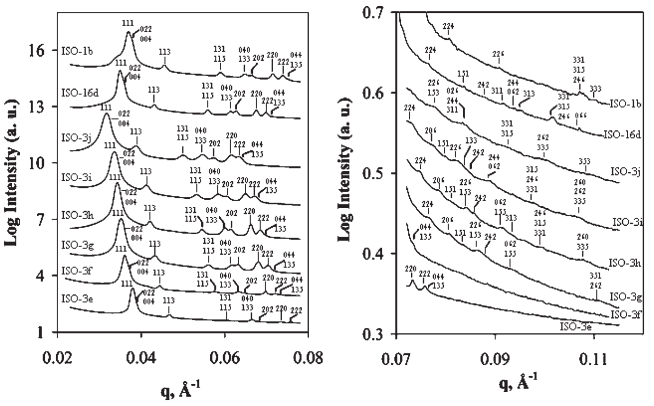

Figure 17. Synchrotron SAXS data acquired from eight PI−PS−PEO specimens in the O^{70} regime. All of the curves are indexed with the allowed reflection for *Fddd* symmetry. Figure reproduced from ref 177.

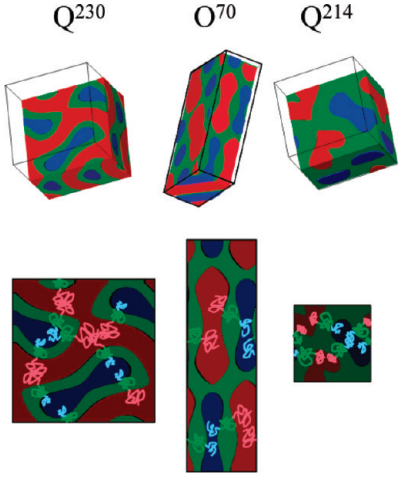

Figure 18. Top row: single unit cell level set models of the Q^{230}, O^{70}, and Q^{214} network morphologies. Bottom row: cross sections of the level set models and sketches of PI−PS−PEO chains demonstrating how each morphology could be assembled. Reproduced from ref 177.

remarkably, none of the allowed peaks are missing in the low-q regime. These data definitively affirm Bailey et al.'s tentative O^{70} assignment. In addition to the six samples prepared by Bailey and co-workers,[188] Epps and Cochran et al. identified the O^{70} network in nine other samples along four different isopleths: (i) $f_I/f_S = 1.1$, $0.15 < f_O < 0.22$, (ii) $f_I/f_S = 0.8$, $f_O = 0.21$, (iii) $f_I/f_S = 0.6$, $0.16 < f_O < 0.25$, and (iv) $f_I/f_S = 0.4$, $0.22 < f_O < 0.29$. Clearly, the O^{70} window encompasses a substantial range of compositions in the PI−PS−PEO system. Note that four of these samples were also listed as forming Q^{214}, as they underwent a melt-phase OOT from Q^{214} to O^{70} upon heating. These OOT's were always reversible, as were O^{70}-to-disorder transitions in materials with experimentally accessible T_{ODT}'s. These reversibilities provide compelling support for the notion that O^{70} is an equilibrium morphology.[176,177]

The microdomain topology of the O^{70} morphology, and those of the more familiar Q^{214} and Q^{230} mesostructures, were further interrogated by Epps and Cochran et al. using a combination of TEM and level set modeling.[177] (Specimens for TEM analysis were rapidly quenched from the melt and the morphology was preserved for room temperature microscopy because the PS domains vitrified prior to PEO crystallization.) This effort was aimed at bridging the gap between the symmetry information present in the reciprocal space SAXS data and the actual domain structure in real space. Level set models are space filling constructs generated using arbitrarily chosen structure factors that have the experimentally determined space group symmetry and divide space into the appropriate volume fractions. These models do not contain any information about individual chain conformations (i.e., polymer statistical mechanics is not considered), but they can be used to simulate TEM projections. Epps and Cochran et al. adjusted the structure factors in their level sets until the simulated TEM projections contained features that closely matched the experimental micrographs. The qualitative visual agreement that was obtained for all three network mesostructures indicated that plausible microdomain models had been proposed and further supported the space group assignments.[177] Level set models of the three network morphologies are provided in Figure 18. Epps and Cochran et al. pointed out that these models do contain some obvious chain packing deficiencies. Namely, there are relatively wide variations in the thickness of individual domains, while SCFT has demonstrated that relatively uniform domains minimize packing frustration and thus overall free energy.[86] Epps and Cochran et al. suggested that SCFT would provide more realistic composition profiles than the level set models, although the latter were useful spatial representations.[177]

The O^{70} network morphology was the first noncubic network structure identified in soft materials,[176,177,188] and it was discussed in numerous subsequent publications.[184−186,190−194] Chatterjee et al. extended the investigations of Bailey, Epps, and Cochran et al.[176,177,188] to PEO-rich PI−PS−PEO triblock terpolymers and identified O^{70} in three different specimens, all of which underwent an OOT from lamellae to O^{70} upon heating.[184] This OOT occurred above the melting temperature of the semicrystalline PEO chains and was not related to the loss of PEO domain crystallinity. Again, the 111, 022, and 004 peaks in the SAXS data were essentially coincident for O^{70}. Chatterjee et al. incorporated both their own and previously published[176,177,188] results into a comprehensive ternary phase map for PI−PS−PEO triblock terpolymers; this portrait is provided in Figure 19. Chatterjee et al. pointed out that a ternary phase map of perfectly symmetric ABC triblock terpolymers would be symmetric about the $f_I = f_O$ isopleth; the asymmetry in Figure 19 was attributed to asymmetries in the block statistical segment lengths and χ parameters.[184] The expansive network windows on this phase portrait validate the strategy of using nonfrustrated ABC triblock terpolymers with symmetric interfacial tensions ($\chi_{AB} \approx \chi_{BC}$) to prepare multiply continuous network morphologies.

Epps and Bates examined the effects of segregation strength on O^{70} network formation.[190] They prepared four series of PI−PS−PEO triblocks along the $f_I \approx f_S$ isopleth with overall molecular weights ~30−130% higher than the previously investigated[176,177,188] O^{70}-forming materials. The melt-phase morphologies of these specimens were probed using a combination of SAXS, TEM, and DMS. Well-ordered O^{70} mesostructures were reported in the network windows for PI−PS−PEO materials with 30 and 75% higher molecular weights, although the precise location of the phase boundaries may have shifted slightly. In contrast, the 80 and 130% higher molecular weight materials with compositions in the network window did not form well-ordered grains of the O^{70} morphology. SAXS data acquired from these specimens contained just two broad peaks, not the assortment of reflections associated with O^{70}. The degree of translational order was sensitive to the symmetry of the underlying morphology, as the 80 and 130% higher molecular weight PI−PS−PEO materials in the LAM regimes did adopt

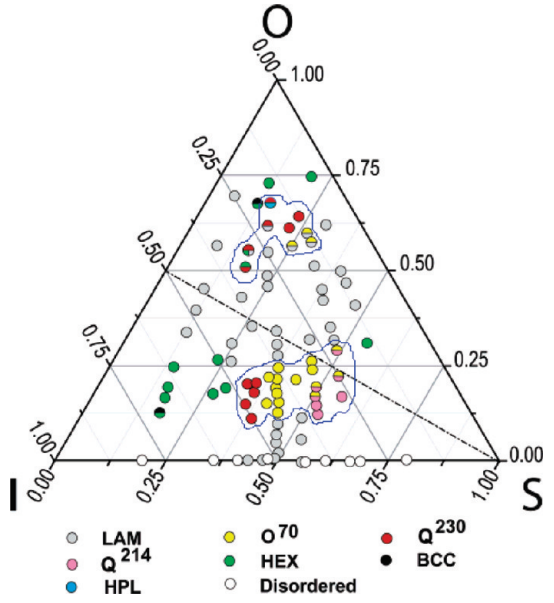

Figure 19. Ternary phase portrait for PI−PS−PEO triblock terpolymers. The axes represent volume fractions of each component, and an imaginary axis normal to the page would represent the segregation strength (all of these samples are located in the plane of the page because they had comparable molecular weights). Six stable ordered morphologies (LAM, HEX, pseudo-BCC (labeled BCC in this figure), O^{70}, Q^{214}, Q^{230}), the metastable hexagonally perforated lamellae (HPL), and a disordered phase are denoted by the colored circles. Symbols containing two colors indicate specimens that underwent OOT's, and the dashed line corresponds to the $f_I = f_O$ isopleth. The blue lines that encompass all of the network-forming specimens are meant to "guide the eye" and are not precise morphology boundaries. Figure reproduced from ref 184.

mesostructures with significant long-range order. Several sample preparation strategies were pursued in an effort to improve the translational order of the mesostructures formed by the high molecular weight PI−PS−PEO materials with compositions in the network window. Neither solvent casting from three different solvents nor annealing at 130 °C for 30 days appreciably altered the state of order of these materials, however. TEM analysis revealed a poorly ordered morphology that appeared to consist of interpenetrating domains of the constituent blocks. Rheological measurements yielded a G' that was relatively invariant with frequency,[190] consistent with a triply periodic morphology.[129] Epps and Bates generically labeled this poorly ordered, triply periodic mesostructure a "network" morphology.[190]

These high molecular weight PI−PS−PEO results appeared to contrast reports detailing network morphologies in AB diblock copolymers. As discussed earlier, it is now generally accepted that the gyroid is a stable morphology for AB diblock copolymers in the SSL,[13,37,136,137] and Urbas et al. published a TEM image of strongly segregated PS−PI diblocks that contained a single gyroid "crystal" that spanned at least several micrometers.[37] The high molecular weight PI−PS−PEO materials did not behave like the diblock counterparts, as they did not adopt a network mesostructure with significant translational order. Epps and Bates suggested the different behaviors derived from differences in molecular diffusion between the PS−PI and PI−PS−PEO systems.[190] In strongly segregated block copolymers, chains do not readily diffuse across domain interfaces.[195,196] Chains can, however, readily diffuse parallel to the domain interfaces. Epps and Bates noted that, due to the large magnitude of χ_{IO}, the PS chains almost exclusively adopt conformations that bridge the terminal domains.[190] As a result, the PI/PS and PS/PEO block junctions would have to move in concert in order for the PI−PS−PEO chains to diffuse parallel to the domain interface. Junction coordination is never present in AB diblock copolymers because no chains contain multiple junctions, and chains are able to freely diffuse parallel to domain interfaces (subject to entanglement effects). The junction coordination in the PI−PS−PEO system apparently does not prevent diffusion that results in the coarsening of lamellae, as well ordered LAM_2 and LAM_3 mesostructures were reported in the high molecular weight samples.[190] Epps and Bates posited that the coordination does inhibit parallel diffusion in network morphologies provided diffusion across domain interfaces is sufficiently suppressed by high segregation strengths. They argued that, since domains in network structures do not have constant thicknesses, PI−PS−PEO chains are not able to freely diffuse parallel to domain interfaces without stretching (compressing) the middle PS block. These stretching requirements are alleviated when the chains can diffuse normal to the domain interface, as they can for lower molecular weight materials. Presumably these entropic stretching considerations inhibit molecular diffusion in the higher molecular weight PI−PS−PEO materials and thus minimize the coarsening of network mesostructures into coherent ordered grains. Epps and Bates noted that the preservation of the triply periodic morphology at higher molecular weights could potentially be very beneficial from a practical applications point of view.[190]

Epps and Bates pointed out that ordered network structures could be the equilibrium state for these generic "network"-forming materials, but the kinetic limitations prevented them from making a definitive determination.[190] Meuler and colleagues subsequently provided evidence that O^{70} was in fact the equilibrium configuration for these "network"-forming samples.[192] They annealed several of the higher molecular weight specimens at 250 °C, above the 200 °C level investigated by Epps and Bates,[190] and probed the morphologies with synchrotron SAXS. While this heat treatment did not alter the state of order of most of the PI−PS−PEO materials, one of the samples did transition from the "network" structure to a (presumably equilibrium) O^{70} morphology at the elevated temperatures.[192] This result supported Epps and Bates' hypothesis that, absent kinetic limitations, the higher molecular weight PI−PS−PEO materials could form ordered network mesostructures.

Meuler et al. extended the investigation of block terpolymers comprised of PI, PS, and PEO chains to PEO−PS−PI−PS−PEO pentablock terpolymers.[192] Previous experimental[140,141] and theoretical[92] reports had identified the familiar gyroid in higher order ABA triblocks; Meuler et al. prepared a series of PEO−PS−PI−PS−PEO pentablocks along the $f_I \approx f_S$ isopleth to determine if, like in the block copolymer materials, the PI−PS−PEO network morphologies persisted in the higher order PEO−PS−PI−PS−PEO pentablocks.[192] A combination of synchrotron SAXS, TEM, and DMS was used to identify O^{70} in an OSISO specimen ($f_O = 0.13$) with approximately the same segregation strength as some previously investigated[176,177,188] PI−PS−PEO materials (i.e., the PEO−PS−PI−PS−PEO sample had about twice the overall molecular weight as a homologous PI−PS−PEO specimen), proving that network morphologies are formed by the higher order PEO−PS−PI−PS−PEO materials.[192] Other investigations focused on the stability of O^{70} in PI−PS−PEO materials with respect to increased PS and PEO block polydispersities,[185,186,191] constituent homopolymer addition,[193] and lithium perchlorate doping.[194]

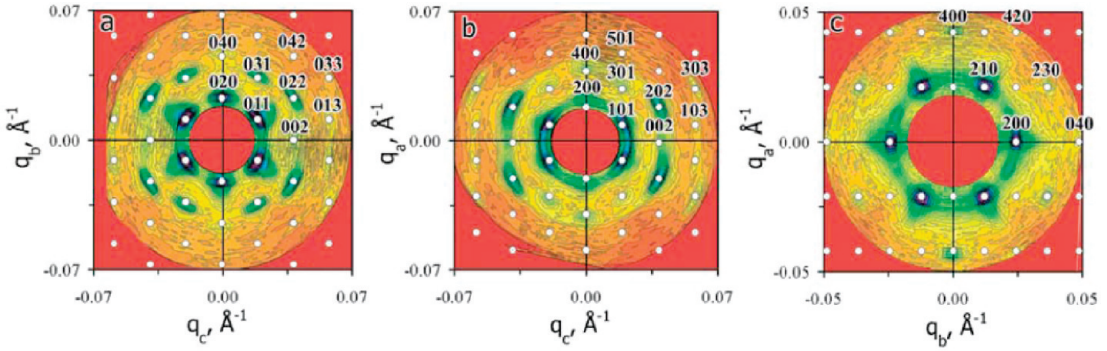

Figure 20. 2-D SAXS patterns from annealed, macroscopically aligned PCHE−PEE−PE. The circles mark the allowed reflection for the O^{52} morphology. The beam is parallel to (a) the shear direction, (b) the shear gradient direction, and (c) the vorticity direction. Figure reproduced with permission from ref 197. Copyright 2004 American Physical Society.

The O^{70} network structure was reported in two nonfrustrated ABC triblock systems besides PI−PS−PEO. Both other systems, like PI−PS−PEO, have symmetrically balanced interfacial tensions ($\chi_{AC} \gg \chi_{AB} \approx \chi_{BC}$), and all of the O^{70}-forming samples were in the weak segregation regime. Epps and Cochran et al. reported that a re-examination of the SAXS and TEM data obtained from a PS−PI−PDMS triblock terpolymer specimen ($f_S = 0.20, f_I = 0.59$)[182] led them to conclude that the sample had formed O^{70}.[177] Cochran and Bates probed the morphology of a PCHE−PEE−PE triblock terpolymer specimen ($f_C = 0.29, f_{EE} = 0.49$) using synchrotron SAXS and reported that it had adopted O^{70}. Once again the first three peaks in the Bragg pattern were nearly coincident.[197] These results indicate that O^{70} may be common to many triblock terpolymer systems.

O^{52}, the Orthorhombic *Pnna* Network. The report of the first known orthorhombic network structure in soft materials (O^{70})[188] was closely followed by a publication identifying a second network morphology with an orthorhombic lattice.[197] This latter research focused on the processing behavior of O^{70}-forming materials. Cochran and Bates subjected a melt of the O^{70}-forming PCHE−PEE−PE triblock sample to reciprocating shear (rate of 5 s^{-1}, 600% strain amplitude) and probed the morphology using SANS (the beam was situated along the shear gradient direction). The 2-D SANS pattern did not change after 6 min of shearing, indicating a steady-state structure had formed. The peaks in this SANS pattern satisfied the extinction rules for multiple space groups, and additional experiments were required to definitively establish the symmetry of the mesostructure. The sheared sample was cooled to room temperature, sectioned, and exposed to X-rays that were coincident with the three orthogonal axes; these SAXS data are provided in Figure 20. Cochran and Bates reported that the multiple orders of reflections and systematic extinctions in these three Bragg patterns conformed uniquely to an orthorhombic (O) space group with *Pnna* symmetry (O^{52}, space group number 52^{64}) and lattice constant ratios of $a = 2.00c$ and $b = 1.73c$.[197] The O^{52} structure is closely related to the O^{70} morphology but fills space in a lower symmetry manner than the latter network. Assuming a simple stick like representation (e.g., Figure 16), both lattices are constructed from 3-fold connectors resulting in 3-D (10,3) loops and networks with orthorhombic symmetry. Connector symmetry (strut length and angles) depends somewhat on the unit cell parameters, which in turn are driven by the block polymer composition and possibly segregation strength. Both the O^{70} and O^{52} connectors contain mirror-plane symmetry, with one strut ~10% shorter than the other two, resulting in an angle of about 125° between the longer struts. Adjusting the angle of rotation between 3-fold units drives the change in symmetry between the *Fddd* (O^{70}) and *Pnna* (O^{52}) unit cell arrangements. For example, using this simple representation O^{70} contains a dense array of indefinitely long, parallel, planar zigzag connector sequences (see Figure 16), which are not found in O^{52}. For a more complete description of these fascinating (10,3) network topologies, the reader is referred to refs 55 and 198. Cochran and Bates presented a level set model of the O^{52} network that contained continuous, triply periodic domains of all three constituent blocks.[197] This reciprocating shear-induced transition from O^{70} to O^{52} was the first known field-induced network-to-network transition in soft materials. The O^{52} morphology persisted following cessation of the shear and several days of thermal annealing above the glass transition temperatures (T_g) of the constituent blocks. Cochran and Bates suggested that O^{52} was a long-lived metastable state, as the (presumably equilibrium) O^{70} always formed upon cooling below T_{ODT} under quiescent conditions. The O^{70} and O^{52} network morphologies apparently had nearly degenerate free energies, and a kinetic barrier prevented a reversal of the shear-induced O^{70} to O^{52} transition.[197]

A morphology with *Pnna* symmetry was recently reported in another nonfrustrated system: PCHE−PE−PCHE−PDMS tetrablock terpolymers ($\chi_{ED} > \chi_{EC} \approx \chi_{CD}$).[199] Bluemle et al. prepared a series of PCHE−PE−PCHE−PDMS specimens ($f_E/f_C = 7/3$) with varying lengths of terminal PDMS chains ($0 < f_D < 0.20$), subjected them to reciprocating shear in the melt, and interrogated the resulting sample morphologies using DMS, SAXS, and TEM (following vitrification of the PCHE domains). All of these specimens adopted hexagonally packed cylinders, except for the sample with $f_D = 0.09$. DMS experiments conducted on this specimen revealed a frequency-independent G' that is suggestive of a triply periodic morphology. SAXS data were acquired with the X-ray beam oriented along each of the orthogonal axes; Bluemle et al. were able to fit nearly all of the spots in these patterns with the allowed reflections of a *Pnna* space group with lattice ratios of $a = 1.75c$ and $b = 0.61c$. TEM analysis of this specimen provided micrographs Bluemle et al. suggested were indicative of discrete spheres of PDMS embedded within the trivalent nodes of the interpenetrating PCHE domains. Although they share *Pnna* symmetry and a (10,3) network lattice, this O^{52} network and the O^{52} structure reported by Cochran and Bates[197] clearly contain different microdomain structures. The lattice parameter ratios are different for the two systems, and the PCHE−PE−PCHE−PDMS version of O^{52} does not contain continuous domains of all of its components,[199] unlike the modeled

PCHE−PEE−PE version.[197] It was unclear if O^{52} represented the equilibrium state of the PCHE−PE−PCHE−PDMS sample[199] or if it was a long-lived metastable state like the O^{52} in the PCHE−PEE−PE specimen.[197]

Theoretical Approaches. In the preceding sections, we discussed selected theoretical publications[162,164−166] that played a role in establishing the $I4_132$ symmetry of the triply continuous Q^{214} mesostructure. Several other[189,200−202] groups have systematically examined triblock terpolymer phase behavior and discussed the network mesostructures adopted by these materials. Erukhimovich et al. developed a weak-segregation theory for ABC triblock terpolymers[203] that, like Leibler's analogous theory for diblock copolymer melts,[7] is rigorously valid only near a critical point. Erukhimovich used this theory to compute the free energies of numerous mesostructural candidates, including the Q^{214} and Q^{230} network morphologies, in various weakly segregated, nonfrustrated ABC triblock terpolymer systems.[200] (Tyler et al. suggested[189] that the phase relations among plane waves used by Erukhimovich to compute the free energy of another network structure were inconsistent with that morphology's reported $I\bar{4}3d$ symmetry. We will therefore omit this phase from our discussion here.) Detailed phase portraits for systems with symmetric χ parameters ($\chi_{AB} = \chi_{BC}$) that satisfy the Hildebrand (i.e., solubility parameter) approximation were provided by Erukhimovich, and these included equilibrium predictions for both Q^{214} and Q^{230}.[200]

Tyler and colleagues used SCFT to interrogate the phase behavior of nonfrustrated ABC triblock terpolymers with $\chi_{AC} \gg \chi_{BC} \approx \chi_{AC}$;[189,201] both the PI−PS−P2VP[159−161,169−172,175] and PI−PS−PEO[176,177,184−186,188,191,192] materials discussed earlier have this sequence of χ parameters. The free energies of 13 ordered morphologies, including Q^{214}, Q^{230}, O^{70}, O^{52}, OTDD (Q^{227}), and core−shell OBDD networks (Q^{228}), were computed, and ternary phase portraits for several model systems were presented.[189] An idealized ABC system, like those studied by Matsen[162] and Erukhimovich,[200] had symmetric interfacial tensions ($\chi_{AB} = \chi_{BC}$) and blocks with equal statistical segment lengths. The Q^{230}, Q^{214}, and O^{70} networks were identified as equilibrium mesostructures for various ranges of compositions in these model materials.[189] While these same three network morphologies were reported in the PI−PS−PEO system,[176,177,184,188] the sizes and positions of the network windows in the model triblocks differed significantly from those in the PI−PS−PEO materials. Tyler et al. aimed to reconcile these differences by incorporating experimentally measured χ and block statistical segment length values into the SCFT calculations. (Note that these values, along with the degree of polymerization, must be computed with respect to a common reference volume for use in SCFT; Tyler and colleagues selected 118 Å^3.) The phase triangle that was computed using these realistic parameters contained stable regions of Q^{230}, Q^{214}, and O^{70} and is provided in Figure 21. It differed significantly from the idealized version, illustrating the sensitivity of ABC triblock phase behavior to the χ and statistical segment length values, and provided a much better qualitative, albeit not quantitative, match to the experimental data shown in Figure 19.[189]

Tyler et al. commented on several other features of the ABC triblock terpolymer phase behavior. They noted that the predicted microdomain structures typically contained diffuse domain interfaces due to the modest segregation strengths considered. Additionally, the predicted microdomain structures in the network morphologies were not always continuous in all three domains, as short terminal chains could either mix with or form discrete domains within the continuous matrix.[189] The overall free energies of competing morphologies were decomposed into individual entropic and enthalpic contributions to provide some physical insight into the thermodynamic phenomena driving network formation. Tyler et al. provided comparisons of these contributions at a number of phase boundaries.[189] Notably, O^{70} was only predicted to be stable for unit cell parameter ratios that would result in a near coincidence of the 111, 004, and 022 peaks in a Bragg pattern, a prediction in agreement with the experimental ISO reports discussed earlier.[176,177,184,188] Additional analysis focused on the sensitivity of the stability of the O^{70} network with respect to variations in the χ parameters; the size and location of the predicted O^{70} window depended strongly on the quantity $\chi_{AB} - \chi_{BC}$ (i.e., the asymmetry of the interfacial tensions).[189]

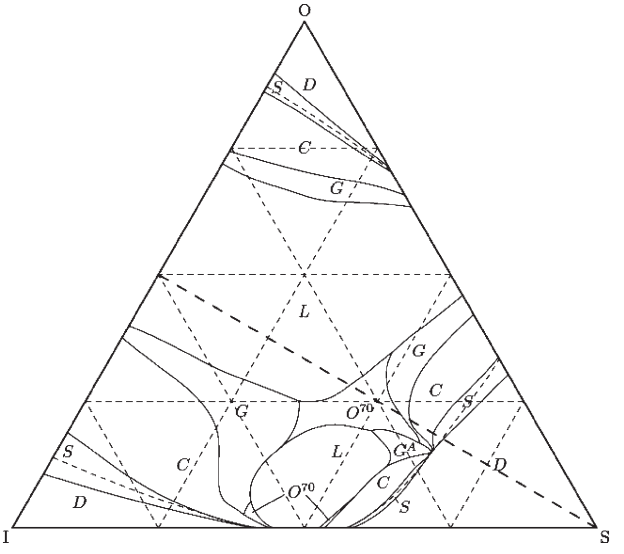

Figure 21. Ternary phase portrait for a model PI−PS−PEO triblock terpolymer. Experimentally measured χ and statistical segment length values were used in the SCFT calculations, and the molecular weights were comparable to those studied by Bates and coworkers[176,177,184,188] (here $\chi_{IS}N = 11.0$, $\chi_{SO}N = 14.2$, $\chi_{IO}N = 45.8$). The predicted equilibrium states are: (D) disorder, (S) BCC, (C) HEX, (L) LAM, (G) Q^{230}, (G^A) Q^{214}, and O^{70}. Figure reproduced from ref 189.

The spectral or pseudo-spectral SCFT implementation strategies utilized by researchers such as Matsen[162] and Tyler and colleagues[189,201] suffer from at least one important limitation: they require the selection of mesostructural candidates. This requirement severely hinders the utility of SCFT as a predictive tool for identifying new equilibrium morphologies, as including every possible space group symmetry in calculations is not practically feasible. Numerical methods that do not require the selection of mesostructural candidates were developed to solve the SCFT equations and overcome this limiting feature beginning in 1999−2000.[204,205] Guo and colleagues recently extended this type of SCFT analysis to ABC triblock terpolymers in three dimensions by using a generic Fourier-space approach.[202] They complemented Tyler et al.'s investigations of nonfrustrated ABC systems[189,201] by focusing on model frustrated ABC triblock terpolymers with equal block statistical segment lengths and $\chi_{AB}N = \chi_{BC}N = 35$ and $\chi_{AC}N = 15$. A ternary phase portrait containing 20 different morphologies that was generated using this methodology is provided in Figure 22b. Included among these morphologies are the traditional Q^{230} (here labeled "G") and Q^{214} (here labeled "G^A") network structures as well as two decorated variations of gyroid that contain embedded, noncontinuous domains: gyroid with spheres at the interfaces (here labeled

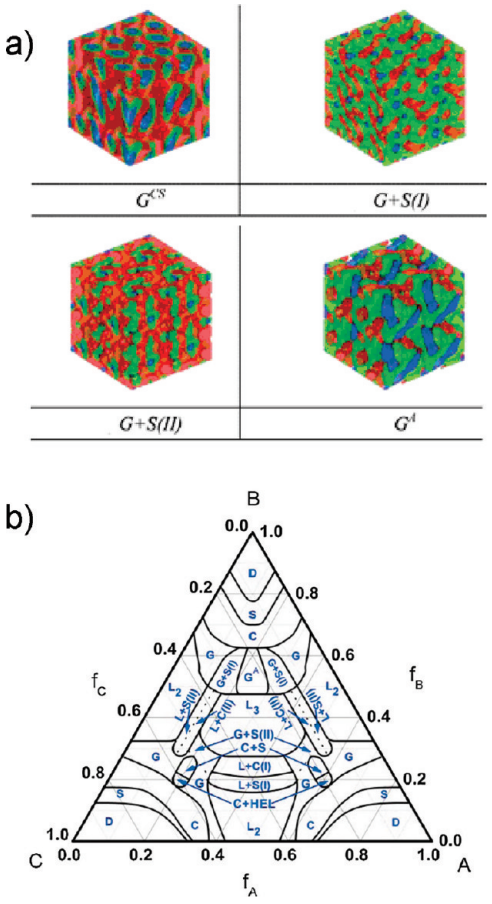

Figure 22. (a) Real space representations of the Q^{230} (here labeled "G^{CS}"), Q^{214} (here labeled "G^{A}"), and decorated variations of the gyroid (gyroid with spheres at the interfaces (here labeled "G + S(I)") and gyroid with spheres inside a domain (here labeled "G + S(II)")) that were obtained by Guo et al. using the generic Fourier-space approach for a model ABC triblock terpolymer with equal block statistical segment lengths and $\chi_{AB}N = \chi_{BC}N = 35$ and $\chi_{AC}N = 15$. (b) Ternary phase map of the predicted equilibrium mesostructures in this model triblock terpolymer system. Figure reproduced with permission from ref 202. Copyright 2008 American Physical Society.

"G + S(I)") and gyroid with spheres inside a domain (here labeled "G + S(II)"); real space representations of these four mesostructures are provided in Figure 22a.[202] The absence of orthorhombic network morphologies such as O^{52} and O^{70} in these model frustrated ABC triblocks is not surprising, given that these mesostructures have only been identified experimentally in nonfrustrated block terpolymer systems.[176,177,184−186,188,190−194,197,199] Guo et al. examined the validity of their methodology by comparing the phase triangle provided in Figure 22b to the reported phase behavior of frustrated PS−PB−PMMA triblock terpolymers.[206] Notably, the SCFT phase portrait contains a LAM_3 ("L_3") → lamellae with cylinders at the interfaces ("L + C(I)") → lamellae with spheres at the interfaces ("L + S(I)") → LAM_2 ("L_2") sequence along the $f_A = f_C$ isopleth;[202] this same mesostructural procession was reported in the PS−PB−PMMA system,[206] an agreement that Guo et al. suggested validated their generic Fourier-space approach.[202] This general approach may prove to be a very powerful tool for investigating ABC triblock terpolymer phase behavior because of its predictive component and the resulting potential to serve as an effective guide for experimentalists preparing designer block polymer materials.

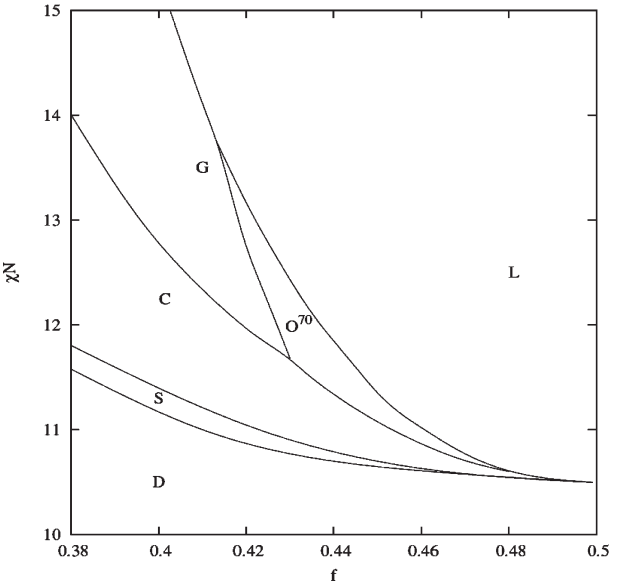

Figure 23. SCFT phase portrait of a conformationally symmetric diblock copolymer: (D) disorder, (L) LAM, (G) gyroid, (C) HEX, (S) BCC. Reproduced with permission from ref 201. Copyright 2005 American Physical Society.

Revisiting AB Diblock Copolymers: O^{70}

The reports of O^{70} in various triblock terpolymer systems[176,177,188,197] led Tyler and Morse to evaluate the stability of this orthorhombic network phase in AB diblock copolymers using SCFT.[201] Their approach, like that employed by Matsen and Schick,[76] involved selecting mesostructural candidates and computing free energies.[201] Tyler and Morse initially investigated O^{70} in ABC triblock terpolymers but, upon finding that O^{70} was predicted to be an equilibrium morphology at certain compositions in the diblock limit (i.e., as the length of the C chain approached zero), decided to recalculate the entire phase portrait for conformationally symmetric AB diblock copolymers. Tyler and Morse included O^{70} as a mesostructural candidate, along with the familiar BCC, HEX, gyroid, and LAM morphologies identified as equilibrium mesostructures by Matsen and Schick,[76] and found that O^{70} has the lowest computed free energy for a narrow range of compositions and segregation strengths.[201] The region of the phase diagram updated by Tyler and Morse is presented in Figure 23;[201] entropic considerations changed a portion of the LAM window to O^{70}, while enthalpic contributions stabilized O^{70} at the expense of gyroid.[189] Guo et al. recently calculated the AB diblock phase diagram using their new, generic Fourier-space SCFT approach that did not rely on a priori assumptions about the symmetry of the structure (i.e., it did not require the selection of mesostructural candidates)[202] and confirmed Tyler and Morse's predictions.[189,201]

As mentioned earlier, orthorhombic unit cells have three independent lattice parameters, while the cubic counterparts are characterized by only one. Tyler and Morse concluded that O^{70} is only stable when the ratios of the cell parameters are approximately $1:2:2\sqrt{3}$;[201] the first three scattering peaks (004, 111, and 022) from unit cells with these exact ratios of lattice parameters are coincident. This near coincidence of the first three reflections was reported in all of the experimental O^{70}-forming block terpolymer systems.[176,177,185,186,188,190,192,193,197] Tyler and Morse suggested that, since O^{70} was predicted to be stable in weakly segregated materials, the rationale for the near coincidence of the scattering peaks and the network structure's stability could be understood in the context of the Landau expansion of the SCFT free energy.[201] Ranjan and Morse subsequently

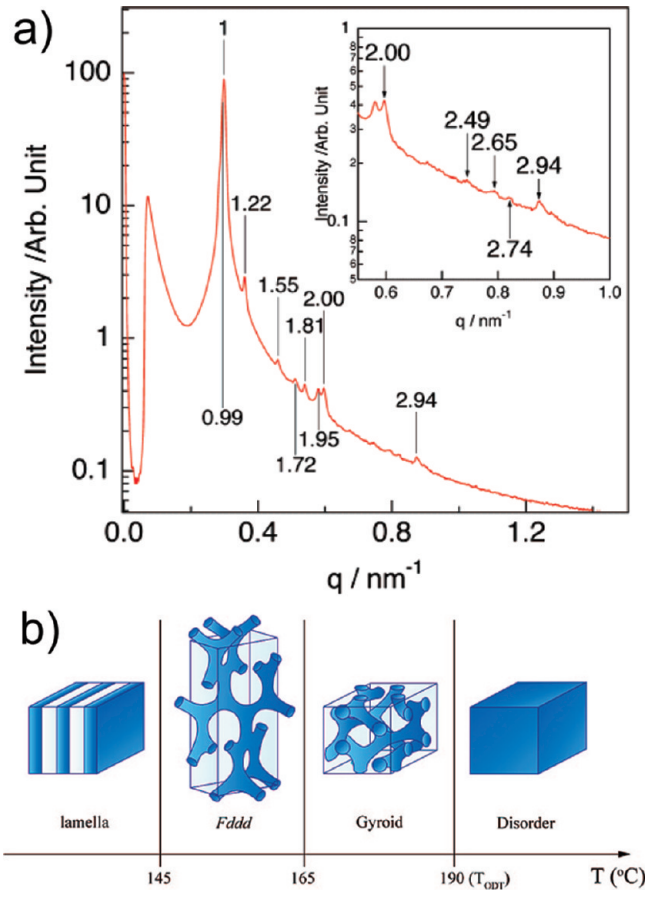

Figure 24. (a) SAXS data used to identify the O^{70} morphology in a PS−PI diblock copolymer with $f_I = 0.638$ and $M_n = 26.4$ kg/mol. Data reproduced from ref 112. (b) Thermally driven order−order transitions identified in the same PS−PI diblock specimen. Transitions to and from the O^{70} (*Fddd*) network are reportedly reversible. Schematic reproduced from ref 114.

extended Leibler's Landau theory[7] and analyzed the stability of O^{70} in diblock copolymers.[207] They assumed that the ratio of unit cell parameters was $1:2:2\sqrt{3}$ and found excellent agreement between the Landau results and the SCFT calculations for weakly segregated ($\chi_{AB}N < 10.55$) diblock materials. Ranjan and Morse speculated that, since it was predicted to be an equilibrium morphology in the context of the Landau theory, the stability of the O^{70} network may be related to geometric considerations and not any specific features of block copolymers.[207] An additional theoretical investigation of the stability of O^{70} was undertaken by Yamada et al.,[208] who calculated the phase diagram of weakly segregated diblock copolymers using two methods: (i) evaluating the free energy of morphological candidates using a Landau expansion in a manner similar to Ranjan and Morse[207] and (ii) direct numerical simulations of the time-evolution free energy equations from starting conditions that include random noise. Both methods led Yamada et al. to conclude that O^{70} was the equilibrium morphology over a small portion of the AB diblock copolymer phase diagram.[208] Curiously, the O^{70} unit cell considered by Yamada et al. did not have lattice parameter ratios of $1:2:2\sqrt{3}$ but was a deformed version of this O^{70} unit cell considered by other groups.[189,207]

These theoretical reports[201,207,208] predicted that O^{70} should be the equilibrium structure of AB diblock copolymers over narrow ranges of composition. Some considered this prediction unlikely,[209] given that many experimental reports in the literature had focused on network structures in AB diblock copolymers, and none of them had identified O^{70}. Takenaka and co-workers provided decisive confirmation of the O^{70} predictions with a 2007 report that a PS−PI diblock with $f_I = 0.638$, $M_n = 26.4$ kg/mol, and a PDI of 1.02 formed O^{70} at temperatures ranging from 145 to 160 °C.[112] The diblock material was first annealed in the disordered state at 230 °C for 30 min to eliminate effects associated with thermal history and then annealed at the target temperatures for 8 h prior to being exposed to synchrotron X-rays or quenched in liquid nitrogen (for TEM analysis). The resulting SAXS data (see Figure 24a) and TEM micrographs were used to identify O^{70} between LAM (at lower temperatures) and the gyroid (at higher temperatures),[112] a sequence of transitions consistent with Tyler and Morse's SCFT prediction.[201] The first three peaks in the SAXS data were essentially coincident,[112] consistent with the findings in block terpolymer systems,[176,177,185,186,188,190,192,193,197] and in agreement with most of the predictions[201,207] for diblock copolymers.

Miao and Wickham were skeptical that the O^{70} morphology reported by Takenaka et al.[112] represented the equilibrium state of the PS−PI diblock sample.[209] They noted that O^{70} was not identified in experimental diblock copolymer reports in the literature prior to 2007, even though a large number of investigations focused on network morphologies in those systems. Miao and Wickham also noted that meastability can be an issue with network mesostructures, as the transition from the metastable HPL to the equilibrium gyroid network reportedly required thermal anneals as long as 31 days, depending on the specific characteristics of the diblock material.[133] Furthermore, composition fluctuations were known to significantly modify the predicted mean-field phase diagram in the weak segregation regime[210] in which O^{70} was identified by Takenaka et al.[112] Miao and Wickham hypothesized that composition fluctuations could suppress the O^{70} network in diblock copolymers,[209] a possibility initially mentioned by Tyler and Morse.[201] They utilized a Hartree-level treatment of a generic Landau−Brazovskii model[211] to theoretically examine whether or not O^{70} was an equilibrium morphology in diblock materials with composition fluctuations.[209] They assumed that the O^{70} unit cell had lattice dimensions in the ratio $1:2:2\sqrt{3}$ (and thus a coincidence of the first three peaks in the predicted Bragg pattern), following experimental[112] and theoretical[201,207] precedent. This theoretical treatment led Miao and Wickham to predict that composition fluctuations render O^{70} metastable with respect to the LAM and disordered states for experimentally relevant molecular weights ($N < 10^4$), and they suggested Takenaka et al.[112] had identified a metastable O^{70} morphology in their PS−PI diblock sample.[209]

Miao and Wickham's report[209] led the Takenaka group to revisit their claim that O^{70} represented the equilibrium state in their PS−PI diblock material.[114,115] The PS−PI diblock copolymer ($f_I = 0.638$, $M_n = 26.4$ kg/mol) was previously reported[112] to undergo order−order transitions from LAM to O^{70} to gyroid upon heating. Kim et al. interrogated the stability of O^{70} by studying the thermoreversibility of these order−order transitions that are summarized in Figure 24b.[114] Two protocols were employed to investigate the respective LAM to O^{70} (i) and O^{70} to gyroid (ii) transitions: (i) anneal at 130 °C for 24 h, anneal at 150 °C for 48 h, and anneal at 130 °C for 48 h and (ii) anneal at 170 °C for 24 h, anneal at 150 °C for 48 h, and anneal at 170 °C for 48 h. The morphology of the PS−PI diblock sample was probed at each temperature using both synchrotron SAXS and TEM. These data conclusively established that protocol (i) yielded transitions from LAM to O^{70} to LAM while protocol (ii) resulted in transitions from gyroid to O^{70} to gyroid. The same sequence of morphological transitions from LAM to O^{70} to gyroid was subsequently reported in five other PS−PI samples with $0.629 < f_I < 0.649$.[115] The thermoreversibility of these transitions, coupled with the long annealing times, provided compelling

evidence that O^{70} is in fact an equilibrium network morphology in PS−PI diblock copolymers.[114,115] It is currently unclear why Miao and Wickham's theoretical investigation[209] found that the formation of O^{70} is completely suppressed in diblock copolymers with composition fluctuations.

Network Mesostructure Stability

Solvents. Numerous theoretical[83,95,212,213] and experimental[134,153−155,212,214−223] investigations have focused on the phase behavior of block copolymers in the presence of solvents. Generally, these specimens adopt the ordered morphologies found in neat diblocks when the volume fraction of block copolymer material exceeds 0.2. The broad features of the phase behavior can generally be understood by viewing the changes in domain volume fractions that result from the partitioning of the solvent as equivalent to changes in block volume fractions of melt-phase AB diblocks, although the addition of solvent typically lowers the segregation strength of the system.[153,154,214−216] The gyroid morphology has been identified in a number of block copolymer/solvent mixtures, some of which are listed in Table 2.

Homopolymers. The phase behavior of blends of block copolymers and constituent homopolymers generally resembles that of neat block copolymers with the same composition, provided the homopolymer is a minority component in the blend and the homopolymer molecular weight is roughly equal to or less than the analogous block molecular weight; macrophase separation can occur when these two conditions are not met.[81,82] Winey et al. first suggested that homopolymer blending could be used to adjust the compositions of block copolymer materials and place them within the narrow gyroid window for AB block copolymers.[66] Multiply continuous network morphologies have since been reported in a number of blends, some of which are listed in Table 3. Theoretical analyses broadly agree with the reported experimental behavior but also suggest that the addition of homopolymer can relieve packing frustration and stabilize morphologies not yet identified in experiments.[81−83,85,149,166]

Table 2. Block Copolymer/Solvent Mixtures in Which the Gyroid (Q^{230}) Has Been Identified

block copolymer	solvent(s)	reference(s)
PS−PI	dioctyl phthalate	214, 216
PS−PI	di-*n*-butyl phthalate	214, 215
PS−PI	diethyl phthalate	215
PS−PI	dimethyl phthalate	215
PEO−PPO−PEO	water/*p*-xylene	218, 219, 221, 223
PEO−PBO−PEO	water/*p*-xylene	220
PEO−PPO−PEO	formamide	222
PS−P4VP	toluene/ethanol	217

Salts. Epps and co-workers have examined the stability of network phases with respect to lithium perchlorate ($LiClO_4$) doping in both PS−PI−PEO and PI−PS−PEO triblock terpolymer systems.[194,227] This research was motivated by the fact that PEO, when complexed with alkali metal salts, can be used as a polymer electrolyte.[228,229] It was hoped that the nonconductive blocks in the block copolymers would lead to improved mechanical toughness of the polyelectrolyte membranes.[227] $LiClO_4$-doped network mesostructures were thought to be particularly attractive because the continuous, percolating PEO domains would not, in principle, require any sort of alignment to ensure that the conducting channels traversed the membrane.[227] (A recent report demonstrated that network morphologies are not, in fact, required for high ionic conductivities.[230]) PS−PI−PEO and PI−PS−PEO triblocks with $f_I \approx f_S$ were doped with $LiClO_4$ at ether oxygen-to-lithium ratios ranging from 48:1 to 3:1. While neat PS−PI−PEO and PI−PS−PEO triblock terpolymers formed Q^{230} and O^{70}, respectively, at certain compositions along this isopleth, the doped materials adopted a core−shell cylindrical mesostructure. This $LiClO_4$-induced morphological transition from the network morphologies to core−shell cylinders was rationalized on the basis of increases in the effective χ parameters in the systems upon the addition of the $LiClO_4$ salt.[194,227]

Ionic Groups. Park et al. investigated symmetric PSS−PMB diblock copolymers with various levels of sulfonation in both the dry and hydrated states.[138,231,232] These materials could potentially find application as polymer electrolyte membranes for fuel cells, with the sulfonic acid-containing PSS domains serving as channels for proton conduction. Park and Balsara et al. hoped to develop an understanding of the relationship between morphology and proton conductivity.[231] PSS−PMB diblock copolymers with sufficient levels of sulfonation adopted ordered morphologies, even at very low molecular weights (~3 kg/mol), due to the relatively large χ between the ionic and nonionic blocks, and well-ordered network mesostructures were obtained even at relatively high ionic contents.[138] Somewhat surprisingly, the gyroid morphology was identified in dry polymers with certain levels of sulfonation, even though f_{SS} lay between 0.45 and 0.50. The PSS−PMB materials also formed coexisting lamellae and perforated lamellae over wide composition ranges (~10% by volume fraction), and Park and Balsara suggested that the "universal phase portrait" for block copolymers[13] did not apply to the PSS−PMB system and that new theories would be required to understand this complex phase behavior.[138] The gyroid network structure persisted as the ambient humidity was increased to modest levels before transitioning to LAM at high humidities.[232] It is not yet clear if the gyroid morphology offers enhanced proton conduction relative to LAM.

Table 3. Block Copolymer/Homopolymer Mixtures in Which Multiply Continuous Network Morphologies Have Been Identified

block copolymer	homopolymer(s)	network(s)	reference(s)
PS−PI	PS	Q^{230} [a]	66−68, 107, 110, 111, 224
PS−PI	PI	Q^{230} [a]	66−68, 225
PS−PB	PS	Q^{230} [a]	66
PS−PB	PB	Q^{230} [a]	66
PS−PB−PS	PVME	Q^{230} [a]	69
PEO−PBO	PBO	Q^{230}	120
PS−PFCDMS	PFCDMS	Q^{230}	226
PFCDMS−PMMA	PFCDMS/ PMMA	Q^{230}	139
PI−PS−PEO	PS	Q^{214}, Q^{230}, O^{70}	193
PI−PS−PEO	PI	Q^{214}, Q^{230}, O^{70}	193
PI−PS−PEO	PI/PS	O^{70}	193

[a] Indicates that the reported network in some of the references is OBDD. These network morphologies are likely the gyroid.

Polydispersity. The effects of polydispersity on block polymer phase behavior have recently been reviewed,[8] and only some features related to network morphologies are discussed here. Experimental[130] and theoretical[233−235] investigations have demonstrated that polydisperse block copolymers generally adopt equilibrium mesostructures that are comparable to those formed by monodisperse materials (i.e., the topologies of the phase diagram are generally the same).[130,233−235] Changes in the shapes of the molecular weight distributions alter the entropic and enthalpic free energy balances and thus the locations of the phase boundaries, however,[130,233−235] and macrophase separation may occur for certain polydispersities, particularly in the gyroid window for intermediately to strongly segregated materials.[234] Polydispersity affects the free energy balance because the longer chains in the molecular weight distribution do not have to stretch as much to fill space, effectively lowering the elastic contribution to the system free energy for the polydisperse ensemble below its monodisperse counterpart.[234] This increased domain elasticity leads to elevated domain periodicity and may drive morphological transitions in which the domain interfaces curve toward the polydisperse block.[130,233−235]

Xie and co-workers first demonstrated that polydisperse block copolymer materials could form multiply continuous network morphologies in 1993.[69] They investigated polydisperse blends of PS−PB−PS triblock copolymers (overall PDI = 1.35) and PVME homopolymers (PDI = 1.70) and reported that the components did not macrophase separate but adopted a network mesostructure (identified as OBDD but likely gyroid).[69] Several subsequent studies focused on blends of nearly monodisperse diblock copolymers. The blends contained bimodal molecular weight distributions in both blocks and typically did not macrophase separate but formed a well-ordered gyroid mesostructure. These results further demonstrated that narrow molecular weight distributions are not required for network formation.[102−104,113]

Some groups have postulated that polydispersity could be used to alter the enthalpic/entropic free energy balance and stabilize ordered network mesostructures. Hasegawa et al. speculated that a distribution of block lengths would alleviate packing frustration and stabilize bicontinuous AB block copolymer mesostructures.[236] Martínez-Veracoechea and Escobedo tested this hypothesis by employing lattice Monte Carlo (MC) simulations to interrogate bimodal blends of AB diblock copolymers.[97] They found that bidisperse materials form the gyroid over a broader temperature range in the simulations because the distribution of chain lengths relieves packing frustration, with the longer chains occupying domain centers. These MC results support the idea that bidispersity could be used to stabilize the gyroid mesostructure.[97] Schröder-Turk et al. suggested polydispersity could be used to relieve the packing frustration of complex multiply continuous morphologies in block terpolymer systems.[237] They used geometric arguments to speculate that a complex triply continuous phase (called I-WP) could be stabilized in certain ABC triblock terpolymers that contain monodisperse A and B domains and a distribution of C chains with varying lengths.

Several investigations have provided experimental data supporting the notion that polydispersity could stabilize network morphologies.[130,185,186] Lynd and Hillmyer identified polydispersity-driven morphological transitions to gyroid at two different compositions in PEP−PLA diblock copolymers with varying polydispersities in the PLA chains.[130] Meuler and colleagues effectively widened the network window in the PI−PS−PEO system using a multicomponent blending strategy.[185,186] This blending process broadened the molecular weight distribution of the PEO chains and drove a morphological transition from lamellae to Q[230] in which the domain interface curved toward the polydisperse PEO blocks. Blending is a generic process whose only "cost" is the preparation of additional block terpolymers with different compositions, and the blending strategy likely can be deployed as a tool to tune phase behavior in many block polymer systems. Note that polydispersity does not always stabilize network mesostructures, however.[186,191] Morphological transitions from networks to lamellae were driven by increases in the breadth of the PS molecular weight distribution in PI−PS−PEO triblock terpolymers,[191] although PS polydispersity did not totally eliminate formation of network morphologies.[186] These results demonstrate that the effects of increasing the polydispersity of blocks with dangling chain ends are fundamentally different than the effects brought about by increases in the polydispersity of middle blocks that, due to enthalpic incompatibilities of the adjacent blocks, are forced to bridge the domain.[186]

Thin Films. Thin films of block copolymers have received considerable research attention due to their potential technological applications in, for example, lithographic processes.[238−241] Generally, the phase behavior of block copolymer thin films differs from the bulk materials due to (i) confinement effects related to the film thickness and (ii) interactions between the constituent blocks with both the surface and the substrate.[239] Relatively few investigations have focused on thin films of block copolymers that adopt network morphologies in the bulk.[22,23,94,106,147,157,242−246] A few groups have used theoretical simulations to examine these materials.[94,242] These investigations suggested that thin film effects frequently, albeit not always, destabilize the gyroid morphology.[94,242] In experimental investigations, the gyroid has been identified using TEM and/or grazing incident SAXS in relatively thin (~400−700 nm thick, $>5\times$ the domain periodicity) films in a few block copolymer systems, including PI−PPMDS−PI triblock copolymers solvent cast onto silicon,[147] PS−PI diblock copolymers solvent cast onto silicon,[106,157,243−245] and P4FS−PLA diblock copolymers solvent cast onto fluorine-doped tin oxide glass substrates.[22,23] The gyroid has not, to the best of our knowledge, been reported in diblock copolymer films with thicknesses of less than twice the bulk domain periodicity. Epps et al. examined films of PI−PS−PEO triblock terpolymers in this thickness range.[246] As was discussed earlier, multiply continuous network morphologies are stable in bulk PI−PS−PEO materials over wide ranges of compositions.[176,177,188] The PI−PS−PEO specimens interrogated by Epps et al. formed Q[214] in the bulk but did not adopt a multiply continuous structure in thin films that were cast onto substrates with a wide variety of surface energies.[246] These results illustrate the difficulties associated with preparing multiply continuous structures in this thickness range. At least a couple of reports of bicontinuous morphologies in thin films have appeared in the literature.[41,247] Daoulas and colleagues prepared blends of PS−PMMA diblock copolymers and PMMA homopolymers that adopted lamellae in the bulk.[247] These blends were deposited onto a substrate with chemically patterned features with a length scale roughly commensurate with the lamellar domain periodicity. A complicated bicontinuous morphology was reported for certain film thicknesses, illustrating the potential utility of lithographic patterning as a strategy for pre-

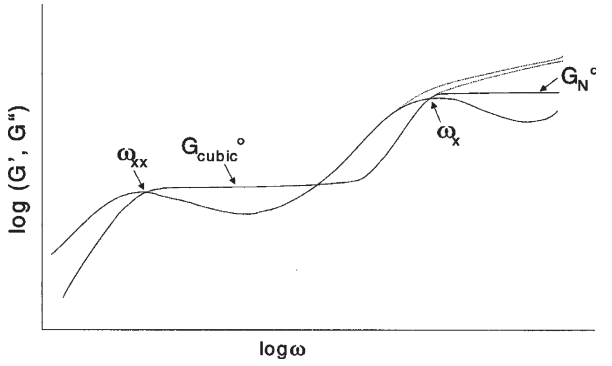

Figure 25. Universal viscoelastic response for block polymers that contain cubic morphologies (including the gyroid) with respect to the entanglement plateau (G°_N, solid line) and the knee in the Rouse spectrum for unentangled systems (dashed lines). Features that are commonly reported in block polymer materials include the plateau in G' (labeled G°_{cubic}) and the crossover of G' and G'' at low frequencies (denoted by ω_{xx}). Figure reproduced with permission from ref 129. Copyright 1999 American Institute of Physics.

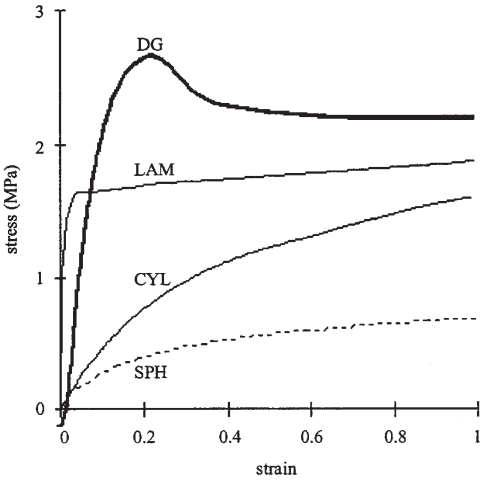

Figure 26. Stress−strain curves of polygranular PS−PI−PS samples containing gyroid (DG), LAM, HEX (CYL), and BCC (SPH) morphologies. Figure reproduced from ref 15.

paring bicontinuous structures in thin films.[247] Liu et al. investigated ~40 nm thick films of ternary blends of PS−PMMA diblock copolymers and equivalent amounts of constituent PS and PMMA homopolymers on substrates coated with random PS−PMMA copolymer.[41] Bicontinuous microemulsions were identified in thin films with a broad range (~20 vol %) of homopolymer compositions.[41]

Physical Properties of Network Morphologies

Viscoelastic Response. While the rheology of microphase-separated block copolymers has been widely studied over the past 30 years,[248] relatively few[46,129] investigations focused on the viscoelastic response of network-forming materials. Schulz et al. reported in 1994 that a gyroid-forming block copolymer sample had an elastic modulus (G') that varied little over a wide range of frequencies (i.e., a plateau in G') above a crossover frequency ω_{xx} (at ω_{xx}, $G' = G''$). For frequencies below ω_{xx}, the specimen exhibited an inelastic response ($G' < G''$) that Schulz et al. suggested was a result of fluctuations driving the local breaking and reforming of the gyroid mesostructure.[46] In 1999, Kossuth and co-workers detailed the rheological behavior of 11 chemically or architecturally distinct block copolymer samples that contained cubic mesostructures (gyroid or BCC spheres).[129] These materials were subjected to isochronal temperature ramps, isochronal strain sweeps, and isothermal frequency sweeps, and time−temperature superposition was successfully used to shift the rheological data. Kossuth et al. reported that block copolymer materials containing cubic morphologies exhibited a universal viscoelastic response that is summarized in Figure 25. This universality was attributed to the 3-D translational order in these mesostructures and demonstrates that rheological data should only be used in a complementary fashion and not as a principal tool for morphological characterization. At frequencies above ω_{xx}, samples with cubic mesostructures typically had G' values that were about an order of magnitude higher than those of noncubic morphologies such as LAM and HEX. Furthermore, nearly all of the samples that contained a cubic mesostructure exhibited a plateau region in plots of G' versus the frequency of the oscillating strain (ω). While the magnitude of the plateau did not depend strongly on the applied strain amplitude, the width of the plateau was highly sensitive to the strain amplitude and degrees of entanglement of the constituent blocks. The materials entered the terminal regime at higher frequencies (i.e., a narrower plateau) for larger applied strain amplitudes and at lower frequencies (i.e., a wider plateau) when at least one of the blocks was well entangled.[129]

The universal viscoelastic response described by Kossuth et al.[129] has been largely confirmed by a number of subsequent publications. Plateaus in G' have been reported in block terpolymers containing cubic Q^{230} (core−shell gyroid)[177,184] and Q^{214} (alternating gyroid)[177] mesostructures as well as the orthorhombic O^{70} network.[177,192] Note that it is the triply periodic nature of the symmetry, and not the "connectedness" of the domains, that is responsible for the plateaus in G' exhibited by materials containing network morphologies. A few groups have reported more detailed theoretical studies of the viscoelastic response of block copolymers containing multiply continuous morphologies.[249−251]

Mechanical Properties. It has long been recognized that network morphologies could enhance the mechanical properties of block polymer materials because of the continuity of multiple domains. Alward et al. did some small-strain mechanical testing in their seminal 1986 paper that first described a bicontinuous morphology in block copolymer materials.[58] They measured the Young's modulus (E') of PS−PI starblock samples with the same composition (30 wt % PS) but different numbers of arms (and thus different mesostructures) over a range of temperatures below the T_g of the PS blocks. The samples that contained a bicontinuous mesostructure had E' values that were about an order of magnitude larger than those of the specimens containing a HEX morphology.[58] Additionally, the bicontinuous material, but not the HEX-containing sample, yielded when subjected to uniaxial extension.[60] Both of these phenomena were attributed to the enhanced continuity of the minority PS domains in the bicontinuous morphology.[58,60]

Dair and co-workers completed the first thorough investigation of the large strain deformation behavior of the gyroid morphology in PS−PI−PS triblock copolymers.[15,16] This research focused on materials in which glassy PS was the minority component, as triblock copolymers with those compositions have been widely used as thermoplastic elastomers.[252] The first study focused on solution cast polygranular materials.[15] Sample morphologies were changed by adjusting the composition of the PS−PI−PS triblocks (with

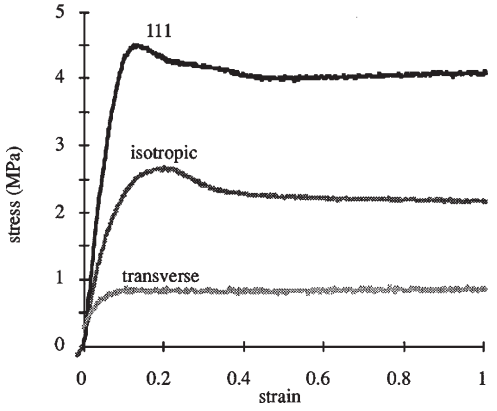

Figure 27. Overlaid stress−strain curves of a polygranular isotropic gyroid PS−PI−PS sample and of an oriented gyroid PS−PI−PS specimen deformed both along and tranverse to the [111] direction. Figure reproduced with permission from ref 16. Copyright 2000 Springer Science and Business Media.

comparable overall M_n). Each specimen was subjected to tensile testing, with stress measured at various strains; representative curves for each morphology are provided in Figure 26. Dair et al. noted that the mechanical properties were sensitive to the underlying mesostructure. The yield stress was highest for the gyroid-containing sample, even though the LAM-forming specimen had a higher glassy block content. Additionally, only the gyroid curve contained a drop in stress at low strains (~0.2 in Figure 26) that was followed by a plateau and subsequent increase in stress with increasing strain. Dair et al. suggested that this stress−strain behavior was consistent with the formation of a stable neck (confirmed with visual inspection) and eventual drawing. Both the higher yield stress and the necking were attributed to the three-dimensionally continuous glassy PS domains that were uniquely present in the gyroid-containing PS−PI−PS triblock material.[15] The evolution of the underlying (initially gyroid) mesostructure during these stress−strain experiments was also probed using SAXS. The Bragg pattern suddenly changed from rings to streaks at the onset of necking, which Dair et al. posited was the result of a disruption of the PS networks.[15] Sakurai et al. reported a similar sudden change in SAXS data while stretching a gyroid-containing PS−PB−PS triblock that was also attributed to the rupture of the glassy 3-D networks.[145]

A second study by Dair et al. focused on the mechanical properties of a PS−PI−PS triblock copolymer film that contained oriented grains of gyroid.[16] This oriented film was prepared by roll casting and annealing a PS−PI−PS triblock. The roll casting process yielded a metastable, aligned HEX mesostructure, and subsequent annealing nucleated and epitaxially grew an equilibrium gyroid morphology with the [111] direction oriented along the cylinder axes.[142,16] This gyroid-containing film was subjected to tensile tests both along and transverse to the [111] direction.[16] The stress−strain curves obtained from these orthogonal directions were markedly different, as shown in Figure 27, indicating that the gyroid exhibits an anisotropic mechanical response. E' had a magnitude of 50 MPa along the [111] direction, but only 10 MPa in the transverse direction. Additionally, the sample necked and exhibited a strong Mullins effect when deformed in the [111] direction but did not neck and only had a weak Mullins effect when stretched in the transverse direction. Dair et al. examined skeletal models of the PS struts and concluded that these mechanical responses were consistent with the PS carrying

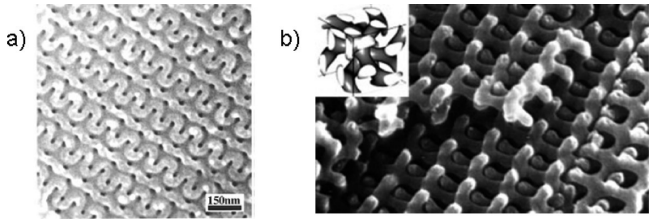

Figure 28. SEM micrographs of nanoporous (a) PS matrix and (b) PS networks following the degradation and removal of the PI chains from gyroid-forming PS−PI diblock copolymers. (a) Reproduced from ref 107. (b) Reproduced with permission from ref 37. Copyright 2002 Wiley-VCH Verlag GmbH & Co.

more of the deformation in the [111] direction and less in the transverse direction. The polygranular isotropic sample exhibited a mechanical response between those of the [111] and transverse deformations because it contained grains with these two extreme, as well as many intermediate, orientations.[16]

Several other groups[143,144,253] have published papers that confirmed one of Dair et al.'s[15] findings and disputed another. Sakurai et al. studied the mechanical properties of PS−PB−PS triblock copolymers with $f_S < 0.35$ that formed HEX, gyroid, and LAM.[144,253] Neither the failure stress nor the strain at break was sensitive to the underlying morphology, but E' was; samples containing the gyroid had E' values ~3 times as large as those containing HEX,[144,253] a result in qualitative agreement with both Dair et al.'s[15] and Alward and co-workers'[58,60] earlier reports. Qiao et al. measured the elastic moduli of PI−PS−PI triblock copolymers and were the first to truly isolate the effects of morphology from factors such as molecular weight and composition.[143] They produced HEX, LAM, and gyroid morphologies from the same PI−PS−PI specimen (M_n = 95 kg/mol, PS wt % = 0.38) by solvent casting the polymer from solvents of varying selectivity. The sample containing the gyroid had an E' that was ~3 times higher than that of the HEX-containing specimen, in good agreement with previous reports.[15,58,60,144,253] The aspect of these reports that was not qualitatively consistent was the magnitude of E' of gyroid (E_G') relative to E' of LAM (E_L'). Dair et al. reported that E_L' was ~4 times *larger* than E_G',[15] Sakurai et al. measured essentially equivalent E_L' and E_G' values,[144,253] and Qiao et al. reported that E_L' was ~2 times *smaller* than E_G'.[143] It is not clear why these relative values differ, although the orientation of LAM and/or gyroid grains may have played a role; both E_G'[16] and E_L'[254] can vary by a factor of ~5 depending on the orientation of the respective mesostructures.

Meuler et al. recently investigated the mechanical properties of network-containing PEO−PS−PI−PS−PEO pentablock terpolymers.[192] They used tensile testing to probe the fracture properties of a number of PEO−PS−PI−PS−PEO pentablock samples, all of which were prepared from the same parent PS−PI−PS triblock. This PS−PI−PS core was designed to impart toughness, while the terminal PEO blocks could potentially provide functionality. Two PEO−PS−PI−PS−PEO specimens had terminal PEO block fractional crystallinities above 0.27: one contained LAM_3 and the other the O[70] network. Phatak and colleagues had previously studied LAM-forming multiblock copolymers that were comprised of a tough triblock core and semicrystalline termini; these materials failed in a brittle fashion for terminal block fractional crystallinities ranging from 0.21 to 0.27.[255] The PEO−PS−PI−PS−PEO materials had fractional crystallinities that exceeded this threshold established by Phatak et al., and the LAM_3-containing specimen failed in a brittle

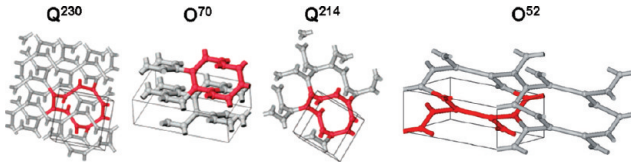

Figure 29. Ball and stick models for the Q^{230}, O^{70}, Q^{214}, and O^{52} (10,3) network lattices that have been definitively identified in block polymer materials. The Q^{230}, O^{70}, and Q^{214} lattices are reproduced from ref 177, and the O^{52} model is reproduced with permission from ref 199. Copyright 2009 The Royal Society of Chemistry.

Table 4. Abbreviations for All of the Polymers Discussed in This Review

polymer	abbreviation
polystyrene	PS
polyisoprene	PI
poly(vinyl methyl ether)	PVME
poly(2-vinylpyridine)	P2VP
poly(4-vinylpyridine)	P4VP
poly(ethylene oxide)	PEO
poly(butylene oxide)	PBO
polydimethylsiloxane	PDMS
polylactide	PLA
poly(ethylene-*alt*-propylene)	PEP
polyethylethylene	PEE
polyethylene	PE
polycyclohexylethylene	PCHE
poly(4-fluorostyrene)	P4FS
polystyrenesulfonate	PSS
polymethylbutylene	PMB
poly(1,1′-ferrocenyldimethylsilane)	PFCDMS
poly(methyl methacrylate)	PMMA
poly(pentamethyldisilylstyrene)	PPMDS
poly(*N*-isopropylacrylamide)	PNIPAM
poly(*tert*-butyl methacrylate)	PtBMA
poly(propylene oxide)	PPO

fashion at a strain of 0.06,[192] a result reminiscent of Phatak et al.'s earlier work.[255] The O^{70}-containing sample, in contrast, was quite tough, yielding and deforming prior to failing at a strain of 1.3 and a stress of 4.2 MPa. Meuler et al. attributed this toughness to the network morphology. Unlike LAM_3, O^{70} does not contain any fragile PEO bilayers, and a crack initiated in the PEO domain would have to break the tough PS−PI−PS subdomain at every unit cell in order to propagate through the material. Meuler et al. suggested that materials with tough cores and fragile bilayers could be toughened by wrapping the bilayers into a 3-D network.[192]

Applications

A number of publications have focused on potential applications of the multiply continuous network morphologies formed by block polymers. Hashimoto et al. prepared the first nanoporous structure from a gyroid precursor in 1997.[107] The PI domains in a gyroid-forming PS−PI diblock copolymer were removed via ozonolysis; an SEM micrograph of the resulting nanoporous structure is provided in Figure 28a. The nanochannels in this structure were nonelectrolytically plated with nickel metal by following a detailed procedure, and Hashimoto et al. suggested this nickel metal could act as a catalyst on the high surface area, nanoporous gyroid support.[107] Nanoporous mesostructures have subsequently been prepared from a variety of gyroid-forming block copolymers. PI chains were removed from PS-PI,[108] P2VP-PI,[108] and PI-PPMDS-PI[147] networks by ozonolysis and from PS−PI diblocks via exposure to ultraviolet radiation,[37] PLA and PEO domains were removed from PS−PLA and PS−PEO network materials, respectively, via treatment with hydroiodic acid,[122] PDMS chains were removed from PS−PDMS specimens by treatment with hydrofluoric acid,[121] and PLA domains were removed from P4FS−PLA samples by exposure to sodium hydroxide.[22,23]

Photonic crystals,[37] hybrid solar cells,[22,23] and ceramic membranes[126,147,256−258] have been prepared using nanoporous block polymer networks. Photonic materials in some butterfly wings have a structure that can be modeled using the gyroid,[259] and detailed calculations suggested that the gyroid is an effective morphology for making photonic crystals, provided the structural features are commensurate with the wavelength of visible light.[29,31−34,36] Urbas et al. prepared a high molecular weight ($M_n \sim 750$ kg/mol, PS wt % = 0.38), gyroid-forming PS−PI diblock copolymer to obtain features on this length scale.[37] Both the intact PS−PI gyroid and the nanoporous PS networks were tested as photonic crystals, proving that network-forming block copolymers can act as photonic materials.[37] Network mesostructures are especially appealing for solar cell applications because they contain multiply continuous domains, and such an interdigitation of continuous donor and acceptor layers is expected to facilitate the separation and extraction of free charges and maximize solar cell efficiency.[21] Crossland et al. used a gyroid-forming P4FS−PLA diblock copolymer as a sacrificial template in the fabrication of dye-sensitized hybrid solar cells[22] whose performance was competitive with optimized, state-of-the-art nanoparticle-based dye-sensitized solar cells.[47] Devices prepared from a gyroid precursor performed better than those prepared from a HEX template, likely a result of the continuity of the donating and accepting channels and the high surface area of the interfaces that were established by the gyroid template.[23] Other studies focused on solar cells prepared from poorly ordered, network-like block copolymer films.[19,20] High surface area nanoporous ceramic films are generally solvent resistant, exhibit good high-temperature chemical and dimensional stability, and could find utility in separations, catalysis, or photonic crystal applications.[147] Ceramic gyroid[126,147,256,257] and plumber's nightmare[258] network mesostructures have been prepared from block copolymer precursors using a sol−gel process.

Concluding Remarks

While cubic network lattices with 3-fold (*n*,3), 4-fold (*n*,4), and 6-fold (*n*,6) connectivity have been reported in low molecular weight surfactant systems,[51−54] the Q^{230}, Q^{214}, O^{70}, and O^{52} block polymer network morphologies described in the previous sections are all characterized by 3-fold-coordinated network lattices; representations of these lattices are provided in Figure 29. Wells identified 30 different network lattices containing 3-fold connectors: one (12,3) net, seven (10,3) nets, three (9,3) nets, 15 (8,3) nets, and four (7,3) nets.[55] The block polymer network mesostructures are characterized by only three of these (10,3) nets: (10,3)a (Q^{230} and Q^{214}), (10,3)c (O^{70}), and (10,3)d (O^{52}).[187] To the best of our knowledge, the existence of a network mesostructure with 4-fold or 6-fold connectors has not been definitively demonstrated in purely polymeric materials.

An open and fascinating question is whether additional network lattices will be identified in block polymer materials, particularly those with complicated architectures (e.g., an ABCD tetrablock), in the coming years. Bates and colleagues have postulated that chain stretching (entropic) considerations, which play only a minor role in surfactant systems, are primarily responsible for the different network morphologies, and 3-fold connectors in particular, found in block polymers.[177,187] The 3-fold connectors (also called "Y-junctions") have a larger angle between struts (120°) than either the 4-fold (109.5°) or 6-fold (90°) connectors. The relatively expansive opening presumably minimizes chain crowding and thus conformational restrictions at the domain interfaces near the 3-fold connectors.[177,187] The 3-fold

connectors also have less variation in both interfacial curvature and domain thickness than the higher order connectors;[187] these factors presumably alleviate packing frustration.[86] A thermodynamic preference for 3-fold connectors would limit the number of possible cubic network mesostructures and may be responsible for the formation of the orthorhombic network morphologies in block polymers.[177] These geometric arguments, while not accounting for detailed molecular factors, are intuitively appealing and suggest that 3-fold connectors may be common structural elements in other polymer systems. The fact that 3-fold connectors have been identified as a component of the disorganized network structures formed in aqueous block copolymer surfactant systems[260,261] supports this reasoning.

Relief of packing frustration may prove critical in the formation of network morphologies that contain lattices with higher order connectors. These mesostructures could prove important in applications that are sensitive to 3-D order. For example, a 4-fold-connected OTDD structure may exhibit a robust band gap that would make it an effective photonic crystal.[35] There are a number of possible avenues for alleviating packing frustration. Numerous theoretical analyses have suggested that the addition of a constituent homopolymer can mitigate packing frustration and stabilize network morphologies such as OBDD,[81−83,85] OTDD,[166] and plumber's nightmare.[83,85,166] These predictions have not, to the best of our knowledge, been verified in experimental block polymer materials, although the addition of a silica precursor to PI−PEO diblock copolymers may have stabilized plumber's nightmare in the hybrid material by reducing packing frustration.[126,258] Selective tuning of block polydispersity,[97,185,186,236,237] asymmetric molecular design,[199] and the tethering of nanoparticles[262−264] are other reported methods for alleviating packing frustration and stabilizing network morphologies. It remains to be seen if these, or any other strategies, prove to be effective tools for stabilizing block polymer based mesostructures characterized by higher order network lattices.

Acknowledgment. Support for this project was provided by the National Science Foundation (DMR-0704192). We thank Jian Qin for useful discussions, thank Eric W. Cochran for providing the software used to generate Figure 2, and thank Michael J. Bluemle for assistance in operating this software.

References and Notes

(1) Szwarc, M. *Nature* **1956**, *178*, 1168–1169.
(2) Inoue, T.; Soen, T.; Hashimoto, T.; Kawai, H. *J. Polym. Sci., Polym. Phys. Ed.* **1969**, *7*, 1283–1301.
(3) Gervais, M.; Gallot, B. *Makromol. Chem.* **1973**, *171*, 157–178.
(4) Hashimoto, T.; Nagatoshi, K.; Todo, A.; Hasegawa, H.; Kawai, H. *Macromolecules* **1974**, *7*, 364–373.
(5) Helfand, E. *Macromolecules* **1975**, *8*, 552–556.
(6) Helfand, E.; Wasserman, Z. R. *Macromolecules* **1976**, *9*, 879–888.
(7) Leibler, L. *Macromolecules* **1980**, *13*, 1602–1617.
(8) Lynd, N. A.; Meuler, A. J.; Hillmyer, M. A. *Prog. Polym. Sci.* **2008**, *33*, 875–893.
(9) Bates, F. S.; Fredrickson, G. H. *Annu. Rev. Phys. Chem.* **1990**, *41*, 525–557.
(10) Matsen, M. W. *J. Phys.: Condens. Matter* **2002**, *14*, R21–R47.
(11) Khandpur, A. K.; Förster, S.; Bates, F. S.; Hamley, I. W.; Ryan, A. J.; Bras, W.; Almdal, K.; Mortensen, K. *Macromolecules* **1995**, *28*, 8796–8806.
(12) Matsen, M. W.; Bates, F. S. *Macromolecules* **1996**, *29*, 1091–1098.
(13) Cochran, E. W.; Garcia-Cervera, C. J.; Fredrickson, G. H. *Macromolecules* **2006**, *39*, 2449–2451.
(14) Potschke, P.; Paul, D. R. *J. Macromol. Sci., Polym. Rev.* **2003**, *C43*, 87–141.
(15) Dair, B. J.; Honeker, C. C.; Alward, D. B.; Avgeropoulos, A.; Hadjichristidis, N.; Fetters, L. J.; Capel, M.; Thomas, E. L. *Macromolecules* **1999**, *32*, 8145–8152.
(16) Dair, B. J.; Avgeropoulos, A.; Hadjichristidis, N.; Thomas, E. L. *J. Mater. Sci.* **2000**, *35*, 5207–5213.
(17) Pernot, H.; Baumert, M.; Court, F.; Leibler, L. *Nat. Mater.* **2002**, *1*, 54–58.
(18) Shefelbine, T. A.; Vigild, M. E.; Matsen, M. W.; Hajduk, D. A.; Hillmyer, M. A.; Cussler, E. L.; Bates, F. S. *J. Am. Chem. Soc.* **1999**, *121*, 8457–8465.
(19) Wang, H.; Oey, C. C.; Djurisic, A. B.; Xie, M. H.; Leung, Y. H.; Man, K. K. Y.; Chan, W. K.; Pandey, A.; Nunzi, J.-M.; Chui, P. C. *Appl. Phys. Lett.* **2005**, *87*, 023507/1–023507/3.
(20) Oey, C. C.; Djurisic, A. B.; Wang, H.; Man, K. K. Y.; Chan, W. K.; Xie, M. H.; Leung, Y. H.; Pandey, A.; Nunzi, J.-M.; Chui, P. C. *Nanotechnology* **2006**, *17*, 706–713.
(21) Yang, X.; Loos, J. *Macromolecules* **2007**, *40*, 1353–1362.
(22) Crossland, E. J. W.; Kamperman, M.; Nedelcu, M.; Ducati, C.; Wiesner, U.; Smilgies, D.; Toombes, G. E. S.; Hillmyer, M. A.; Ludwigs, S.; Steiner, U.; Snaith, H. J. *Nano Lett.*, **2009**, *9*, 2807−2812.
(23) Crossland, E. J. W.; Nedelcu, M.; Ducati, C.; Ludwigs, S.; Hillmyer, M. A.; Steiner, U.; Snaith, H. J. *Nano Lett.*, **2009**, *9*, 2813−2819.
(24) Yang, S. Y.; Ryu, I.; Kim, H. Y.; Kim, J. K.; Jang, S. K.; Russell, T. P. *Adv. Mater.* **2006**, *18*, 709–712.
(25) Phillip, W. A.; Rzayev, J.; Hillmyer, M. A.; Cussler, E. L. *J. Membr. Sci.* **2006**, *286*, 144–152.
(26) Phillip, W. A.; Amendt, M.; O'Neill, B.; Chen, L.; Hillmyer, M. A.; Cussler, E. L. *ACS Appl. Mater. Interfaces* **2009**, *1*, 472–480.
(27) Cho, B.-K.; Jain, A.; Gruner, S. M.; Wiesner, U. *Science* **2004**, *305*, 1598–1601.
(28) Lin, S. Y.; Fleming, J. G.; Hetherington, D. L.; Smith, B. K.; Biswas, R.; Ho, K. M.; Sigalas, M. M.; Zubrzycki, W.; Kurtz, S. R.; Bur, J. *Nature* **1998**, *394*, 251–253.
(29) Martín-Moreno, L.; Garcia-Vidal, F. J.; Somoza, A. M. *Phys. Rev. Lett.* **1999**, *83*, 73–75.
(30) Campbell, M.; Sharp, D. N.; Harrison, M. T.; Denning, R. G.; Turberfield, A. J. *Nature* **2000**, *404*, 53–56.
(31) Babin, V.; Garstecki, P.; Holyst, R. *Phys. Rev. B: Condens. Matter* **2002**, *66*, 235120/1–235120/9.
(32) Maldovan, M.; Urbas, A. M.; Yufa, N.; Carter, W. C.; Thomas, E. L. *Phys. Rev. B: Condens. Matter* **2002**, *65*, 165123/1–165123/5.
(33) Maldovan, M.; Carter, W. C.; Thomas, E. L. *Appl. Phys. Lett.* **2003**, *83*, 5172–5174.
(34) Maldovan, M.; Ullal, C. K.; Carter, W. C.; Thomas, E. L. *Nat. Mater.* **2003**, *2*, 664–667.
(35) Maldovan, M.; Thomas, E. L. *Nat. Mater.* **2004**, *3*, 593–600.
(36) Michielsen, K.; Kole, J. S. *Phys. Rev. B: Condens. Matter* **2003**, *68*, 115107/1–115107/13.
(37) Urbas, A. M.; Maldovan, M.; DeRege, P.; Thomas, E. L. *Adv. Mater.* **2002**, *14*, 1850–1853.
(38) Scriven, L. E. *Nature* **1976**, *263*, 123–125.
(39) Bates, F. S.; Maurer, W. W.; Lipic, P. M.; Hillmyer, M. A.; Almdal, K.; Mortensen, K.; Fredrickson, G. H.; Lodge, T. P. *Phys. Rev. Lett.* **1997**, *79*, 849–852.
(40) Ellison, C. J.; Meuler, A. J.; Qin, J.; Evans, C. M.; Wolf, L. M.; Bates, F. S. *J. Phys. Chem. B* **2009**, *113*, 3726–3737.
(41) Liu, G.; Stoykovich, M. P.; Ji, S.; Stuen, K. O.; Craig, G. S. W.; Nealey, P. F. *Macromolecules* **2009**, *42*, 3063–3072.
(42) Court, F.; Yamaguchi, D.; Hashimoto, T. *Macromolecules* **2006**, *39*, 2596–2605.
(43) Chen, L.; Phillip, W. A.; Cussler, E. L.; Hillmyer, M. A. *J. Am. Chem. Soc.* **2007**, *129*, 13786–13787.
(44) Thomas, E. L.; Alward, D. B.; Kinning, D. J.; Martin, D. C.; Handlin, D. L. , Jr.; Fetters, L. J. *Macromolecules* **1986**, *19*, 2197–2202.
(45) Hajduk, D. A.; Harper, P. E.; Gruner, S. M.; Honeker, C. C.; Kim, G.; Thomas, E. L.; Fetters, L. J. *Macromolecules* **1994**, *27*, 4063–4075.
(46) Schulz, M. F.; Bates, F. S.; Almdal, K.; Mortensen, K. *Phys. Rev. Lett.* **1994**, *73*, 86–89.
(47) Snaith, H. J.; Schmidt-Mende, L. *Adv. Mater.* **2007**, *19*, 3187–3200.
(48) Hyde, S. T. *Acta Crystallogr., Sect. A: Found. Crystallogr.* **1994**, *A50*, 753–759.
(49) O'Neill, B. *Elementary Differential Geometry*; 2nd revised ed.; Academic Press: New York, 2006.
(50) Meier, W. M.; Olson, D. H. *Atlas of Zeolite Structure Types*; Butterworth-Heinemann: London, 1992.
(51) Luzzati, V.; Spegt, P. A. *Nature* **1967**, *215*, 701–704.
(52) Mariani, P.; Luzzati, V.; Delacroix, H. *J. Mol. Biol.* **1988**, *204*, 165–189.

(53) Seddon, J. M. *Biochim. Biophys. Acta* **1990**, *1031*, 1–69.
(54) Fontell, K. *Colloid Polym. Sci.* **1990**, *268*, 264–285.
(55) Wells, A. F. *Three-Dimensional Nets and Polyhedra*; John Wiley & Sons: New York, 1977.
(56) Schoen, A. H. NASA TN D-5541, **1970**.
(57) Anderson, D. M.; Davis, H. T.; Scriven, L. E.; Nitsche, J. C. C. *Adv. Chem. Phys.* **1990**, *77*, 337–396.
(58) Alward, D. B.; Kinning, D. J.; Thomas, E. L.; Fetters, L. J. *Macromolecules* **1986**, *19*, 215–224.
(59) Aggarwal, S. L. *Polymer* **1976**, *17*, 938–956.
(60) Kinning, D. J.; Thomas, E. L.; Alward, D. B.; Fetters, L. J.; Handlin, D. L. , Jr. *Macromolecules* **1986**, *19*, 1288–1290.
(61) Herman, D. S.; Kinning, D. J.; Thomas, E. L.; Fetters, L. J. *Macromolecules* **1987**, *20*, 2940–2942.
(62) Hajduk, D. A.; Harper, P. E.; Gruner, S. M.; Honeker, C. C.; Thomas, E. L.; Fetters, L. J. *Macromolecules* **1995**, *28*, 2570–2573.
(63) Hasegawa, H.; Tanaka, H.; Yamasaki, K.; Hashimoto, T. *Macromolecules* **1987**, *20*, 1651–1662.
(64) Hahn, T., Ed. *International Tables for Crystallography*, 4th revised ed.; Kluwer Academic: Boston, 1994; Vol. *A*.
(65) Thomas, E. L.; Anderson, D. M.; Henkee, C. S.; Hoffman, D. *Nature* **1988**, *334*, 598–601.
(66) Winey, K. I.; Thomas, E. L.; Fetters, L. J. *Macromolecules* **1992**, *25*, 422–428.
(67) Spontak, R. J.; Smith, S. D.; Ashraf, A. *Macromolecules* **1993**, *26*, 956–962.
(68) Spontak, R. J.; Smith, S. D.; Ashraf, A. *Microsc. Res. Tech.* **1994**, *27*, 412–419.
(69) Xie, R.; Yang, B.; Jiang, B. *Macromolecules* **1993**, *26*, 7097–7099.
(70) Wang, Z. G.; Safran, S. A. *Europhys. Lett.* **1990**, *11*, 425–430.
(71) Anderson, D. M.; Thomas, E. L. *Macromolecules* **1988**, *21*, 3221–3230.
(72) Likhtman, A. E.; Semenov, A. N. *Macromolecules* **1994**, *27*, 3103–3106.
(73) Olmsted, P. D.; Milner, S. T. *Phys. Rev. Lett.* **1994**, *72*, 936–939.
(74) Olmsted, P. D.; Milner, S. T. *Phys. Rev. Lett.* **1995**, *74*, 829.
(75) Semenov, A. N. *Sov. Phys. JETP* **1985**, *61*, 733–742.
(76) Matsen, M. W.; Schick, M. *Phys. Rev. Lett.* **1994**, *72*, 2660–2663.
(77) Gobran, D. A. Doctoral Thesis, Department of Chemical Engineering, University of Massachusetts, Amherst, MA, **1990**.
(78) Koppi, K. A.; Tirrell, M.; Bates, F. S. *Phys. Rev. Lett.* **1993**, *70*, 1449–1452.
(79) Matsen, M. W.; Schick, M. *Macromolecules* **1994**, *27*, 7157–7163.
(80) Matsen, M. W.; Schick, M. *Macromolecules* **1994**, *27*, 6761–6767.
(81) Matsen, M. W. *Phys. Rev. Lett.* **1995**, *74*, 4225–4228.
(82) Matsen, M. W. *Macromolecules* **1995**, *28*, 5765–5773.
(83) Martínez-Veracoechea, F. J.; Escobedo, F. A. *Macromolecules* **2007**, *40*, 7354–7365.
(84) Huse, D. A.; Leibler, S. *J. Phys.* (*Paris*) **1988**, *49*, 605–620.
(85) Martínez-Veracoechea, F. J.; Escobedo, F. A. *Macromolecules* **2009**, *42*, 1775–1784.
(86) Matsen, M. W.; Bates, F. S. *Macromolecules* **1996**, *29*, 7641–7644.
(87) Matsen, M. W.; Bates, F. S. *J. Chem. Phys.* **1997**, *106*, 2436–2448.
(88) Gruner, S. M. *J. Phys. Chem.* **1989**, *93*, 7562–7570.
(89) Jinnai, H.; Nishikawa, Y.; Spontak, R. J.; Smith, S. D.; Agard, D. A.; Hashimoto, T. *Phys. Rev. Lett.* **2000**, *84*, 518–521.
(90) Matsen, M. W. *J. Chem. Phys.* **2000**, *113*, 5539–5544.
(91) Matsen, M. W.; Bates, F. S. *J. Polym. Sci., Part B* **1997**, *35*, 945–952.
(92) Matsen, M. W.; Thompson, R. B. *J. Chem. Phys.* **1999**, *111*, 7139–7146.
(93) Nonomura, M.; Yamada, K.; Ohta, T. *J. Phys.: Condens. Matter* **2003**, *15*, L423–L430.
(94) Podariu, I.; Chakrabarti, A. *J. Chem. Phys.* **2003**, *118*, 11249–11257.
(95) Sun, P.; Yin, Y.; Li, B.; Chen, T.; Jin, Q.; Ding, D.; Shi, A. *Phys. Rev. E: Stat., Nonlinear, Soft Matter Phys.* **2005**, *72*, 061408/1–061408/6.
(96) Abu-Sharkh, B.; AlSunaidi, A. *Macromol. Theory Simul.* **2006**, *15*, 507–515.
(97) Martínez-Veracoechea, F. J.; Escobedo, F. A. *Macromolecules* **2005**, *38*, 8522–8531.
(98) Martínez-Veracoechea, F. J.; Escobedo, F. A. *J. Chem. Phys.* **2006**, *125*, 104907/1–104907/12.
(99) Ranjan, A.; Qin, J.; Morse, D. C. *Macromolecules* **2008**, *41*, 942–954.
(100) Tselikas, Y.; Hadjichristidis, N.; Lescanec, R. L.; Honeker, C. C.; Wohlgemuth, M.; Thomas, E. L. *Macromolecules* **1996**, *29*, 3390–3396.
(101) Förster, S.; Khandpur, A. K.; Zhao, J.; Bates, F. S.; Hamley, I. W.; Ryan, A. J.; Bras, W. *Macromolecules* **1994**, *27*, 6922–6935.
(102) Spontak, R. J.; Fung, J. C.; Braunfeld, M. B.; Sedat, J. W.; Agard, D. A.; Kane, L.; Smith, S. D.; Satkowski, M. M.; Ashraf, A.; Hajduk, D. A.; Gruner, S. M. *Macromolecules* **1996**, *29*, 4494–4507.
(103) Sakurai, S.; Umeda, H.; Furukawa, C.; Irie, H.; Nomura, S.; Hyun Lee, H.; Kon Kim, J. *J. Chem. Phys.* **1998**, *108*, 4333–4339.
(104) Sakurai, S.; Irie, H.; Umeda, H.; Nomura, S.; Lee, H. H.; Kim, J. K. *Macromolecules* **1998**, *31*, 336–343.
(105) Park, S.; Cho, D.; Ryu, J.; Kwon, K.; Lee, W.; Chang, T. *Macromolecules* **2002**, *35*, 5974–5979.
(106) Park, I.; Lee, B.; Ryu, J.; Im, K.; Yoon, J.; Ree, M.; Chang, T. *Macromolecules* **2005**, *38*, 10532–10536.
(107) Hashimoto, T.; Tsutsumi, K.; Funaki, Y. *Langmuir* **1997**, *13*, 6869–6872.
(108) Hashimoto, T.; Nishikawa, Y.; Tsutsumi, K. *Macromolecules* **2007**, *40*, 1066–1072.
(109) Hwang, J.; Huh, J.; Jung, B.; Hong, J.; Park, M.; Park, C. *Polymer* **2005**, *46*, 9133–9143.
(110) Mareau, V. H.; Matsushita, T.; Nakamura, E.; Hasegawa, H. *Macromolecules* **2007**, *40*, 6916–6921.
(111) Mareau, V. H.; Akasaka, S.; Osaka, T.; Hasegawa, H. *Macromolecules* **2007**, *40*, 9032–9039.
(112) Takenaka, M.; Wakada, T.; Akasaka, S.; Nishitsuji, S.; Saijo, K.; Shimizu, H.; Kim, M. I.; Hasegawa, H. *Macromolecules* **2007**, *40*, 4399–4402.
(113) Chen, F.; Kondo, Y.; Hashimoto, T. *Macromolecules* **2007**, *40*, 3714–3723.
(114) Kim, M. I.; Wakada, T.; Akasaka, S.; Nishitsuji, S.; Saijo, K.; Hasegawa, H.; Ito, K.; Takenaka, M. *Macromolecules* **2008**, *41*, 7667–7670.
(115) Kim, M. I.; Wakada, T.; Akasaka, S.; Nishitsuji, S.; Saijo, K.; Hasegawa, H.; Ito, K.; Takenaka, M. *Macromolecules* **2009**, *42*, 5266–5271.
(116) Schulz, M. F.; Khandpur, A. K.; Bates, F. S.; Almdal, K.; Mortensen, K.; Hajduk, D. A.; Gruner, S. M. *Macromolecules* **1996**, *29*, 2857–2867.
(117) Valkama, S.; Ruotsalainen, T.; Nykaenen, A.; Laiho, A.; Kosonen, H.; ten Brinke, G.; Ikkala, O.; Ruokolainen, J. *Macromolecules* **2006**, *39*, 9327–9336.
(118) Okumura, A.; Nishikawa, Y.; Hashimoto, T. *Polymer* **2006**, *47*, 7805–7812.
(119) Hamley, I. W.; Fairclough, J. P. A.; Ryan, A. J.; Mai, S.-M.; Booth, C. *Phys. Chem. Chem. Phys.* **1999**, *1*, 2097–2101.
(120) Xu, J.; Turner, S. C.; Fairclough, J. P. A.; Mai, S.; Ryan, A. J.; Chaibundit, C.; Booth, C. *Macromolecules* **2002**, *35*, 3614–3621.
(121) Ndoni, S.; Vigild, M. E.; Berg, R. H. *J. Am. Chem. Soc.* **2003**, *125*, 13366–13367.
(122) Mao, H.; Hillmyer, M. A. *Soft Matter* **2006**, *2*, 57–59.
(123) Floudas, G.; Ulrich, R.; Wiesner, U. *J. Chem. Phys.* **1999**, *110*, 652–663.
(124) Floudas, G.; Ulrich, R.; Wiesner, U.; Chu, B. *Europhys. Lett.* **2000**, *50*, 182–188.
(125) Floudas, G.; Vazaiou, B.; Schipper, F.; Ulrich, R.; Wiesner, U.; Iatrou, H.; Hadjichristidis, N. *Macromolecules* **2001**, *34*, 2947–2957.
(126) Toombes, G. E. S.; Finnefrock, A. C.; Tate, M. W.; Ulrich, R.; Wiesner, U.; Gruner, S. M. *Macromolecules* **2007**, *40*, 8974–8982.
(127) Almdal, K.; Mortensen, K.; Ryan, A. J.; Bates, F. S. *Macromolecules* **1996**, *29*, 5940–5947.
(128) Bates, F. S.; Schulz, M. F.; Khandpur, A. K.; Förster, S.; Rosedale, J. H.; Almdal, K.; Mortensen, K. *Faraday Discuss.* **1994**, 7–18.
(129) Kossuth, M. B.; Morse, D. C.; Bates, F. S. *J. Rheol.* **1999**, *43*, 167–196.
(130) Lynd, N. A.; Hillmyer, M. A. *Macromolecules* **2005**, *38*, 8803–8810.
(131) Vigild, M. E.; Almdal, K.; Mortensen, K.; Hamley, I. W.; Fairclough, J. P. A.; Ryan, A. J. *Macromolecules* **1998**, *31*, 5702–5716.
(132) Hillmyer, M. A.; Bates, F. S.; Almdal, K.; Mortensen, K.; Ryan, A. J.; Fairclough, J. P. A. *Science* **1996**, *271*, 976–978.
(133) Hajduk, D. A.; Takenouchi, H.; Hillmyer, M. A.; Bates, F. S.; Vigild, M. E.; Almdal, K. *Macromolecules* **1997**, *30*, 3788–3795.

(134) Hajduk, D. A.; Kossuth, M. B.; Hillmyer, M. A.; Bates, F. S. *J. Phys. Chem. B* **1998**, *102*, 4269–4276.
(135) Zhao, J.; Majumdar, B.; Schulz, M. F.; Bates, F. S.; Almdal, K.; Mortensen, K.; Hajduk, D. A.; Gruner, S. M. *Macromolecules* **1996**, *29*, 1204–1215.
(136) Davidock, D. A.; Hillmyer, M. A.; Lodge, T. P. *Macromolecules* **2003**, *36*, 4682–4685.
(137) Davidock, D. A.; Hillmyer, M. A.; Lodge, T. P. *Macromolecules* **2004**, *37*, 397–407.
(138) Park, M. J.; Balsara, N. P. *Macromolecules* **2008**, *41*, 3678–3687.
(139) Kloninger, C.; Rehahn, M. *Macromolecules* **2004**, *37*, 8319–8324.
(140) Laurer, J. H.; Hajduk, D. A.; Fung, J. C.; Sedat, J. W.; Smith, S. D.; Gruner, S. M.; Agard, D. A.; Spontak, R. J. *Macromolecules* **1997**, *30*, 3938–3941.
(141) Avgeropoulos, A.; Dair, B. J.; Hadjichristidis, N.; Thomas, E. L. *Macromolecules* **1997**, *30*, 5634–5642.
(142) Dair, B. J.; Avgeropoulos, A.; Hadjichristidis, N.; Capel, M.; Thomas, E. L. *Polymer* **2000**, *41*, 6231–6236.
(143) Qiao, L.; Leibig, C.; Hahn, S. F.; Winey, K. I. *Ind. Eng. Chem. Res.* **2006**, *45*, 5598–5602.
(144) Sakurai, S.; Isobe, D.; Okamoto, S.; Nomura, S. *Mater. Sci. Res. Int.* **2001**, *7*, 225–228.
(145) Sakurai, S.; Isobe, D.; Okamoto, S.; Yao, T.; Nomura, S. *Phys. Rev. E: Stat., Nonlinear, Soft Matter Phys.* **2001**, *63*, 061803/1–061803/5.
(146) Avgeropoulos, A.; Chan, V. Z.-H.; Lee, V. Y.; Ngo, D.; Miller, R. D.; Hadjichristidis, N.; Thomas, E. L. *Chem. Mater.* **1998**, *10*, 2109–2115.
(147) Chan, V. Z.-H.; Hoffman, J.; Lee, V. Y.; Latrou, H.; Avgeropoulos, A.; Hadjichristidis, N.; Miller, R. D.; Thomas, E. L. *Science* **1999**, *286*, 1716–1719.
(148) Nykaenen, A.; Nuopponen, M.; Laukkanen, A.; Hirvonen, S.; Rytelae, M.; Turunen, O.; Tenhu, H.; Mezzenga, R.; Ikkala, O.; Ruokolainen, J. *Macromolecules* **2007**, *40*, 5827–5834.
(149) Likhtman, A. E.; Semenov, A. N. *Macromolecules* **1997**, *30*, 7273–7278.
(150) Olmsted, P. D.; Milner, S. T. *Macromolecules* **1998**, *31*, 4011–4022.
(151) Lipic, P. M.; Bates, F. S.; Matsen, M. W. *J. Polym. Sci., Part B* **1999**, *37*, 2229–2238.
(152) Matsen, M. W. *Phys. Rev. Lett.* **1998**, *80*, 4470–4473.
(153) Wang, C.; Lodge, T. P. *Macromol. Rapid Commun.* **2002**, *23*, 49–54.
(154) Wang, C.; Lodge, T. P. *Macromolecules* **2002**, *35*, 6997–7006.
(155) Chastek, T. Q.; Lodge, T. P. *Macromolecules* **2003**, *36*, 7672–7680.
(156) Ahn, J.; Zin, W. *Macromol. Res.* **2003**, *11*, 152–156.
(157) Park, H.; Jung, J.; Chang, T.; Matsunaga, K.; Jinnai, H. *J. Am. Chem. Soc.* **2009**, *131*, 46–47.
(158) Bates, F. S.; Fredrickson, G. H. *Phys. Today* **1999**, *52*, 32–38.
(159) Mogi, Y.; Kotsuji, H.; Kaneko, Y.; Mori, K.; Matsushita, Y.; Noda, I. *Macromolecules* **1992**, *25*, 5408–5411.
(160) Mogi, Y.; Mori, K.; Matsushita, Y.; Noda, I. *Macromolecules* **1992**, *25*, 5412–5415.
(161) Mogi, Y.; Nomura, M.; Kotsuji, H.; Ohnishi, K.; Matsushita, Y.; Noda, I. *Macromolecules* **1994**, *27*, 6755–6760.
(162) Matsen, M. W. *J. Chem. Phys.* **1998**, *108*, 785–796.
(163) Bailey, T. S.; Pham, H. D.; Bates, F. S. *Macromolecules* **2001**, *34*, 6994–7008.
(164) Phan, S.; Fredrickson, G. H. *Macromolecules* **1998**, *31*, 59–63.
(165) Dotera, T.; Hatano, A. *J. Chem. Phys.* **1996**, *105*, 8413–8427.
(166) Dotera, T. *Phys. Rev. Lett.* **2002**, *89*, 205502/1–205502/4.
(167) Xi, H.; Milner, S. T. *Macromolecules* **1996**, *29*, 2404–2411.
(168) Verdier, P. H.; Stockmayer, W. H. *J. Chem. Phys.* **1962**, *36*, 227–235.
(169) Matsushita, Y.; Suzuki, J.; Seki, M. *Physica B* **1998**, *248*, 238–242.
(170) Matsushita, Y.; Torikai, N.; Suzuki, J.; Seki, M. *J. Phys. Chem. Solids* **1999**, *60*, 1279–1284.
(171) Seki, M.; Suzuki, J.; Matsushita, Y. *J. Appl. Crystallogr.* **2000**, *33*, 285–290.
(172) Suzuki, J.; Seki, M.; Matsushita, Y. *J. Chem. Phys.* **2000**, *112*, 4862–4868.
(173) Matsushita, Y.; Tamura, M.; Noda, I. *Macromolecules* **1994**, *27*, 3680–3682.
(174) Zheng, W.; Wang, Z. *Macromolecules* **1995**, *28*, 7215–7223.
(175) Suzuki, J.; Nakane, K.; Takano, A.; Matsushita, Y. *Polymer* **2004**, *45*, 8989–8997.
(176) Epps, T. H., III; Cochran, E. W.; Hardy, C. M.; Bailey, T. S.; Waletzko, R. S.; Bates, F. S. *Macromolecules* **2004**, *37*, 7085–7088.
(177) Epps, T. H., III; Cochran, E. W.; Bailey, T. S.; Waletzko, R. S.; Hardy, C. M.; Bates, F. S. *Macromolecules* **2004**, *37*, 8325–8341.
(178) Frielinghaus, H.; Hermsdorf, N.; Almdal, K.; Mortensen, K.; Messe, L.; Corvazier, L.; Fairclough, J. P. A.; Ryan, A. J.; Olmsted, P. D.; Hamley, I. W. *Europhys. Lett.* **2001**, *53*, 680–686.
(179) Goldacker, T.; Abetz, V. *Macromolecules* **1999**, *32*, 5165–5167.
(180) Goldacker, T.; Abetz, V.; Stadler, R.; Erukhimovich, I.; Leibler, L. *Nature* **1999**, *398*, 137–139.
(181) Hückstädt, H.; Goldacker, T.; Goepfert, A.; Abetz, V. *Macromolecules* **2000**, *33*, 3757–3761.
(182) Sugiyama, M.; Shefelbine, T. A.; Vigild, M. E.; Bates, F. S. *J. Phys. Chem. B* **2001**, *105*, 12448–12460.
(183) Hardy, C. M.; Bates, F. S.; Kim, M.; Wignall, G. D. *Macromolecules* **2002**, *35*, 3189–3197.
(184) Chatterjee, J.; Jain, S.; Bates, F. S. *Macromolecules* **2007**, *40*, 2882–2896.
(185) Meuler, A. J.; Ellison, C. J.; Hillmyer, M. A.; Bates, F. S. *Macromolecules* **2008**, *41*, 6272–6275.
(186) Meuler, A. J.; Ellison, C. J.; Qin, J.; Evans, C. M.; Hillmyer, M. A.; Bates, F. S. *J. Chem. Phys.* **2009**, *130*, 234903/1–234903/17.
(187) Bates, F. S. *MRS Bull.* **2005**, *30*, 525–532.
(188) Bailey, T. S.; Hardy, C. M.; Epps, T. H., III; Bates, F. S. *Macromolecules* **2002**, *35*, 7007–7017.
(189) Tyler, C. A.; Qin, J.; Bates, F. S.; Morse, D. C. *Macromolecules* **2007**, *40*, 4654–4668.
(190) Epps, T. H., III; Bates, F. S. *Macromolecules* **2006**, *39*, 2676–2682.
(191) Meuler, A. J.; Ellison, C. J.; Evans, C. M.; Hillmyer, M. A.; Bates, F. S. *Macromolecules* **2007**, *40*, 7072–7074.
(192) Meuler, A. J.; Fleury, G.; Hillmyer, M. A.; Bates, F. S. *Macromolecules* **2008**, *41*, 5809–5817.
(193) Epps, T. H., III; Chatterjee, J.; Bates, F. S. *Macromolecules* **2005**, *38*, 8775–8784.
(194) Epps, T. H., III; Bailey, T. S.; Waletzko, R.; Bates, F. S. *Macromolecules* **2003**, *36*, 2873–2881.
(195) Cavicchi, K. A.; Lodge, T. P. *Macromolecules* **2003**, *36*, 7158–7164.
(196) Cavicchi, K. A.; Lodge, T. P. *Macromolecules* **2004**, *37*, 6004–6012.
(197) Cochran, E. W.; Bates, F. S. *Phys. Rev. Lett.* **2004**, *93*, 087802/1–087802/4.
(198) Cochran, E. W. Doctoral Thesis, Department of Chemical Engineering and Materials Science, University of Minnesota, Minneapolis, MN, **2004**.
(199) Bluemle, M. J.; Fleury, G.; Lodge, T. P.; Bates, F. S. *Soft Matter* **2009**, *5*, 1587–1590.
(200) Erukhimovich, I. Y. *Eur. Phys. J. E* **2005**, *18*, 383–406.
(201) Tyler, C. A.; Morse, D. C. *Phys. Rev. Lett.* **2005**, *94*, 208302/1–208302/4.
(202) Guo, Z.; Zhang, G.; Qiu, F.; Zhang, H.; Yang, Y.; Shi, A. *Phys. Rev. Lett.* **2008**, *101*, 028301/1–028301/4.
(203) Erukhimovich, I.; Abetz, V.; Stadler, R. *Macromolecules* **1997**, *30*, 7435–7443.
(204) Drolet, F.; Fredrickson, G. H. *Phys. Rev. Lett.* **1999**, *83*, 4317–4320.
(205) Bohbot-Raviv, Y.; Wang, Z. *Phys. Rev. Lett.* **2000**, *85*, 3428–3431.
(206) Abetz, V.; Goldacker, T. *Macromol. Rapid Commun.* **2000**, *21*, 16–34.
(207) Ranjan, A.; Morse, D. C. *Phys. Rev. E: Stat., Nonlinear, Soft Matter Phys.* **2006**, *74*, 011803/1–011803/6.
(208) Yamada, K.; Nonomura, M.; Ohta, T. *J. Phys: Condens. Matter* **2006**, *18*, L421–L427.
(209) Miao, B.; Wickham, R. A. *J. Chem. Phys.* **2008**, *128*, 054902/1–054902/5.
(210) Fredrickson, G. H.; Helfand, E. *J. Chem. Phys.* **1987**, *87*, 697–705.
(211) Brazovskii, S. A. *Sov. Phys. JETP* **1975**, *41*, 85.
(212) Hamley, I. W.; Castelletto, V.; Mykhaylyk, O. O.; Yang, Z.; May, R. P.; Lyakhova, K. S.; Sevink, G. J. A.; Zvelindovsky, A. V. *Langmuir* **2004**, *20*, 10785–10790.
(213) Yu, B.; Li, B.; Sun, P.; Chen, T.; Jin, Q.; Ding, D.; Shi, A. *J. Chem. Phys.* **2005**, *123*, 234902/1–234902/8.
(214) Hanley, K. J.; Lodge, T. P.; Huang, C. *Macromolecules* **2000**, *33*, 5918–5931.
(215) Lodge, T. P.; Pudil, B.; Hanley, K. J. *Macromolecules* **2002**, *35*, 4707–4717.
(216) Lodge, T. P.; Hanley, K. J.; Pudil, B.; Alahapperuma, V. *Macromolecules* **2003**, *36*, 816–822.
(217) Park, S.; Sul, W. *Polymer* **2008**, *49*, 3327–3334.

(218) Alexandridis, P.; Olsson, U.; Lindman, B. *Macromolecules* **1995**, *28*, 7700–7710.
(219) Alexandridis, P.; Olsson, U.; Lindman, B. *J. Phys. Chem.* **1996**, *100*, 280–288.
(220) Alexandridis, P.; Olsson, U.; Lindman, B. *Langmuir* **1997**, *13*, 23–34.
(221) Alexandridis, P.; Olsson, U.; Lindman, B. *Langmuir* **1998**, *14*, 2627–2638.
(222) Alexandridis, P. *Macromolecules* **1998**, *31*, 6935–6942.
(223) Svensson, B.; Alexandridis, P.; Olsson, U. *J. Phys. Chem. B* **1998**, *102*, 7541–7548.
(224) Bodycomb, J.; Yamaguchi, D.; Hashimoto, T. *Macromolecules* **2000**, *33*, 5187–5197.
(225) Laurer, J. H.; Hajduk, D. A.; Dreckoetter, S.; Smith, S. D.; Spontak, R. J. *Macromolecules* **1998**, *31*, 7546–7549.
(226) Lammertink, R. G. H.; Hempenius, M. A.; Thomas, E. L.; Vancso, J. *J. Polym. Sci., Part B* **1999**, *37*, 1009–1021.
(227) Epps, T. H., III; Bailey, T. S.; Pham, H. D.; Bates, F. S. *Chem. Mater.* **2002**, *14*, 1706–1714.
(228) Robitaille, C. D.; Fauteux, D. *J. Electrochem. Soc.* **1986**, *133*, 315–325.
(229) Chandrasekhar, V. *Adv. Polym. Sci.* **1998**, *135*, 139–205.
(230) Singh, M.; Odusanya, O.; Wilmes, G. M.; Eitouni, H. B.; Gomez, E. D.; Patel, A. J.; Chen, V. L.; Park, M. J.; Fragouli, P.; Iatrou, H.; Hadjichristidis, N.; Cookson, D.; Balsara, N. P. *Macromolecules* **2007**, *40*, 4578–4585.
(231) Park, M. J.; Downing, K. H.; Jackson, A.; Gomez, E. D.; Minor, A. M.; Cookson, D.; Weber, A. Z.; Balsara, N. P. *Nano Lett.* **2007**, *7*, 3547–3552.
(232) Park, M. J.; Nedoma, A. J.; Geissler, P. L.; Balsara, N. P.; Jackson, A.; Cookson, D. *Macromolecules* **2008**, *41*, 2271–2277.
(233) Cooke, D. M.; Shi, A. *Macromolecules* **2006**, *39*, 6661–6671.
(234) Matsen, M. W. *Phys. Rev. Lett.* **2007**, *99*, 148304/1–148304/4.
(235) Lynd, N. A.; Hillmyer, M. A.; Matsen, M. W. *Macromolecules* **2008**, *41*, 4531–4533.
(236) Hasegawa, H.; Hashimoto, T.; Hyde, S. T. *Polymer* **1996**, *37*, 3825–3833.
(237) Schröder-Turk, G. E.; Fogden, A.; Hyde, S. T. *Eur. Phys. J. B* **2007**, *59*, 115–126.
(238) Russell, T. P. *Curr. Opin. Colloid Interface Sci.* **1996**, *1*, 107.
(239) Fasolka, M. J.; Mayes, A. M. *Annu. Rev. Mater. Res.* **2001**, *31*, 323–355.
(240) Park, C.; Yoon, J.; Thomas, E. L. *Polymer* **2003**, *44*, 6725–6760.
(241) Cheng, J. Y.; Ross, C. A.; Smith, H. I.; Thomas, E. L. *Adv. Mater.* **2006**, *18*, 2505–2521.
(242) Yin, Y.; Sun, P.; Jiang, R.; Li, B.; Chen, T.; Jin, Q.; Ding, D.; Shi, A. *J. Chem. Phys.* **2006**, *124*, 184708/1–184708/8.
(243) Lee, B.; Park, I.; Yoon, J.; Park, S.; Kim, J.; Kim, K.; Chang, T.; Ree, M. *Macromolecules* **2005**, *38*, 4311–4323.
(244) Jin, S.; Yoon, J.; Heo, K.; Park, H. W.; Kim, J.; Kim, K. W.; Shin, T. J.; Chang, T.; Ree, M. *J. Appl. Crystallogr.* **2007**, *40*, 950–958.
(245) Park, H.; Im, K.; Chung, B.; Ree, M.; Chang, T.; Sawa, K.; Jinnai, H. *Macromolecules* **2007**, *40*, 2603–2605.
(246) Epps, T. H., III; DeLongchamp, D. M.; Fasolka, M. J.; Fischer, D. A.; Jablonski, E. L. *Langmuir* **2007**, *23*, 3355–3362.
(247) Daoulas, K. C.; Muller, M.; Stoykovich, M. P.; Park, S.; Papakonstantopoulos, Y. J.; de Pablo, J. J.; Nealey, P. F.; Solak, H. H. *Phys. Rev. Lett.* **2006**, *96*, 036104/1–036104/4.
(248) Fredrickson, G. H.; Bates, F. S. *Annu. Rev. Mater. Sci.* **1996**, *26*, 501–550.
(249) Tyler, C. A.; Morse, D. C. *Macromolecules* **2003**, *36*, 3764–3774.
(250) Yamada, K.; Ohta, T. *Europhys. Lett.* **2006**, *73*, 614–620.
(251) Tamate, R.; Yamada, K.; Vinals, J.; Ohta, T. *J. Phys. Soc. Jpn.* **2008**, *77*, 034802/1–034802/6.
(252) Holden, G.; Legge, N. R. In *Thermoplastic Elastomers*, 2nd ed.; Holden, G., Legge, N. R., Quirk, R. P., Schroeder, H. E., Eds.; Hansen Publishers: New York, 1996; pp 48−69.
(253) Sakurai, S.; Isobe, D.; Okamoto, S.; Nomura, S. *J. Macromol. Sci., Phys.* **2002**, *B41*, 387–395.
(254) Cohen, Y.; Albalak, R. J.; Dair, B. J.; Capel, M. S.; Thomas, E. L. *Macromolecules* **2000**, *33*, 6502–6516.
(255) Phatak, A.; Lim, L. S.; Reaves, C. K.; Bates, F. S. *Macromolecules* **2006**, *39*, 6221–6228.
(256) Finnefrock, A. C.; Ulrich, R.; Du Chesne, A.; Honeker, C. C.; Schumacher, K.; Unger, K. K.; Gruner, S. M.; Wiesner, U. *Angew. Chem., Int. Ed.* **2001**, *40*, 1208–1211.
(257) Finnefrock, A. C.; Ulrich, R.; Toombes, G. E. S.; Gruner, S. M.; Wiesner, U. *J. Am. Chem. Soc.* **2003**, *125*, 13084–13093.
(258) Jain, A.; Toombes, G. E. S.; Hall, L. M.; Mahajan, S.; Garcia, C. B. W.; Probst, W.; Gruner, S. M.; Wiesner, U. *Angew. Chem., Int. Ed.* **2005**, *44*, 1226–1229.
(259) Michielsen, K.; Stavenga, D. G. *J. R. Soc. Interface* **2008**, *5*, 85–94.
(260) Jain, S.; Bates, F. S. *Science* **2003**, *300*, 460–464.
(261) Jain, S.; Gong, X.; Scriven, L. E.; Bates, F. S. *Phys. Rev. Lett.* **2006**, *96*, 138304/1–138304/4.
(262) Iacovella, C. R.; Keys, A. S.; Horsch, M. A.; Glotzer, S. C. *Phys. Rev. E: Stat., Nonlinear, Soft Matter Phys.* **2007**, *75*, 040801/1–040801/4.
(263) Iacovella, C. R.; Horsch, M. A.; Glotzer, S. C. *J. Chem. Phys.* **2008**, *129*, 044902/1–044902/10.
(264) Iacovella, C. R.; Glotzer, S. C. *Nano Lett.* **2009**, *9*, 1206–1211.